Angle of Incidence and Non-Intrusive Cell Quantum Efficiency

Measurements of Commercial Photovoltaic Modules

by

Brett Knisely

A Thesis Presented in Partial Fulfillment
of the Requirements for the Degree
Master of Science in Technology

Approved September 2013 by the
Graduate Supervisory Committee:

Govindasamy Tamizhmani, Chair
Bradley Rogers
Narciso Macia

ARIZONA STATE UNIVERSITY

December 2013

ABSTRACT

This is a two-part thesis:

Part 1 of this thesis tests and validates the methodology and mathematical models of the International Electrotechnical Commission (IEC) 61853-2 standard for the measurement of angle of incidence (AOI) effects on photovoltaic modules. Flat-plate photovoltaic modules in the field operate under a wide range of environmental conditions. The purpose of IEC 61853-2 is to characterize photovoltaic modules' performance under specific environmental conditions. Part 1 of this report focuses specifically on AOI.

To accurately test and validate IEC 61853-2 standard for measuring AOI, meticulous experimental setup and test procedures were followed. Modules of five different photovoltaic technology types with glass superstrates were tested. Test results show practically identical relative light transmission plots for all five test modules. The experimental results were compared to theoretical and empirical models for relative light transmission of air-glass interface. IEC 61853-2 states "for the flat glass superstrate modules, the AOI test does not need to be performed; rather, the data of a flat glass air interface can be used." The results obtained in this thesis validate this statement. This work was performed in collaboration with another Master of Science student (Surynarayana Janakeeraman) and the test results are presented in two masters theses.

Part 2 of this thesis is to develop non-intrusive techniques to accurately measure the quantum efficiency (QE) of a single-junction crystalline silicon cell within a commercial module. This thesis will describe in detail all the equipment and conditions necessary to measure QE and discuss the factors which may influence this measurement.

i

The ability to utilize a non-intrusive test to measure quantum efficiency of a cell within a module is extremely beneficial for reliability testing of commercial modules. Detailed methodologies for this innovative test procedure are not widely available in industry because equipment and measurement techniques have not been explored extensively. This paper will provide a literature review describing relevant theories and measurement techniques related to measuring the QE of a cell within a module. The testing methodology and necessary equipment will be described in detail. Results and conclusions provide the overall accuracy of the measurements and discuss the parameters affecting these measurements.

DEDICATION

This thesis is dedicated to my parents, Mark and Cindy Knisely. Without their love and support, none of this would be possible.

ACKNOWLEDGMENTS

I would like to thank my advisor, Dr. Govindasamy Tamizhimani for his guidance and leadership throughout my thesis work. It's an honor to be mentored by such a hard-working and dedicated figure to the solar industry.

I also express my appreciation to my committee members Dr. Rogers and Dr. Macia for their help with my thesis development.

My sincere appreciation goes out to Joseph Kuitche for giving me the opportunity to work at Arizona State University Photovoltaic Reliability Laboratory. I value the experience and knowledge that I gained while working under his supervision at PRL.

I would also like to thanks all past and present employees at PRL. It was an honor working with such a diverse and dedicated group of people. Special thanks go out to Suryanarayana Vasantha Janakeeraman, Sai Tatapudi, Jaya Mallineni, Karan Rao Yeddidi, Jonathan Belmont, Kolapo Olakonu, Cameron Anderson, Bulent Bicer and Cassie Yan.

TABLE OF CONTENTS

LIST OF TABLES

LIST OF FIGURES

DEFINITION OF TERMS

AOI = Angle of incidence (angle between solar beam and normal vector in degrees)

PV = photovoltaic

ASU-PRL = Arizona State University Photovoltaic Reliability Laboratory

IEC = International Electrotecnical Commission

Mono-Si = monocrystalline silicon

Poly-Si = polycrystalline silicon

a-Si = amorphous silicon

CdTe = cadmium telluride

CIGS = copper indium gallium selenide

$\mathbf{I_{sc}}$ = Short circuit current (A)

$\mathbf{V_{oc}}$ = Open circuit voltage (V)

$\mathbf{E_e}$ = Solar irradiance actually captured and used by module (dim or suns)

$\mathbf{E_{dni}}$ = Direct normal solar irradiance (W/m^2)

$\mathbf{E_{poa}}$ = Global solar irradiance in the plane-of-array (module) (W/m^2)

$\mathbf{E_o}$ = Reference global solar irradiance, typically 1000 W/m^2

$\mathbf{T_c}$ = Measured module (cell) temperature (°C)

$\mathbf{\alpha_{Isc}}$ = Short-circuit current temperature coefficient (1/°C)

$\mathbf{f_1(AM_a)}$ = Empirical relationship for solar spectral influence on Isc versus air mass

C-M-QE = Cell-module quantum efficiency measurement

FF = Fill factor

C-QE = Cell Quantum Efficiency

M-QE = Module Quantum Efficiency

PART 1: ANGLE OF INCIDENCE EFFECT ON PHOTOVOLTAIC MODULES

1-1 INTRODUCTION

About the IEC 61853-2 Standard

The International Electrotechnical Commission (IEC) is a standard development organization (SDO) for the preparation and publication of International Standards for all electrical, electronic and related technologies. IEC 61853 is a standard governing photovoltaic (PV) module performance testing and energy rating. The overall scope of the IEC 61853 standard is to test and characterize PV modules over a wide range of temperatures, irradiance levels, angles of incidence, and solar spectra.

Part 1 of IEC 61853: *Photovoltaic Module Performance Testing and Energy Rating* measures PV module power under specific conditions: air mass spectrum of 1.5, angle of incidence of 0°, seven different irradiance levels, and four different temperatures. Part 2 of IEC 61853 aims to test and measure power ratings over a wide range of air mass spectrum and angle of incidences from 0° to 90°. Currently, IEC 61853-2 is a draft form and is projected to be finalized in the 2014/2015 timeframe. IEC Technical Group 82 developed the procedures and mathematical models used in the first two parts of the standard (IEC 61853-1 and IEC 61853-2). The accuracy of these procedures and models must be independently tested and validated.

Statement of the Problem

The amount of sunlight reaching solar cells is dictated by the reflected and transmitted fractions of the incident light. The transmissions and reflections are influenced by the module design: reflections within superstrate and encapsulant, and at

the air/superstate, superstrate/encapsulant and encapsulant/cell interfaces; transmittances through superstrate and encapsulant. These reflections and transmittances are the functions of the solar incidence angle. The surface roughness and antireflective coatings of the superstrates heavily influence the incident angle effect.

As shown in Figure 1, there are two primary ways angle of incidence (AOI) influences the short circuit current of photovoltaic modules. The first is a purely mechanical/geometrical effect due to the module's orientation with respect to the incident sunlight. It is often referred to as the 'cosine effect'. It states that the irradiance incident on the module decreases with increasing AOI and it is proportional to cos(AOI). The second way AOI influences short circuit current is due to the optical effects or surface characteristics of the module itself and will be referred to as the 'optical effect'. PV manufacturers go through great lengths to improve the optical characteristics of modules, specifically the superstrate, by incorporating anti-reflective coatings, rolled or textured glass, or other methods.
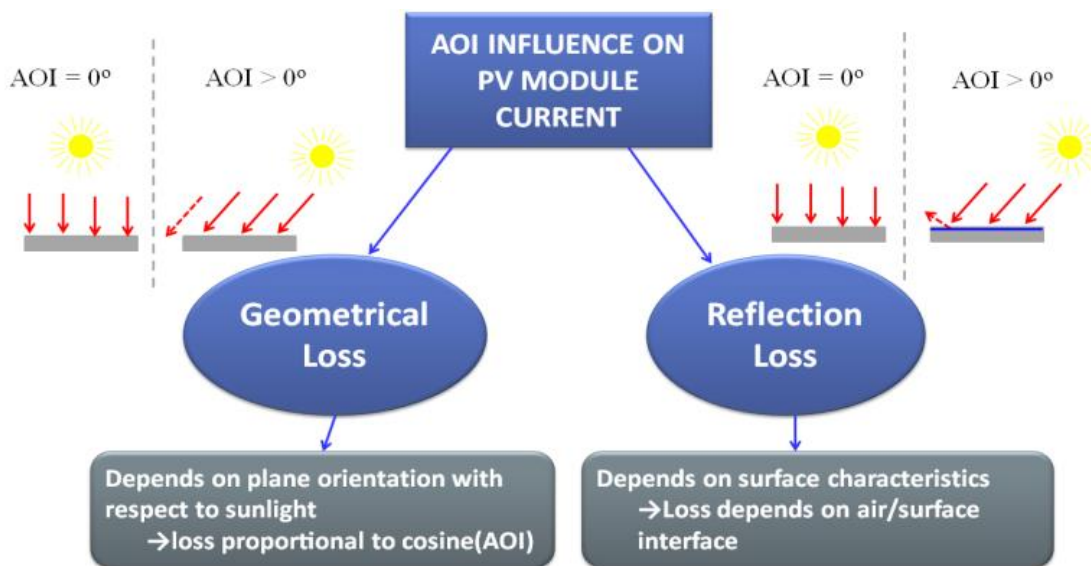
Figure 1.   Summary of geometrical and reflection losses for flat-plate PV modules

This report presents the effects of AOI on short circuit current for five different module technologies: monocrystalline silicon (Mono-Si), polycrystalline silicon (Poly-Si), amorphous silicon (a-Si), cadmium telluride (CdTe), and copper indium gallium selenide (CIGS). The superstrate/encapsulant/substrate materials of these modules are respectively: glass/EVA/polymer (mono-Si); glass/EVA/polymer (poly-Si); glass/EVA/glass (a-Si); glass/EVA/glass (CdTe); glass/EVA/polymer (CIGS). All measurements were carried out on clear sunny days using a 2-axis tracker. A novel device, described later in this thesis, was used to accurately measure the angle of incidence (AOI) and three conventional reference devices were used to measure the irradiance: pyranometer (global irradiance), pyrheliometer (direct normal irradiance), and polycrystalline silicon reference cell (global irradiance).

The data collected during this experiment was then processed and analyzed according to equations specified by IEC 61853-1. To cross check this data analysis procedure, the data was also processed using the method developed by Sandia National Laboratory. Both results are plotted and compared to existing theoretical curves for the reflectance of an air-glass interface. A comprehensive uncertainty analysis was also calculated by quantifying the error for each measurement device used in the experiment. A major report based on this work was published by Solar ABCs and this report can be downloaded from SolarABCs website (solarabcs.org).

1-2 LITERATURE REVIEW

Outdoor Measurement Procedure of IEC 61853-2 Standard

The measurement procedure of IEC 61853-2 for AOI effects is based on collecting Isc data of the test modules over a wide range of incident angles. The required test apparatus, experimental setup, and measurement procedures are briefly presented below. For detailed and exact procedures, refer to the IEC standard.

The standard identifies the use of various test apparatus and the technical requirements of these apparatus. Irradiance sensors are used to measure the global and direct irradiance levels (reference cell for global irradiance and direct irradiance level using shadowing/collimating method as described in the "measurement procedure" below; or a combination of pyranometer for global irradiance and pyheliometer for direct normal irradiance). Thermal sensors are used to measure the temperature of ambient, test module and reference cell. A data acquisition system collects and stores the output of thermal sensors and the short circuit current of the test modules and reference cell. Two-axis trackers are used to mount the test modules and change the incident angles on the test modules. An AOI measuring device determines the tilt angle to the sun and verified the co-planarity of test modules and irradiance sensors

If the diffuse component does not exceed 10% of the total irradiance, then directly measured Isc at various angles of incidence, Isc(θ), can be used to calculate the relative angular light transmission data, $\tau(\theta)$, as given in (3). If the diffuse component exceeds 10% of the total irradiance, then the measured Isc(θ) should be corrected before use in the

calculation of $\tau(\theta)$. The Isc(θ) correction depends on the type of irradiance sensor used (PV reference cell or pyranometer).

If a PV reference cell device is used as an irradiance sensor, the diffuse light component should not exceed 10% of the total irradiance during the Isc(θ) measurement period. If the diffuse component exceeds 10%, it can be subtracted after measuring the angular response with blocked direct light component or the diffuse component can be blocked to below 10% by reducing the field of view of the diffuse component; for example, by collimating the incident light reaching the test module.

If the pyranometer and pyrheliometer are used as irradiance sensors, the diffuse component visible to the module is given in Equation (1).

$$G_{diff} = G_{tpoa} - G_{dni}\cos(\theta) \qquad (1)$$

Where G_{diff} is global diffuse irradiance, G_{tpoa} is the total irradiance in the plane of the module (as measured by a pyranometer in the module plane), G_{dni} is direct normal irradiance as measured by the pyrheliometer and θ corresponds to the tilt angle between the module normal and the direct solar irradiance.

Isc induced by the direct incident light can be estimated in the presence of the diffuse light component in Equation (2).

$$I_{SC}(\theta) = I_{sc_{measured}}(\theta)\left(1 - \frac{G_{diff}}{G_{tpoa}}\right) \qquad (2)$$

Use the two-axis tracker to rotate the test module with respect to the normal solar irradiance. Vary the angle between module normal and sunlight between -80° and +80° in steps of maximum 10°. Do a minimum of nine different angles to span the angles from 0 to 80°.

The relative angular light transmission (or relative angular optical response) into the module is given by Equation (3).

$$\tau(\theta) = \frac{I_{SC}(\theta)}{\cos(\theta)I_{SC}(0)} \qquad (3)$$

Sandia National Laboratory Method

In June 2012, Sandia National Laboratory published a paper titled "Measuring Angle-of-Incidence (AOI) Influence on PV Module Performance" [1]. This paper stated the difference between "mechanical" and "optical" effects and the contributing factors of angle of incidence losses. Mechanical effects deal strictly with the module's orientation with respect to the incident sunlight. Mechanical effects have nothing to do with the material construction of the module; rather it is an unavoidable physical effect when changing the angle of incidence. The mechanical effect is proportional to the cosine of AOI and is often referred to as the cosine effect. The optical effect depends on the surface characteristics of the module and affects the PV module by increasing reflectance losses as AOI increases. All modules used in this report were of an air-glass interface.

Both mechanical and optical influences apply mainly to the direct component of sunlight. Therefore, it was essential to perform the experiments on a clear sunny day when the direct component beam was greater than 90% of the total global irradiance. The Sandia model accounts for both mechanical and optical influences using an expanded expression to determine the effective solar irradiance. By taking to account the direct and diffused components of sunlight, the optical effect (f_2(AOI)) can be measured empirically and calculated using the following Equations (4) and (5).

$$f_2(\text{AOI}) = \frac{E_0\left(\frac{I_{SC}}{\left(1+\alpha_{Isc}(T_C-25)\right)I_{scr}}\right)-\left(E_{poa}-E_{dni}\cos(AOI)\right)}{E_{dni}\cos(AOI)} \qquad (4)$$

$$I_{scr} = \frac{I_{sc}E_0}{E_{poa}\left(1+\alpha_{Isc}(T_c-25)\right)} \qquad (5)$$

Empirical measurements for f_2(AOI) were carried out at Sandia National Laboratory for conventional flat-plate PV modules with planar glass-air interfaces. The results for these tests are given in Figure 2.
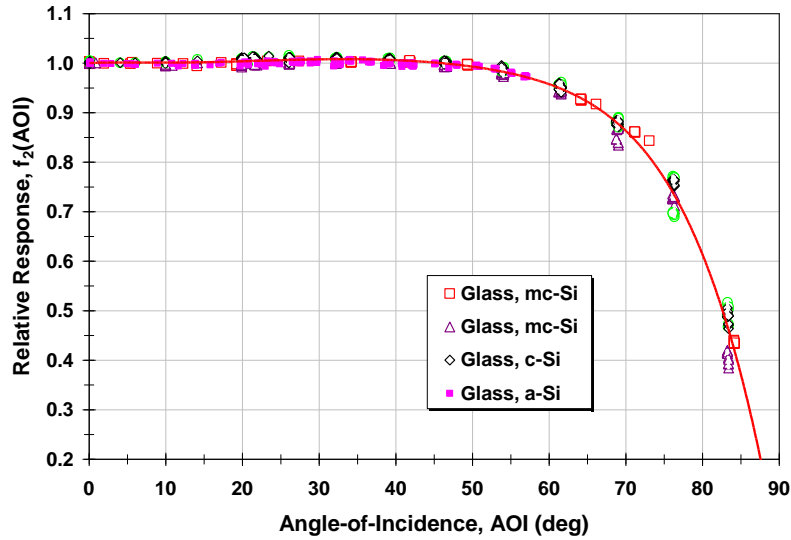
Figure 2.   Empirical f_2(AOI) measurements by Sandia National Laboratories for conventional flat-plate modules with a planar glass front surfaces [1]

After sufficient data had been collected for the relative optical response of modules with an air-glass interface, Sandia National Laboratories fit a fifth order polynomial to the measured data. This polynomial is shown in red in Figure 2. The generic polynomial used to describe the typical optical response for modules with an air-glass interface is given in Equation (6) below.

8

$$f_2(AOI) = 1-2.4377E\text{-}3(AOI)+3.1032E\text{-}4(AOI)^2-1.2458E\text{-}5(AOI)^3+$$

$$2.1122E\text{-}7(AOI)^4-1.3593E\text{-}9(AOI)^5 \qquad (6)$$

Theoretical Models for Reflectance Losses

The Sandia National Laboratory polynomial for typical optical response of air-glass interface PV modules gives an empirically derived model for the reflective behaviors of PV modules in the field. This study will also consider an analytical module to determine how they compare with measured data. "Angular Reflection Losses in PV Modules" by N. Martin and J. M. Ruiz was published in 2004 with the purpose of obtaining a universal model for calculating the annual angular reflection losses of PV modules in real conditions [2]. The calculation for the optical losses, developed by the authors, is given in Equation (7).

$$AL(\alpha) = 1 - \left[\frac{1-exp[-\cos(\alpha)/a_r]}{1-\exp(-\frac{1}{a_r})} \right] \qquad (7)$$

Where:

α = Angle of incidence

a_r = angular loss coefficient (an empirical dimensionless parameter dependent on each technology; typical values range from 0.16 to 0.17 for commercial clean x-Si and a-Si modules, 0.20 if the modules' surfaces have a moderate quantity of dust [for this report, 0.17 was used])

Equation (7) was plotted and compared to the Sandia National Laboratory generalized polynomial as shown in Figure 3. Both the empirically derived curve and analytically derived curves are in good agreement with each other. The measured results from this experiment were plotted and compared to the Sandia National Laboratory generalized polynomial and the Martin and Ruiz theoretically derived polynomial to check accuracy.
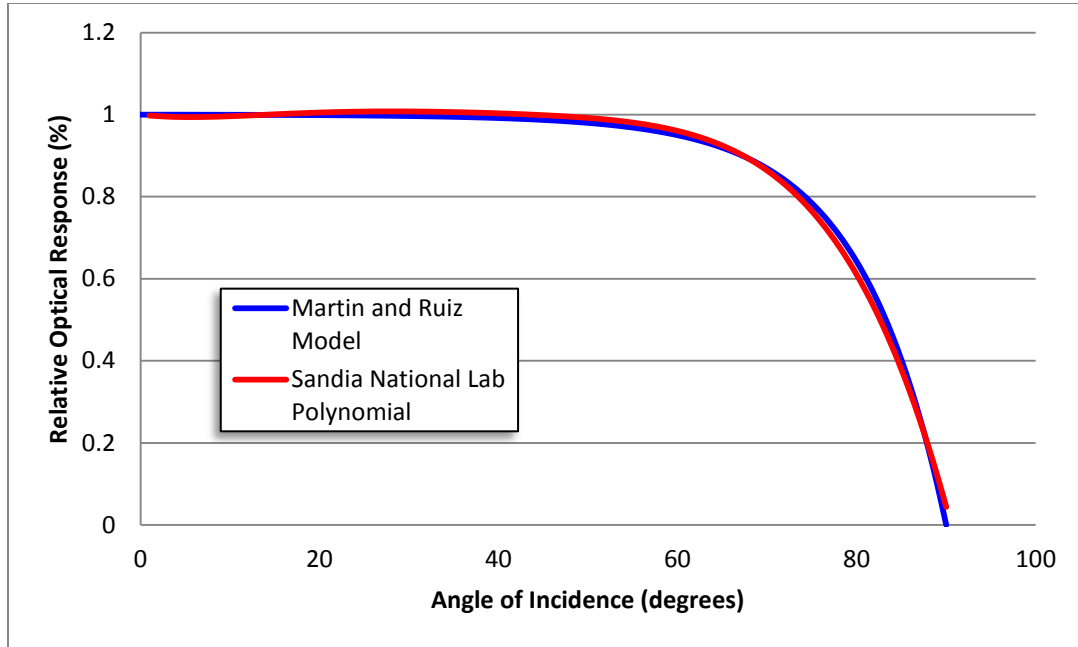
Figure 3.   Comparison of relative optical response for Sandia National Laboratory polynomial and Martin and Ruiz model

1-3 METHODOLOGY

Outdoor Measurement Procedure at ASU-PRL

During the outdoor measurements at ASU-PRL, the measurement procedures of IEC 61853-2 standard were closely followed. The test apparatus, experimental setup and measurement procedures used in this work are presented below.

Test Apparatus

- Test modules: The test modules of five different technologies were used: monocrystalline silicon (Mono-Si), polycrystalline silicon (Poly-Si), amorphous silicon (a-Si), cadmium telluride (CdTe), and copper indium gallium selenide (CIGS). In all the five modules, glass was used as the superstrate. The superstrate/encapsulant/substrate materials of these five modules are: glass/EVA/polymer (mono-Si); glass/EVA/polymer (poly-Si); glass/EVA/glass (a-Si); glass/EVA/glass (CdTe); glass/EVA/polymer (CIGS).

- Irradiance sensors: A PV reference cell (poly-Si), two pyranometers from two vendors (Eppley PSP and Kipp & Zonnen) and a pyrheliometer (Kipp & Zonen) were used. All the irradiance sensors were calibrated. Only the data obtained using the pyranometers and pyrheliometer were processed for the data analysis in this report. The data obtained using the PV reference cell will be processed and presented in a future publication.

- Thermal sensors: Omega T-type thermocouples were attached to the center of the backsheet of each module using a thermal tape. The accuracy of the thermocouples is given by the manufacturer as +/- 1°C or 0.75% for temperatures above 0°C.

- Short Circuit Current Measurement: CR Magnetic direct current (DC) transducers were used to measure the short circuit current for each module (Figure 4A). The transducers were kept in an air conditioned facility to maintain a constant operating temperature and to comply with the manufacturer rated accuracy of 1%. A linear relation is given between current passing through the transducer and the voltage output by the transducer.

- Data acquisition system: A Campbell Scientific CR1000 data logger was used to record and store all the simultaneously collected data: module short circuit current; module temperature; and irradiance. Since temperatures of the five modules also had to be recorded, a multiplexer was used to provide the necessary number of inputs (Figure 4B). The CR1000 was also kept inside a temperature controlled facility to meet the manufacture rated accuracy of 1%.
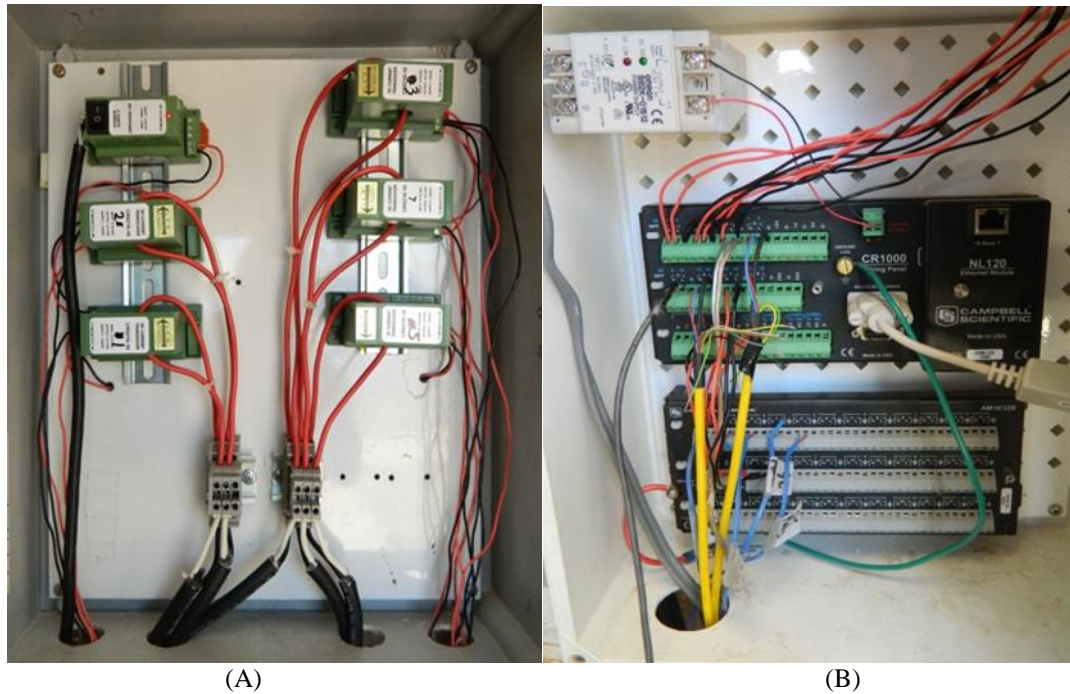
Figure 4.   (A) DC current transducers (B) CR1000 data logger with multiplexer

- <u>Two-axis tracker:</u> A two axis tracker was used to mount the test modules, irradiance sensors and AOI measuring device. Ideally, the tracker used should have full range of motion in both azimuth and elevation angles to achieve high angles of incidence for any time of day. The tracker used for this experiment was limited to 180° rotation about the azimuth angle and 65° of rotation about the elevation angle. High AOI could be achieved by starting the experiment at a certain time of day (around 14:30 MST for this experiment) to allow the tracker to utilize its full azimuth range. Since it was necessary to obtain E_{dni} measurements throughout the experiment, the pyrheliometer was allowed to track the sun using a manual 2-axis tracking method.

- <u>AOI measuring device:</u> To determine the tilt angle to the sun for all modules and reference devices mounted on the two-axis tracker, a 3DM-GX3-25 miniature attitude heading reference system (Figure 5A) was used. This device is a high-

13

performance, miniature attitude heading reference system purchased from MicroStrain (www.microstrain.com). It consists of a triaxial accelerometer, triaxial magnetometer, temperature sensors and processor that run an algorithm which provides static and dynamic orientation measurements with a manufacturer rated accuracy of +/- 0.5° static accuracy and a +/- 0.2° repeatability. To comply with the static accuracy of the device, the tracker was stopped for six seconds at each AOI. This allowed a stable AOI reading from the device. AOI software was used to calculate the position of the sun relative to the modules orientation, therefore providing the AOI. The device was mounted on the surface of a plastic platform (Figure 5B) at the end of a plastic bar extending from the tracker and coplanar to the modules. AOI data was measured and recorded by a laptop that was kept outside. The tracker operator manually rotated the two-axis tracker while referring to the laptop with the AOI software which displayed the AOI of the tracker and thus the modules and irradiance devices. The AOI data and data recorded by the Campbell Scientific CR1000 data logger were combined by synchronizing the laptop's clock to that of the data logger.

| (A) | (B) |

Figure 5.   (A) AOI measurement device. (B) AOI device mounted on plastic arm

Ideally, to ensure that all modules and reference devices are coplanar with respect to each other, the altitude heading reference device was placed on each module and the AOI was read from the software and checked for consistency. However, the accuracy of the device is greatly affected by any magnetic material. Care was taken to insure the device was mounted on a plastic platform with non-magnetic screws to avoid magnetic interference which may influence AOI measurements. When the AOI measurement device was placed near the modules, an accurate reading of AOI was unobtainable. To check that all modules where coplanar with respect to each other, the tracker was then set to automatic mode and allowed to track at an angle normal to the solar incidence beam. Both the AOI device and a sundial were placed on the plastic mounting arm of the AOI device and the tracker was 'zeroed' so that the AOI device measured a maximum AOI of 0.3°or lower and there was no visible shadow on the sundial (Figure 6A). The sundial was then placed at the center and corner (Figure 6B) of each module. The shadow of the sundial was measured for each location. As shown in the equation below, the point on the tracker with the longest shadow length represented the least accurate point with respect to

15

AOI ($AOI_{max\ error}$). This maximum shadow length was measured and the corresponding angle was calculated to be 0.7°. Given that the initial AOI reading was a maximum of 0.3°, the projected maximum uncertainty for AOI was +/-1.0°.

Test Setup

The setup used for this experiment is shown in Figure 7. As required by the standard, all the modules were cleaned before beginning the measurements. The name of each module technology is labeled next to the respective module. All the components and test apparatus used in this work are identified in Figure 7.

(A)   (B)
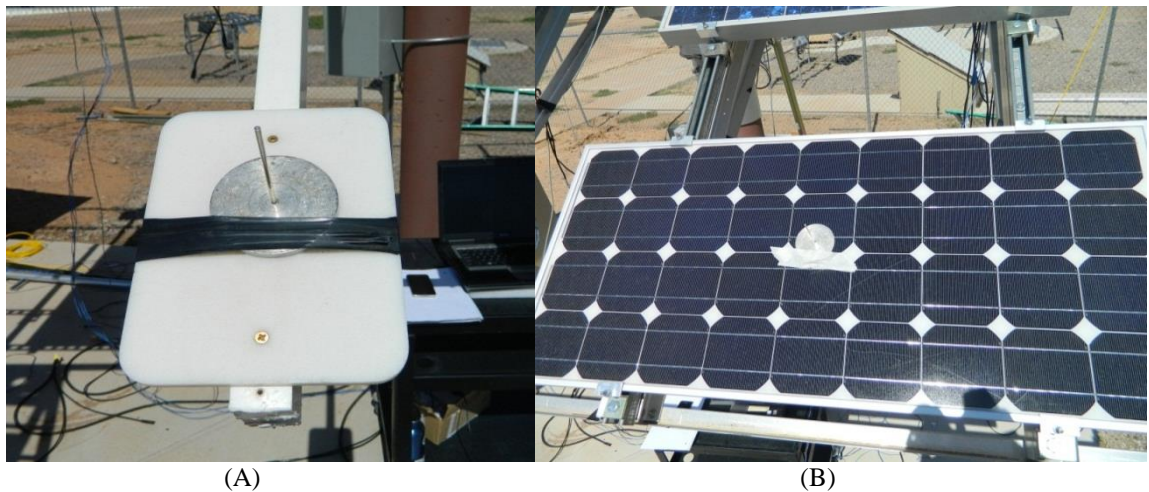
Figure 6.   (A) Sundial "zeroed" to AOI platform with essentially no shadow present (B) Sundail used to check the accuracy of the AOI for the mono-Si module
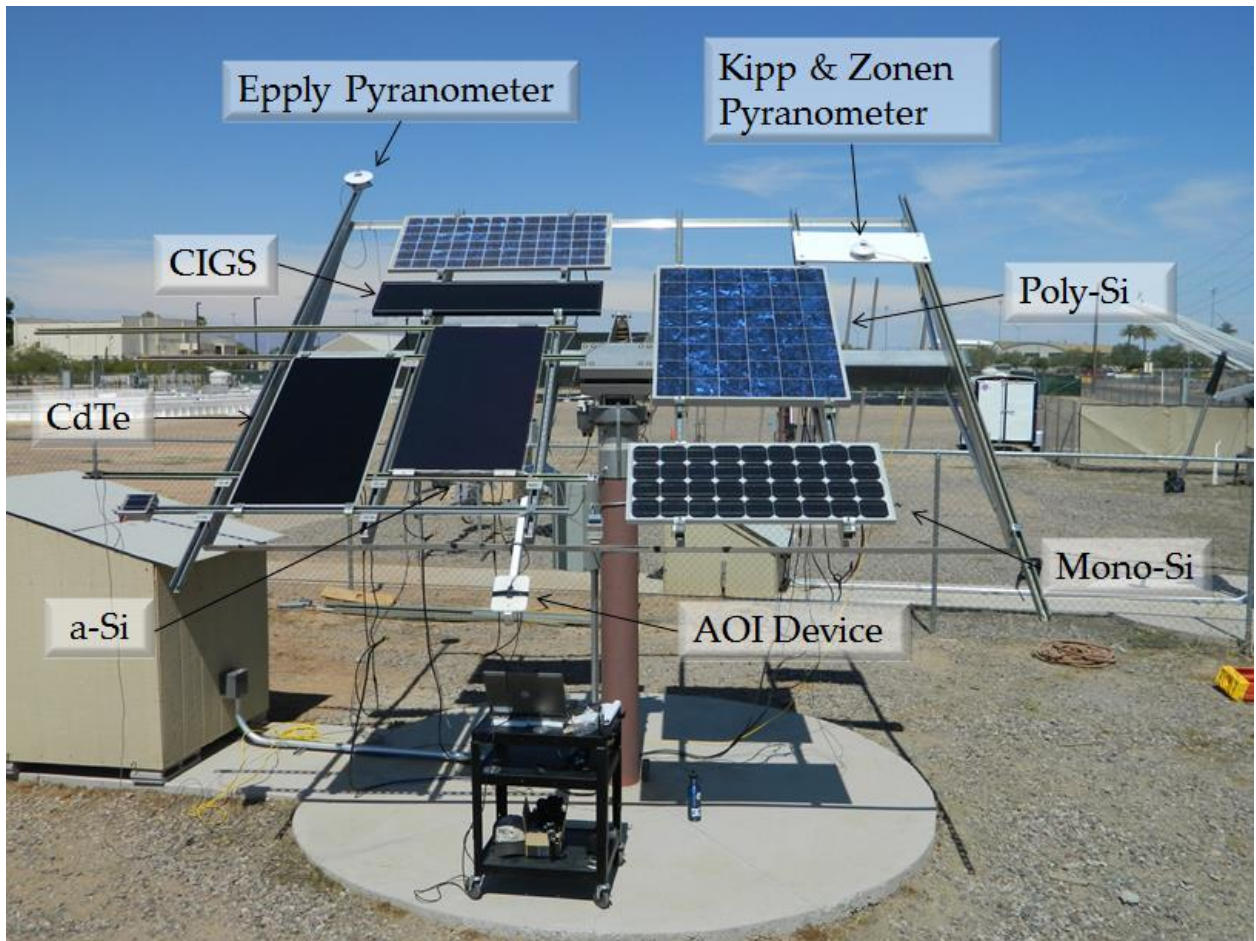
Figure 7.   AOI measurement setup on two-axis tracker

Measurement Procedure

To reduce the effects of module temperature, solar irradiance and solar spectral variations, the data was collected as quickly as possible. For this experiment, data was simultaneously collected from five different modules and irradiance sensors. These factors were given great importance and attention when performing the experiment:

1. Soiling: Dust on the surface of the modules can be expected to influence the irradiance incident on the surface of the module. Therefore, all modules where cleaned before each experiment was performed.

17

2. Reflection from the surroundings: No objects of abnormally high solar reflectance were present at the test sight. Care was taken to prevent reflection from the surroundings. Any unnecessary devices on the tracker that protruded from the plane of array of the modules were removed. The ground surrounding the tracker was a flat gravel surface.

3. Standard and constant irradiance: Ideally, if the entire global irradiance of about 1000 W/m^2 is made of direct irradiance, then AOI measurements on PV modules would become very simple. However, even on very clear days, there is always some diffused light. Clouds will further increase the ratio of diffused to direct irradiance. This ratio plays a prominent role on the measurement accuracy, especially at higher AOI. Therefore, all the tests were performed under clear sky conditions when the ratio of direct normal irradiance (measured by the normal incidence pyrheliometer) to global normal irradiance (measured by the pyranometer) was higher than 0.85.

4. Standard and constant spectrum: Ideally, the test should be performed in a short period of time near solar noon to minimize the influence of spectral variation during the test period. Due to the physical limitation of the tracker, this test was performed around 14:30 MST to utilize the full range of the tracker. However, the test was done quickly (about 10 minutes) to maintain a constant spectrum throughout the experiment. The AOI was changed by rotating the tracker in azimuth and elevation from west to east, up to angles close to 90°. The data obtained in the opposite direction, east to west, is presented in Appendix F.

5. Standard and constant temperature: Ideally, the measurements shall be done at a constant module temperature. However, when AOI is changed, the module temperature cannot be kept constant due to varying irradiance levels on the module surface. The temperature of each module, under a very low wind speed condition, was measured by attaching a thermocouple to the center of the backsheet and recording the temperature throughout the experiment. Using the measured temperature coefficient for current of each module, the Isc values were corrected to 25°C to eliminate the influence of varying temperature during the test period.

6. Maximum number of data points: A higher number of data points will improve the confidence level in the accuracy of measurements. The minimum time interval that the data logger could collect data was 30 seconds. To obtain enough data points, with nearly constant irradiance and air mass conditions, the tracker was moved 5° every 30 seconds up to AOI close to 85° (or as far as the tracker would allow). This allowed for a minimum of 18 data points to generate the Isc vs. AOI plots. The actual number of data points collected was 21 as the tracker was rotated slower at higher AOI to obtain more data points.

1-4 RESULTS AND DISCUSSION

Relative I_sc with Diffuse Component and Cosine Effects

The first set of data was selected when the ratio of direct normal irradiance (G_{dni}) to total plane of irradiance (G_{tpoa}) was 87%. During this experiment, the Isc data of each module and the corresponding AOI was simultaneously measured. Figure 8 shows the Isc data relative to the Isc data obtained at zero AOI. This plot indicates the data is nearly identical for all the modules with glass superstrate regardless of the test technology (mono-Si, poly-Si, a-Si, CdTe, or CIGS). It is important to note that both optical and cosine effects of both the direct component and the diffuse component of the incident irradiance influence relative Isc data. To obtain the true Isc value (relative light transmission or relative optical response) free from the influence of the diffuse light component and the cosine effect, the Isc data shown in Figure 8 needs to be corrected.
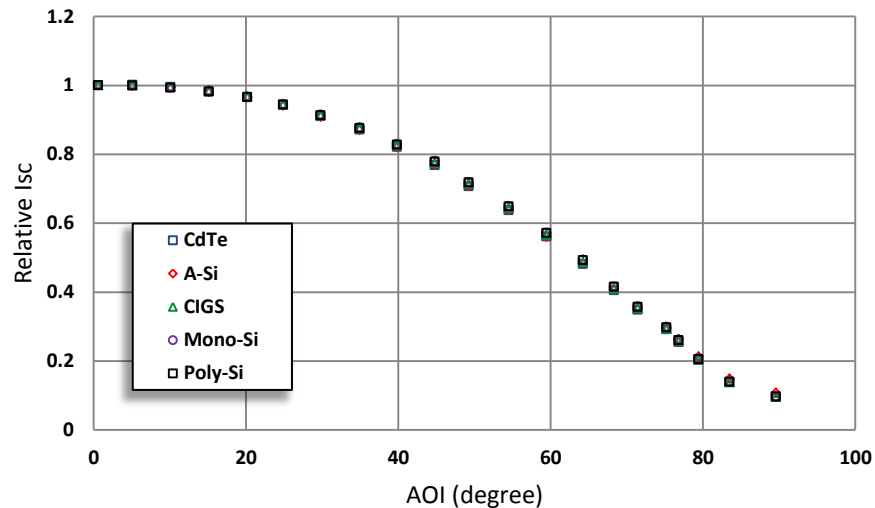
Figure 8   Relative Isc with diffused component and cosine effects

Relative I_{sc} without Diffuse Component and Cosine Effects

Relative I_{sc} without Diffuse Component and Cosine Effects

According to the requirements of the standard, the diffuse component of the incident light should not exceed 10% of the total irradiance during the experiment. If it does, then the data should be corrected to eliminate the influence of the diffuse component. This correction can be made using the reference cell method or the pyranometer/pyrheliometer method described in IEC 61853-2 [3].

To make the correction using the reference cell method, follow the procedure delineated in the standard: "If the diffuse component exceeds 10%, it can be subtracted after measuring the angular response with blocked direct light component or the diffuse component can be blocked to below 10% by reducing the field of view of the diffuse component, for example by collimating the incident light reaching the test module." The Isc data obtained with this correction method is now influenced only by the direct irradiance without any influence from diffuse irradiance, because the Isc contribution from diffuse irradiance is subtracted from the Isc value obtained with total irradiance.

This Isc data, referred to as Isc(θ), can then be directly used in Equation (3) of this report (or Equation (2) of the standard) to obtain the relative light transmission (or relative optical response) data, which is the true corrected data after eliminating the cosine and diffuse component effects.

For the correction using the pyranometer/pyheliometer method, the IEC 61853-2 [3] and Sandia [1] procedures/models were implemented. The Sandia procedure/model involves Equations (4) and (5) and the details of this procedure are provided in Appendix A. The relative optical response, f_2(AOI), is given in Equation (4).

The plots obtained using the IEC Equations (1) (2) and (3) are provided in Figure 9 and the plots obtained using the Sandia Equations (4) and (5) are provided in Figure 10. Both the IEC model and the Sandia model yield approximately the same results. As shown in Figure 11, the modeled data can be slightly influenced at higher AOI values (>60°) by the pyranometer type (Eppley or Kipp & Zonen) probably due to the AOI sensitivity of the calibration factors of the pyranometers above 60°.
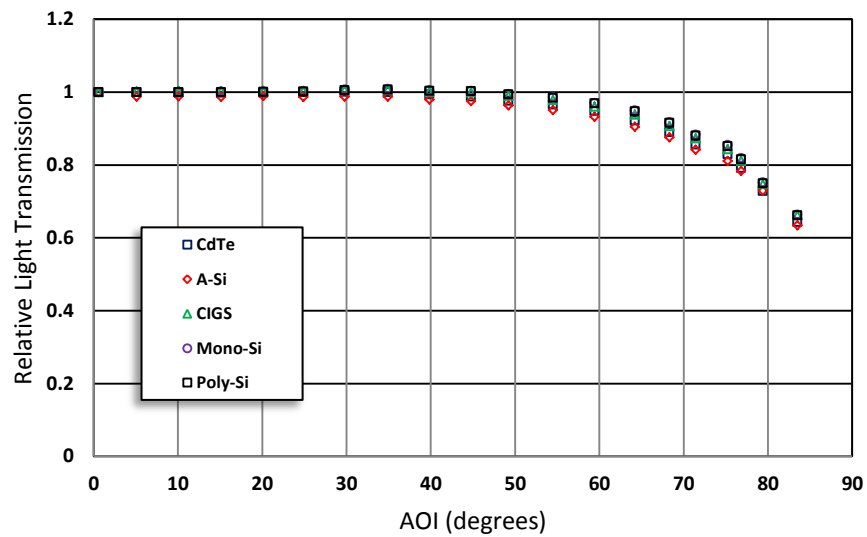
Figure 9.   Relative Isc without diffused component and cosine effects – IEC Method
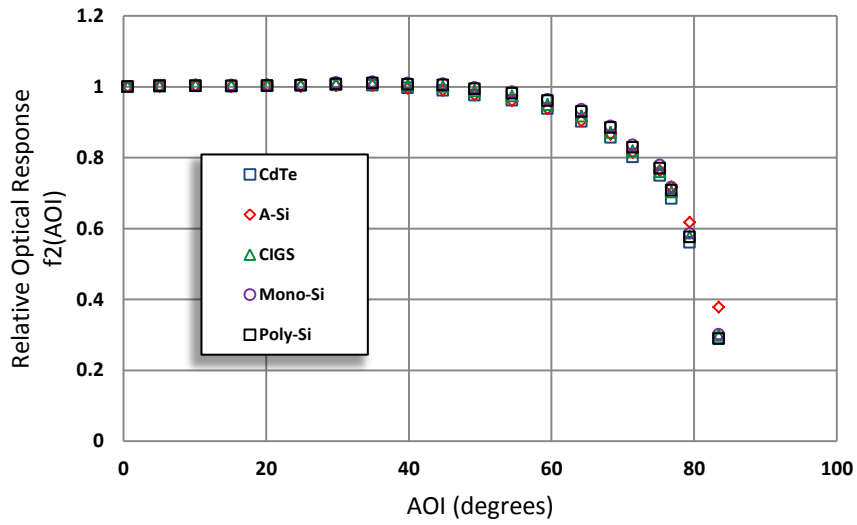
Figure 10.   Relative Isc without diffused component and cosine effects – Sandia method
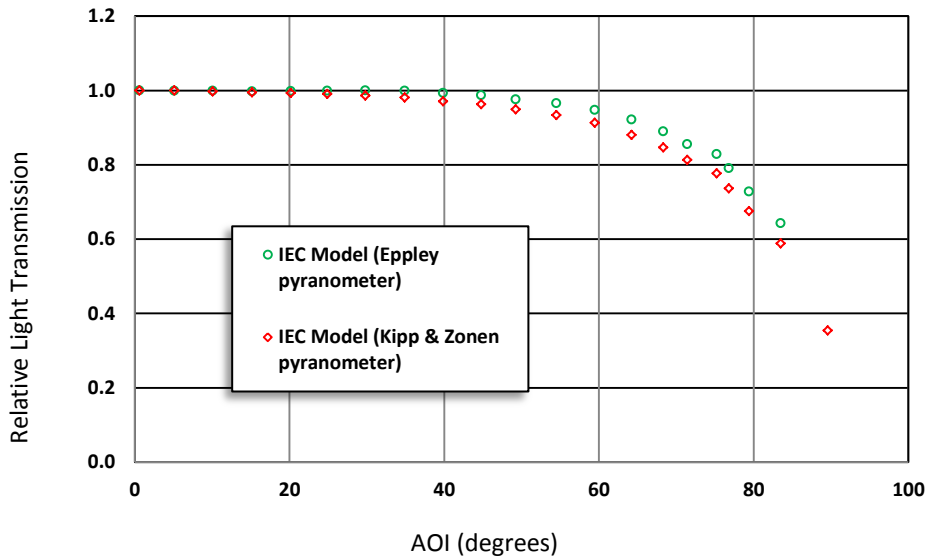
Figure 11.   Comparison between Eppley and Kipp & Zonen pyranometers – CdTe module

Comparison between the models

Based on the $f_2(AOI)$ data obtained for various PV module technologies with glass superstrate, Sandia developed a "generic" polynomial model as shown in (6).

$$f_2(AOI) = 1 - 2.437E\text{-}3(AOI) + 3.103E\text{-}4(AOI)^2 - 1.246E\text{-}5(AOI)^3 + 2.112E\text{-}7(AOI)^4$$

$$- 1.359E\text{-}9(AOI)^5 \qquad (6)$$

The data obtained was compared using the Sandia model and the IEC model for the CdTe module (glass superstrate) with the "generic" polynomial model of Sandia and glass/air AOI model of Martin and Ruiz (Martin & Ruiz, 2005). They all have an excellent match with each other, confirming that the relative optical response of all the glass superstrate modules is almost exclusively dictated by the glass/air interface. The draft standard states: "For modules with a flat uncoated front glass plate made of standard solar glass, the relative light transmission into the module is primarily influenced by the first glass-air interface. In this case, the test does not need to be performed; rather, the data of a flat glass air interface can be used." The experimental and modeled data presented in this report fully validate this statement.
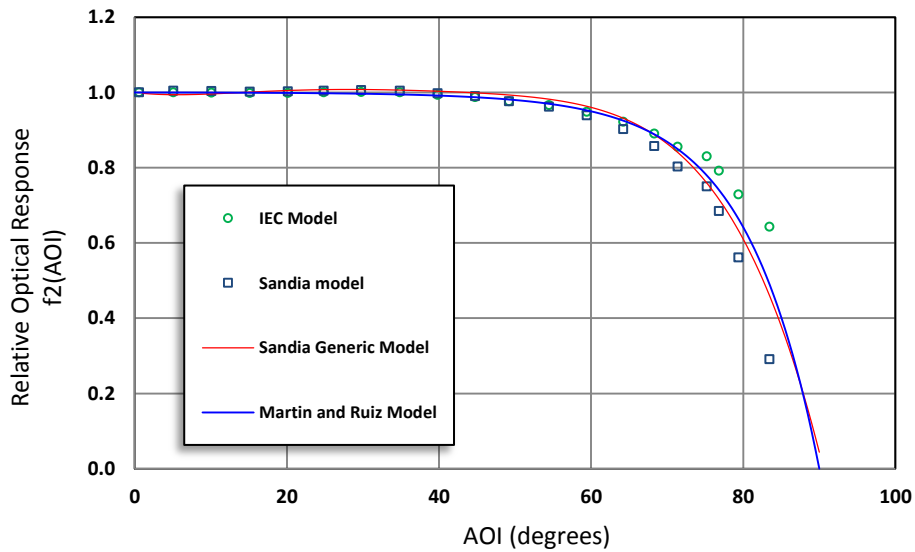
Figure 12.   Comparison between various models developed by different institutions

For a more accurate and repeatable process to test antireflective coated glass or non-planar glass superstrate modules, follow the approach suggested by Sandia National

Laboratories [1]. Since all the models for the flat glass-air interface lead to identical results, the reference module (flat glass with matched cell technology) and test module may be tested side-by-side to quickly identify and eliminate experimental and data processing errors, if any.

Uncertainty Analysis

Great care was taken during the test setup and procedure to ensure accuracy, but minor errors are inevitable. For Equations (4) and (5), each uncertainty contributor was taken into account and the magnitude of the associated uncertainty was assigned based on the calibration report or manufacturer specifications. Table 1 lists the uncertainty contributors and their uncertainties.

Uncertainty Contributor (U_i)	Uncertainty
Isc (U_{Isc})	1.00%
Global Irradiance (U_{epoa})	1.40%
Temperature Coefficient (U_α)	0.01%
Module Temperature (U_t)	0.75%
Direct Irradiance (U_{dni})	1.10%
Angle of Incidence (U_{AOI})	1.00%

Table 1.   Uncertainty of various uncertainty contributors in Equations (3) and (4)

The combined standard uncertainty for $f_2(AOI)$ was quantified by taking the square root of the sum of the squares of the uncertainty estimates multiplied by the squares of their corresponding sensitivity coefficients. The sensitivity coefficients are determined by taking the derivative of the $f_2(AOI)$ equation with respect to the uncertainty contributor.

25

$$u_c = \sqrt{\sum c_i^2 u_i^2} \qquad (7)$$

The resulting uncertainties are presented as error bars in Figure 13 for each module. As calculated from the equation, the combined uncertainty for $f_2(AOI)$ increases with increasing AOI. This can be attributed to a greater dependence on the accuracy of the pyranometer at higher AOI. For this experiment, a single sensitivity/calibration factor for the pyranometers was used for all AOI values. However, as discussed previously, the sensitivity factor is expected to vary slightly with an increase in AOI beyond 60°. Therefore, the accuracy of the pyranometer decreases with increasing AOI and the uncertainty of $f_2(AOI)$ is expected to increase.
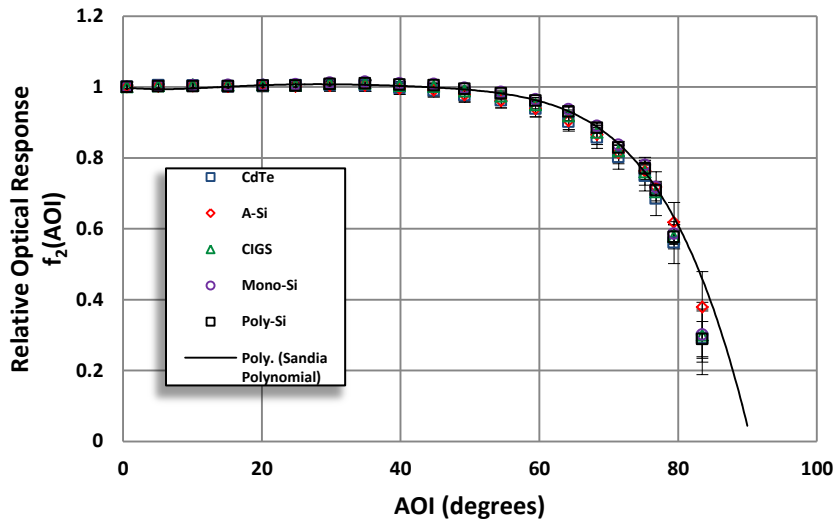
Figure 13. Relative optical response with error bars for all five module technologies

1-5 CONCLUSION

This study related to the testing and validation of the IEC 61853-2 standard procedure for the measurement of incident angle effects on photovoltaic modules was successfully carried out using an outdoor test method for five modules of different technologies. The major conclusions resulting from this project are:

1. The results show nearly identical relative light transmission plots for all the five test modules with glass superstrate irrespective of the type of PV cell technology (mono-Si, poly-Si, a-Si, CdTe or CIGS). This indicates that the reflective losses are governed almost exclusively by the air-glass interface of the PV modules.

2. The relative light transmission plots obtained using the IEC 61853-2 model were in agreement with the plots obtained using the theoretical air-glass interface models and the empirical model developed by Sandia National Laboratories for the glass superstrate PV modules.

3. Obtaining accurate results required careful experimental setup and rigorous test procedures.

4. The standard states that "for the flat glass superstrate modules, the AOI test does not need to be performed; rather, the data of a flat glass air interface can be used." The results obtained in the current study validate this statement.

5. For more accurate and repeatable process to test non-glass or non-planar superstrate modules, the reference module approach suggested by Sandia National Laboratories should be followed. The reference module and test module should be tested side-by-side to quickly identify and eliminate the experimental and data processing issues, if any.

PART 2: NON-INTRUSIVE CELL QUANTUM EFFICIENCY OF PV MODULES

2-1 INTRODUCTION

About Quantum Efficiency Measurements

Quantum efficiency (QE) is defined as the ratio of the number of electron carriers generated by the solar cell to the number of photons of a given wavelength that are incident on the solar cell [4]. QE is a dimensionless ratio and can be directly correlated to the spectral responsivity of a solar cell. The spectral responsivity of a solar cell is measured as the output current over input intensity (A/W) as a function of wavelength. External quantum efficiency is calculated using the intensity of photons incident on the surface of the solar cell and includes optical losses such as transmission and reflection. Correspondingly, internal quantum efficiency is calculated from external quantum efficiency by factoring in the reflection and transmission of the particular device. This paper will focus explicitly on external quantum efficiency.

The two primary ways QE measurements are made in the industry is at the cell level and the module level. At the cell level, individual cells are illuminated with light of a specific wavelength. When measuring the QE of a single-junction cell, the output current is measured by connecting directly to the positive and negative terminals of the device under test. In this way, the cell can be held at short circuit conditions and electrons generated by the light of a specific wavelength are directly collected by the QE system. The test method for measuring QE measurements of single-junction photovoltaic cells is defined by ASTM E1021-12 *Standard Test Method for Spectral Responsivity Measurements of Photovoltaic Devices* [5]. Module level QE measurements illuminate the entire module with light of a certain wavelength using a band-pass filter and white

light source. The short circuit current of the module is measured with respect to the intensity of the incident light. These two quantities are used to calculate the QE at that particular wavelength. The result is an external quantum efficiency measurement for the entire module.

The focus of this report is to accurately measure the QE of a cell within a module using a non-intrusive procedure. The methodology and equipment needed to perform this non-intrusive cell-module QE (C-M-QE) will be explained in detail in this paper. Measuring C-M-QE is an intrinsically more difficult procedure than measuring cell QE (C-QE) or module QE (M-QE). C-M-QE measurements require the use of module bias light, cell bias light, and bias voltage. The cell under test is shaded to function as the current limiting cell. Each of the remaining cells in the module is illuminated with module bias light so they are forward biased. A voltage bias is applied to the module to bring the voltage of the cell under test close to zero voltage. With the device close to short circuit current (zero volts) the quantum efficiency system is able to extract the electrons from the cell under test through the module and thus measure QE. This paper discusses this process in detail and reports the optimal module bias lighting, cell bias lighting and bias voltage that should be applied to the module under test in order to obtain the most accurate results.

However, even when the optimum module bias lighting and voltage bias are applied to the module under test, measurement artifacts can cause a decrease in the module quantum efficiency curve. This decrease is influenced by the series and shunt resistances of the cell under test as well as the component cells connected in series within the module. An absolute module QE measurement could be challenging for modules that

30

have experienced severe degradation via accelerated testing, field degradation, or potentially induced degradation. However, relative QE curves in conjunction with electroluminescence imaging, I-V curves, and dark I-V curves can provide useful information in determining cell failure modes of stressed modules.

Statement of the Problem

The purpose of this thesis is to explain the methodology for obtaining accurate module QE measurement on the module quantum efficiency system at Arizona State University Photovoltaic Reliability Laboratory (ASU-PRL). The testing focuses primarily on commercial size crystalline silicon PV modules. Analysis of module light bias, cell light bias and voltage bias settings and their effects on the quantum efficiency curve were studied and reported. Module QE curves were compared to direct cell QE curves by cutting into a module's backsheet and accessing the cell's positive and negative leads directly. Direct cell measurements (obtained without the need of module light bias and bias voltage) were used to determine the absolute quantum efficiency curve for a specific location on the cell. The methodology used for obtaining direct cell QE measurements is provided by ASTM E1021-12 *Standard Test Method for Spectral Responsivity Measurements of Photovoltaic Devices*. QE curves measured through the module were compared to the direct cell curves and checked for accuracy.

The effects of measuring QE for cells with high and low fill factors (FF) were also investigated. The interconnects of each cell in the module under test were accessed by cutting into the backsheet and encapsulant. The installation of soldering ribbons to the positive and negative ends of each cell allowed the QE system to test any number of cells

31

within the module. Systematically increasing the number of cells connected in series allowed the cell under test to be measured under a variety of voltage bias conditions in order to further understand the effect of applying bias voltage. For cells measured at the module level that showed a low quantum efficiency curve compared to the direct quantum efficiency curve, an explanation for the loss is provided by correlating the results with light I-V, dark I-V, and electroluminescent imaging.

It is important to understand that for this study, the module under test was affected by cutting into the backsheet to access individual cells. This is an intrusive test that would not be performed if the module was intended to undergo further rounds of characterization, field aging, or accelerated stress testing. However, the focus of this study is to determine and demonstrate the accuracy of cell-module QE by comparing with cell QE. Therefore, an intrusive test was also performed to compare QE curves at the module level with QE curves at the cell level. The relationship between cell level QE measurements and module level QE measurements will be discussed in detail in the results of this paper. Once this relationship is understood, future cell measurements will be performed at the module level and intrusive testing will not be necessary.

2-2 LITERATURE REVIEW

Quantum Efficiency Measurements for Single-junction PV Cells

In order to interpret the results for QE measurements for a cell within a module, a thorough understanding of QE measurements for single-junction PV devices is necessary. For this thesis report, the American Society for Testing and Materials (ASTM) Designation: E1021-12 Standard *Test Method for Spectral Responsivity Measurements of Photovoltaic Devices* was used to ensure that direct cell measurements (obtained by cutting into the backsheet and connecting directly to the cell under test) are obtained according to the standard. This section delineates the test methods outlined by ASTM E1021-12 and compares them to the equipment and measurement techniques for the module quantum efficiency system at ASU-PRL. The basic diagram of the optical components required for quantum efficiency measurements is given in Figure 14. Each component of the optical setup is discussed in this section.
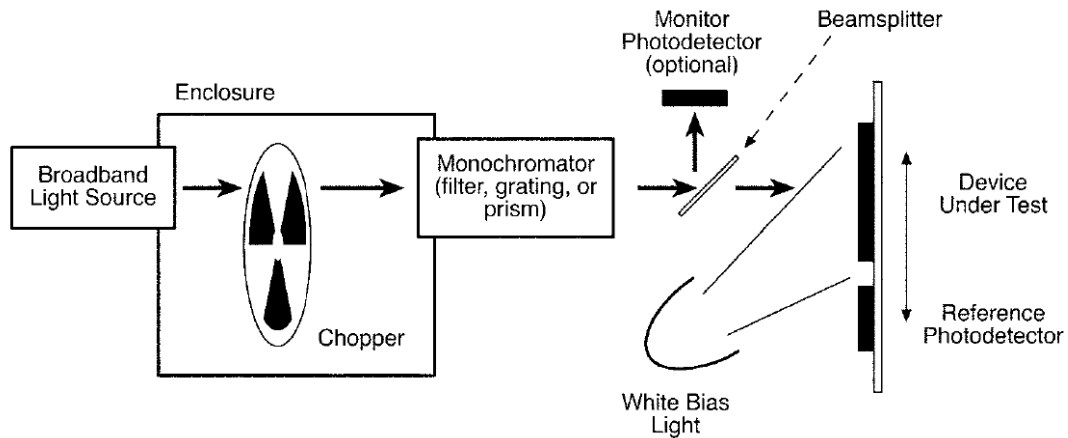

Figure 14.   Diagram of basic optical components necessary for QE measurement [5]

Broadband Light Source: The broadband light source provides the initial polychromatic light that will be incident on the monochromator. The ASU-PRL Cell-Module Quantum Efficiency (C-M-QE) system uses a xenon arc lamp for the broadband light source. An ellipsoidal reflector collects light from the xenon arc lamp and concentrates it on the monochromator. To maximize the intensity of broadband light incident on the monochromator, adjustments to the ellipsoidal reflector can be made via three set screws on the back of the device. Simultaneously adjusting the reflector screws and monitoring the output intensity measured by the reference photodiode ensured that the maximum intensity was incident on the monochromator.

Chopper: Before the light from the xenon arc lamp is focused on the monochromator, it passes through a mechanical chopper mechanism. The chopper is a rotating disk with slits for light to pass through. The chopper modulates the light source at a specific frequency in order to provide a reference signal to the signal processor. The frequency range for the C-M-QE system is 4 Hz to 200 Hz. The reason that the light must be chopped at a certain frequency is that the monochromatic beam itself might not have enough intensity for the device under test to respond. Just shining a weak monochromatic light source on the module might not induce enough output current to be accurately measured apart for the inherent noise of the system. Therefore, the monochromatic light is chopped at a known frequency that can be identified by the signal processor.

ASTM E1021-12 delineates that 'the chopper blades should be designed to minimize stray light. To minimize modulation of room light or bias light, the chopper should be configured to be close to the monochromatic light source [5].' The C-M-QE system incorporates all the optical components of the machine in an enclosed case that uses black

plastic to block out ambient room light. The chopper is mounted directly in between the xenon arc lamp broadband light source and the monochromator. A baffle between the xenon arc lamp ant the chopper serves to block light that is reflected off the chopper blades from reaching the test device. The chopper is also mounted as close as possible to the monochromatic light source and therefore complies with the standard.

Monochromator and filter wheel: The monochromator separates the broadband light source into individual wavelengths by using dual-grating diffraction. The filter wheel positions a filter to attenuate stray light and pass the monochromatic light through to the device under test. The monochromatic light generated with the C-M-QE is approximately 4 nm full width half maximum (FWHM). The associated wavelength uncertainty is +/- 2 nm.

ASTM E1021-12 states that "the monochromatic light source shall be capable of providing wavelengths that extend beyond the response range of the device to be tested [5]". The C-M-QE system has a wavelength range of 300 nm to 1400 nm. For crystalline silicon modules, the response is measured from 300 nm to 1100 nm. The standard also states "a minimum of 12 wavelengths within the spectral response range of the device to be measured is recommended. All increments between wavelengths should be less than 50 nm [5]". The QE curves collected for this experiment were measured at 10 nm intervals and collected a total of 81 data points within the 300 nm to 1100 nm range.

Monitor photodetector, beamsplitter, and associated optics: The C-M-QE system uses a photodiode as the monitor photodetector. A beam splitter directs a portion of the monochromatic light to the monitor photodiode. The signal generated by the monitor cell is amplified and provided to the digital signal processing equipment. Associated optics

35

then direct the monochromatic beam and focus it on the device under test. ASTM E1021-12 delineates "the monitor photodetector can be a pyroelectric radiometer, a photodiode, or a solar cell [5]".

One unique aspect of the C-M-QE system is that it is designed to measure commercially available modules. Since the average size of a PV module is 1m x 1.9m, it was necessary to design the system so the module would remain on a stationary test fixture while the associated optical components are moveable to scan different locations on the module. Therefore, the optical components of the device are mounted in a moveable compartment that is covered with light-blocking plastic to prevent ambient light from interfering. The optical components move to the selected location via a set of x-y positioning motors that are controlled by the QE software.

Cell bias light: A continuous cell bias light (also referred to as dc white light beam) is used to illuminate the device under test simultaneously with the chopped monochromatic light source. The biased light serves to amplify the dc current output and increase the photoconductivity of the photovoltaic device under test. Therefore, the PV device sees both chopped monochromatic light and white bias light. ASTM E1021-12 states, "the bias light should be of sufficient intensity to ensure the device under test is operating in its linear response region [5]".

Lockin a mplifier and signal processing equipment: The purpose of the Lockin amplifier is to accurately separate the current generated from the chopped monochromatic light from the white bias light. The frequency of light modulation dictated by the chopper is fed into the signal processing equipment. The signal processor then detects the signal that has a specific phase relationship with the chopper's reference

36

signal. The signal generated by the monitor photodiode is also fed into the signal processing equipment to monitor the incident external light on the test device. The signal processing equipment is then able to quantify the alternating current producted by the device under test and generate the corresponding QE curve.

Quantum Efficiency Measurements for Modules

Module QE (or spectral responsivity) measurements are performed by illuminating the entire module with light of a selected wavelength. Band pass filters are commonly used to block out unwanted wavelengths. The module is then illuminated only by the wavelength range allowed to pass through the selected filter. Once the entire module is illuminated, the bias voltage is set to keep the module at zero volts [6]. The resulting QE measurement obtained is for the entire module, not individual cells. However, the problem with this method is that different cells may be current limiting at different wavelengths, and the bias point of the current-limiting cell whose QE is being measured is not at zero volts [6].

Quantum Efficiency in Multi-junction Cells

A multi-junction cell is a device that consists of more than one photovoltaic junction stacked on top of each other and electrically connected in series. The individual photovoltaic junctions are referred to as component cells. Since a multi-junction cell consists of multiple component cells in series, measuring the quantum efficiency of the device cannot be achieved using the same procedure as single junction cells. When

connected to a single-junction cell, quantum efficiency measurements can be achieved by directly measuring the current extracted at the pn (positive-negative) junction by the monochromatic light for the cell under test. However, when measuring multi-junction cells, if only monochromatic light is incident on the component cells it will be absorbed by one junction while the other two junctions remain in the dark. The current from PV cells in series is dictated by the current-limiting cells (in this case, the cells left in the dark). Therefore, the output photocurrent will not represent the current of the junction under test. To resolve this issue, light bias and voltage bias must be applied to the junction under test.
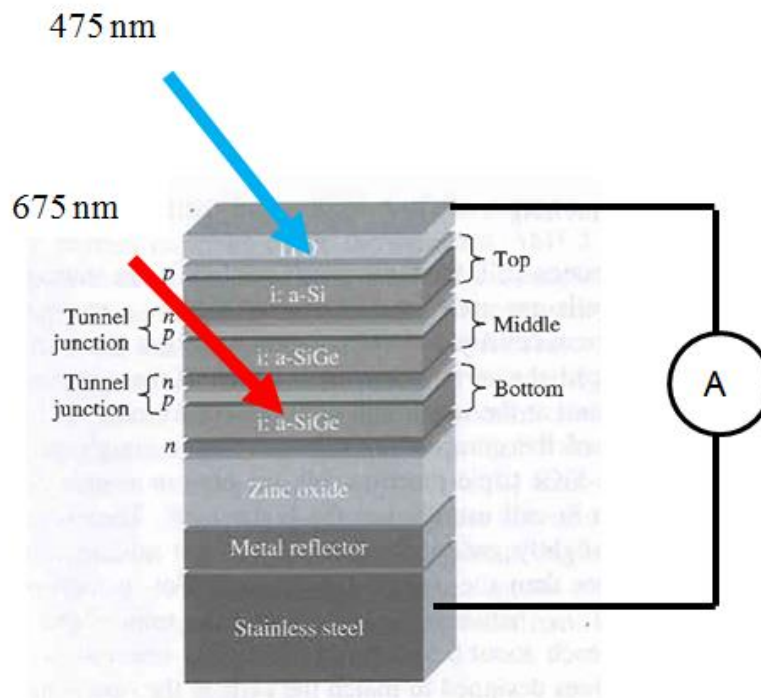

Figure 15.   Structure of a triple-junction nip substrate type solar cell [7] source: Handbook of Photovoltaic Science and Engineering

In Figure 15, a blue light bias of around 475 nm is applied to the top cell corresponding with its band gap. A red light bias of around 675 nm is applied to the bottom component cell. This light bias illuminates the top and bottom component cell essentially leaving the middle component cell in the dark. The component cell with the lowest current will dictate the overall current flow out of the cell. Since the middle component cell is now the current-limiting cell, any current out of the cell from the monochromatic light is generated by the middle component cell. To quantify the current generated by the monochromatic light, the light is modulated by applying an optical chopper at a specific frequency. A lock-in amplifier then detects this frequency of current and separates it from the base current generated to give just the current generated from the middle component cell.

A voltage bias must also be applied to the component cell under test in order to control its operating point. When the component cell under test is kept in the dark but connected to other component cells which are generating current, the component cell under test is under reverse bias conditions. The voltage of this reverse biased component cell will be equal and opposite to the sum of the Voc for the other two component cells. If the FF of the component cell is high, then the resulting QE curve of the reverse biased cell is very close to the QE under short circuit conditions [7]. Therefore, if the fill factor

(FF) for all cells is high, the cell under test operates close to short circuit conditions and an applied voltage bias will have minimal effect on the QE. However, when shunted cells resulting in a low FF are measured in series with the component cell under test, the resulting QE curve is lower than its true value. Therefore, a voltage biased must be externally applied to cancel the voltage of the other two cells and shift the component cell under test to short circuit conditions.

ASTM E2236-10 *Standard Test Methods for Measurement of Electrical Performance and Spectral Response of Nonconcentrator Multijunction Photovoltaic Cells and Modules* defines the methodology for measuring spectral responsivity (quantum efficiency) for multi-junction photovoltaic modules. The scope of this test method provides special techniques needed to determine the electrical performance and spectral response of two-terminal, multijunction PV devices, both cell and module. In a series-connected multijunction PV device, the incident total spectral irradiance determines which component cell will generate the smallest photocurrent and thus limits the current through the entire series-connected device. Light-biasing and voltage-biasing techniques of each component cell are necessary to successfully measure the spectral response of the device under test [7]. This section will summarize the contents of this standard that are relevant to the overall goal of measuring quantum efficiency of a single-junction module.

Spectrally adjustable solar simulator - A spectrally adjustable solar simulator which has the additional capability of allowing different wavelength regions of its spectral irradiance to be independently adjusted is to be used. Ideally, the adjustable wavelength

ranges of the spectrally adjustable solar simulator should correspond to the spectral response ranges of each component cell in the multi-junction device to be tested. The cell-module quantum efficiency system at Arizona State University Photovoltaic Reliability Laboratory (ASU-PRL) has the capability to supply spectrally adjustable monochromatic light with a bandwidth of no more than five nanometers. The wavelength range of the MQES is from 300 to 1400 nm which allows for adjustable wavelength ranges corresponding to the spectral response ranges of the test device.

Reference Cells – Photovoltaic reference cells are used are used to measure source irradiance in the wavelength regions that correspond to each component cell in the multijunction device to be tested. For best results, the spectral responses of the reference cells should be similar to the spectral responses of the corresponding component cells. The C-M-QE has two calibrated photodiode reference cells: mono-crystalline silicon and Germanium. For this experiment, the mono-crystalline reference cell was used to calibrate the equipment before each test was made.

Module Bias Light Source – A dc bias light that is equipped with appropriate spectral filters to block wavelength regions corresponding to the expected spectral response range of the individual component cell being tested is to be used. The bias light source of the C-M-QE system consists of 150 electrically isolated Indus Star^{TM} high-power LED light modules. Each light module is arranged in a tri-emitter configuration with an aluminum heat sink mounted to the back. Each light module emits a 6500K white light capable of supplying 0.17 suns at 100% intensity. This experiment will deal with single-junction crystalline silicon modules. Therefore, the bias light source corresponds to the expected spectral response range of the individual component cells being tested.
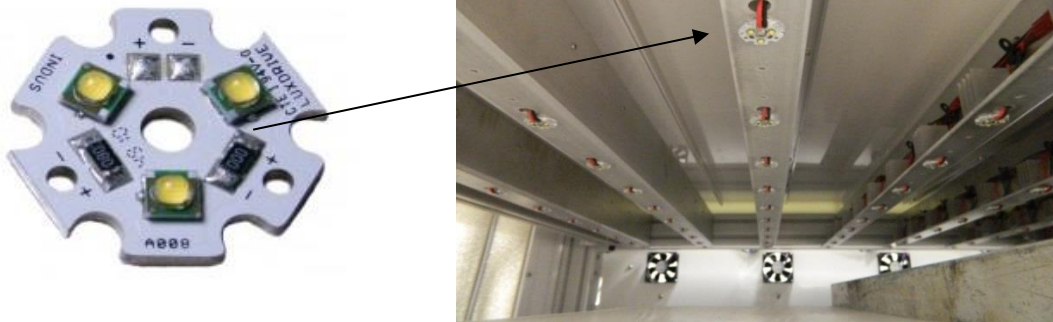
41

Figure 16   Indus StarTM high-power LED light modules mounted to the MQES

Bias Voltage Source − A variable dc power supply capable of providing a voltage equal to the open-circuit voltage of the multijunction device to be tested is to be used. The C-M-QE system was designed to measure quantum efficiency of standard sized modules and was equipped with a variable dc power supply capable of providing a voltage up to +40VDC and -10VDC.

Cell-Module QE Measurements

Both cell QE measurements and module QE measurements are extremely useful data for characterizing solar cells and modules. However, measuring the QE of a specific location of a cell within a module using a non-intrusive measurement procedure is an extremely valuable characterization technique for reliability testing. Understanding single-junction cell, multi-junction cell, and module level QE measurement techniques lends insight to the methodology and equipment necessary to perform C-M-QE measurement. However, there are some significant differences present when extracting the current from a single cell that is connected in series with multiple cells in a

42

commercial module. This section will outline the methodology for obtaining cell-module quantum efficiency curves.

The basic approach to measuring C-M-QE is similar to the methodology for measuring multi-junction cells. First, the cell under test must be forced to be the current limiting cell so that the current output of the module is dictated by the current passing through the test cell. For C-M-QE measurements, this can be achieved by partially shading the cell under test with a light blocking cover. The next step is to apply dc cell bias lighting to the portion of the cell that is to be measured. An AC monochromatic light generated using the same techniques specified by ASTM E1021-12 is also incident on the portion of the cell in addition to bias light. Next, the cells connected in series with the cell under test (the remaining cells in the module) must be illuminated so they are forward biased. This is achieved through the use of module bias light. Once the bias lighting is applied, the cell under test is reversed biased with a voltage equal to the summation of the open circuit voltage of all the other cells in the module. A voltage bias is applied to bring the cell under test close to zero volts. For devices with component cells that contribute similar voltages, the bias voltage is calculated according to (8).

$$V_b = \frac{n-1}{n} V_{OC} \qquad (8)$$

The current of the cell under test is then measured when the cell is operating near short circuit current (zero volts). A lockin amplifier isolates the current generated by the monochromatic light based on the chopping frequency. The C-M-QE system also monitors the intensity of the monochromatic light using a monitor photodiode. Calculating the output current (A) and the input intensity (W) for a specific wavelength will yield the absolute power spectral responsivity of the device. The absolute spectral

43

responsivity may also be converted to external quantum efficiency, with the dimensionless units of collected electrons per incident photon, using (9).

$$QE(\lambda) = \frac{hc}{q}\frac{R_{pa}(\lambda)}{\lambda} \qquad (9)$$

The QE is then reported and plotted as a function of wavelength from 300nm to 1100nm in 10nm increments.

Cell-Module QE Measurements Artifacts

Appling voltage bias, module light bias, and cell bias makes it possible to measure absolute quantum efficiency of a specific location on a cell within a module by connecting to the external leads of the module. However, even after optimizing all the input parameters some cases exist where an absolute QE measurement is not obtainable due to sever degradation. To further explain these measurement artifacts, consider the case of three cells connected in series where two cells have high FF and one cell is shunted (resulting in a lower FF) as shown in Figure 17.
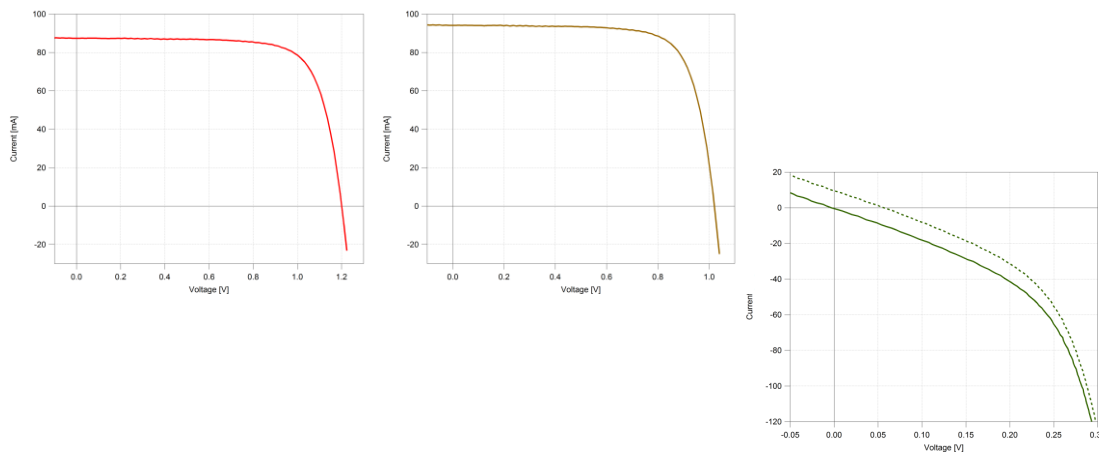

Figure 17.   I-V curves of three cells where cells 1 and 2 have high FF and cell 3 is shunted (has a lower FF); cell 3 is shifted down to show that it is in the dark

A QE measurement is to be obtained for the shunted cell. The two high FF cells will be illuminated with a bias light so that they are operating in forward bias. Meanwhile, the shunted cell is kept in the dark and therefore its corresponding I-V curve is shifted down, where I_{sc} is zero. When the monochromatic light is shined on the dark cell, the I-V curve is shifted slightly upwards and the I_{sc} value is increased to 10 mA (shown as the dotted line in cell three).

If measured as an individual solar cell, the QE system would hold the voltage at zero and measure a current of 10 mA which is the true current extracted from the cell as a result of the monochromatic light. However, the cell cannot be measured as an individual cell and must be measured in series with cells 1 and 2. When the QE system is connected to the three cells in series, the current passing through the lowest cell will dictate the current through cells 1 and 2. Therefore, the operating point on all cells will be at 10 mA as shown in Figure 18.
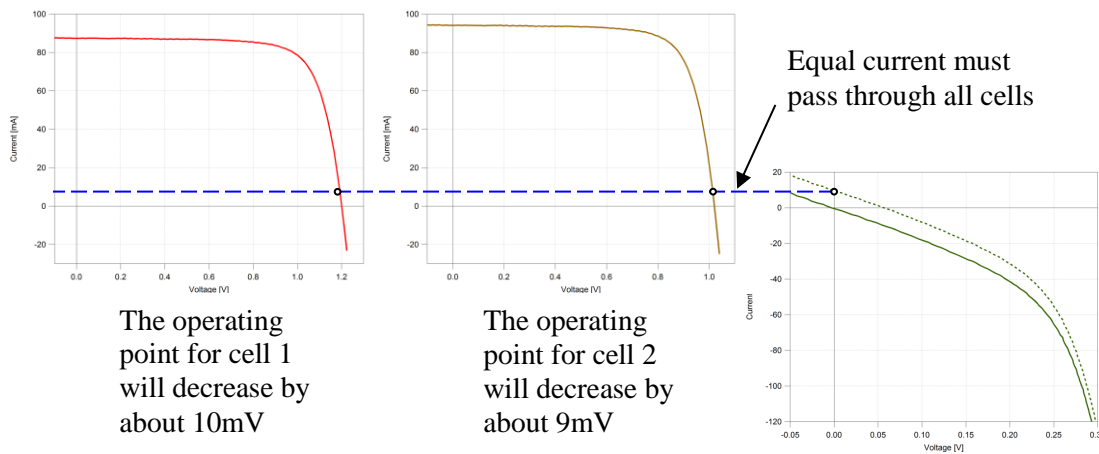

Figure 18.   Operating points for the three cells connected in series and their corresponding voltage shifts

Since cells 1 and 2 are now passing 10mA, their voltage will decrease by an amount corresponding to the slope of the I-V curve near Voc (for this example 10mV for cell 1 and 9mV for cell 2). The voltage of cell 3 must be equal and opposite to the sum of the Voc for cell 1 and 2. Therefore, the voltage of cell 3 will increase by 19mV. This shift in voltage for cell 3 will cause a drop in current proportional to the slope of the I-V curve near Isc as shown in Figure 19.
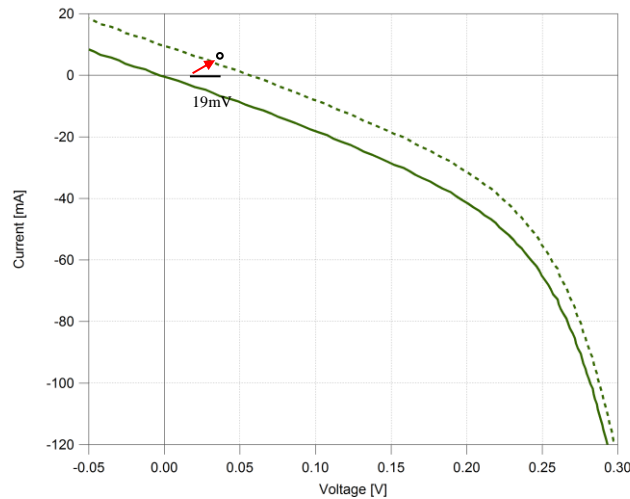

Figure 19.   The voltage increase of cell 3 and the corresponding shift in the operating point resulting in lower current

Since cell 3 is shunted, a 19mV increase in voltage causes a significant drop in the current. In this example, the current decreases from 10mA to 7mA. Since the actual current is near 7mA instead of 10mA, the actual voltage shift due to cells 1 and 2 is smaller (around 14mV in this example). Since the current is decreased in cell 3, the QE curve will be affected. The expected results for the QE curve of a cell in this example would be about 7mA/10mA or about 0.7 times what it would be if measured individually.

2-3 METHODOLOGY

Measuring Direct Cell QE for Nine Isolated Cells

The Arizona State University Photovoltaic Reliability Laboratory (ASU-PRL) Cell-Module Quantum Efficiency (C-M-QE) system is novel equipment that measures the QE of a specific point on a cell *within* a module non-intrusively. The hardware and software of the C-M-QE was developed by PV Measurements and is shown in Figure 20. The C-M-QE system measures external quantum efficiency of a cell within a module without having to cut into the backsheet to access the cell directly. This offers several advantages for PV module characterization and reliability testing. Although it is not necessary to cut into the backsheet to access individual cells for normal module QE measurements, this test is concerned with determining the accuracy between direct cell measurements and cell-module QE measurements. To understand this relation, individual cells within the module were accessed by cutting into the backsheet and soldering an interconnect ribbon to the positive and negative terminals. This section will focus on using the MQES to obtain direct QE cell measurements for an isolated portion of a module. These direct QE measurements will be compared to cell I-V curves and electroluminescent images for each cell within the isolated section.

Figure 20.   The Arizona State University Photovoltaic Reliability Laboratory Cell-Module Quantum Efficiency (C-M-QE) System

The module selected for this test was a 220W mono-crystalline silicon PV module (specifications given in Table 2). This module had previously undergone accelerated PID (potential induced degradation) stress testing in an environmental chamber at 85°C dry heat and was given a module code of Manufacturer 6 DH1. The history of this module was that it underwent PID stress testing at -400V for 35 hours under disrupted surface conductivity (a carbon paste applied to the front surface of the module except around the edges). The module did not show significant signs of degradation and the power after stress testing was at 96.9% of the original power output of the module. This module was selected for QE tests because the electroluminescence image showed that most cells within the module where in relatively good condition. However, cells 1 and 2 in the corner of the module showed significant signs of degradation/shunting as shown by the dark portions in Figure 21. This provided the ideal case study because healthy cells

within the module could be measured and compared to cells that showed signs of degradation.

To determine the health of each cell in the module, an electroluminescence image was collected. The EL image is shown in Figure 21. The target cells are identified as cells 1 to 9 on the lower side of the module. These cells were selected because cells 9 to 3 are in relatively good condition and show strong electroluminescence characteristics. Cells 1 and 2 are in poor condition relative to the other cells in the string. Therefore, this PV module fits the initial criteria and was selected for further testing.

PV Module Specifications	
Type	Mono-crystalline
Cells	60
Pmax	220W
Voc	35.4V
Isc	8.36A

Table 2.   Specifications for the PV module selected for QE measurements
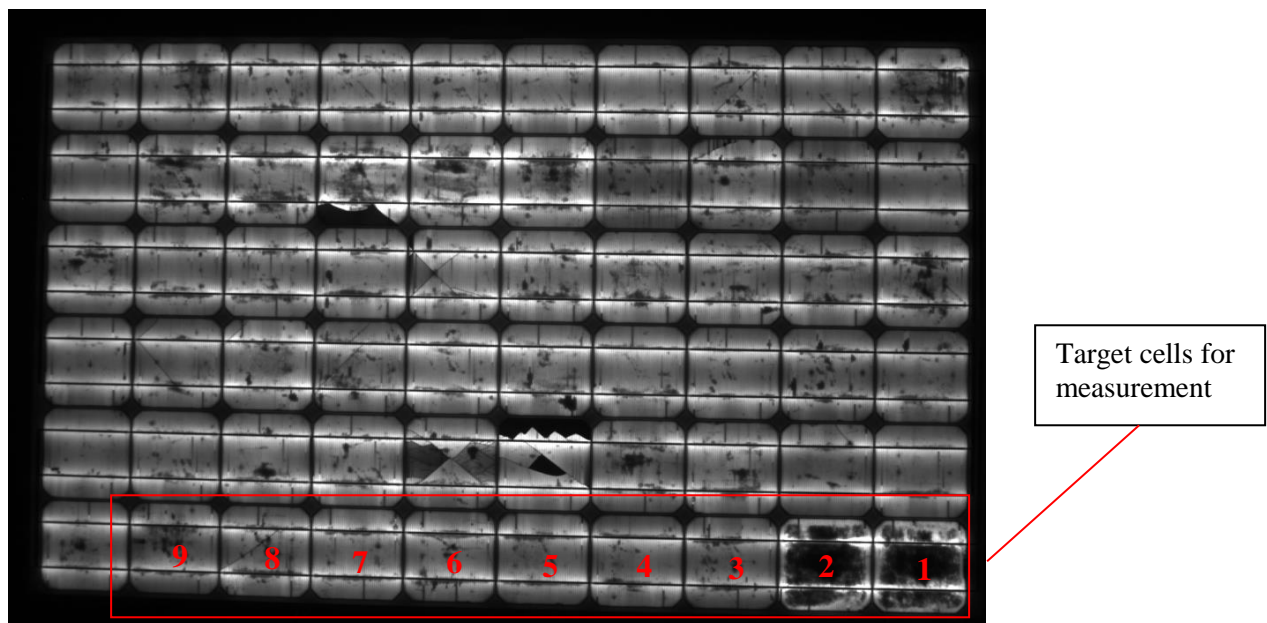

Figure 21.   Electroluminescence image of PV module showing healthy cells (white) and dead cells (black)

To obtain a more accurate measurement of the condition for each individual cell in the target string, individual cell I-V curves were measured. To measure the I-V characteristics of individual cells in a string, it was necessary to cut the backsheet of the module to access the interconnect ribbons between each cell. The backsheet and EVA encapsulant was carefully peeled away using a sharp precision razor blade. Once the interconnect ribbons between the cells where exposed, they were scrapped clean of EVA with the blade. Two inch lengths of new ribbon where then soldered onto the exposed ribbon interconnecting the cells. This new ribbon now serves as an open circuited contact point to access individual cells for measurements. To anchor the ribbon securely and ensure that it would not be pulled out when making connections, a piece of thermal tape was adhered to the backsheet and part of the ribbon. The thermal tape also served to protect open area of the cell to ensure that no moisture or dirt could penetrate. An image of the module with the ribbons connected is given in Figure 22.
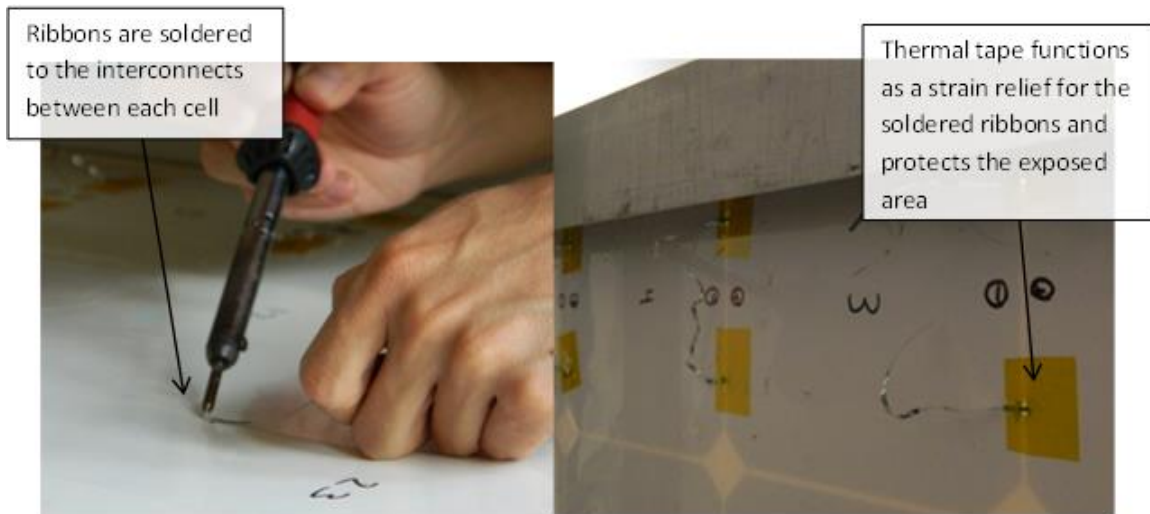

Figure 22.   The PV module with ribbons soldered to the cell interconnects

The methodology for measuring QE of a single-junction cell is outlined by ASTM E1021-12 and was followed closely in this section for measuring direct cell QE. The leads of the C-M-QE system were connected directly to the cell under test. DC cell bias light and AC monochromatic light were shined on a specific location on the cell. For this module, the response as a function of bias light intensity was linear. Therefore, the QE curve did not change with increasing bias light intensity (results shown in appendix A). No module bias light was needed because the connections were made directly to the cell under test. No bias voltage was needed because the C-M-QE system holds the cell at short circuit current throughout the measurement. Since no other forward biased cells were connected in series, the cell under test was not reverse biased and the current could be measured directly. A diagram of the connections and input parameters is given in Figure 23.
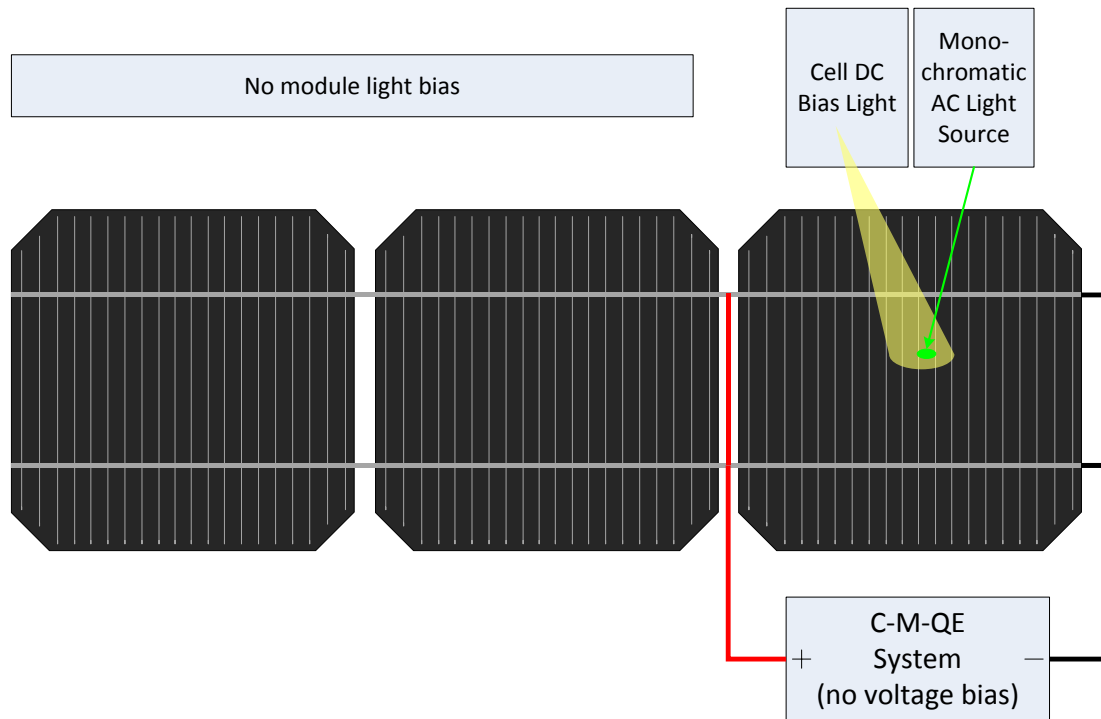

Figure 23.   Diagram of connections and equipment setup for direct QE cell measurement

Measuring Cell QE through Multiple Cells

This section explains the methodology used to measure QE for a specific location on one cell when that cell is connected to multiple other cells in series. Direct cell QE was obtained for the previous section by connecting the leads of the C-M-QE system straight to the cell under test. No module bias light or bias voltage was required. For this test, the current output of the cell under test was measured by connecting the C-M-QE leads to the positive and negative leads of a string of multiple cells connected in series. The negative terminal of the MQE system will remain anchored to the negative of the cell under test. The number of cells in the series connected circuit will be given by n. For direct cell QE measurements n = 1. This section explains the methodology for measuring QE through multiple cells up to n = 22. A diagram of the connections and equipment setup for the multiple cell QE measurement for n = 2 is given in Figure 24.
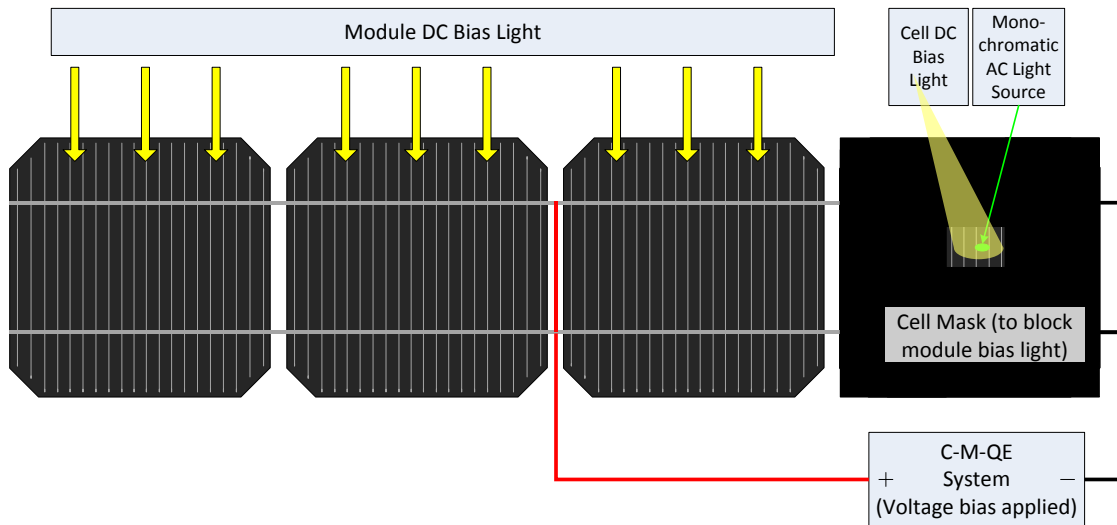

Figure 24.　　Diagram for connections of multiple cell QE for two cells (n = 2)

The methodology for measuring QE for multiple cells is discussed in this section. To make the cell under test the current limiting cell, a black vinyl mask was taped to the surface of the cell under test. The purpose of the mask is to block ambient light from the module bias lights from shining on the cell under test. A 2 cm x 4 cm opening was cut out of the vinyl material to allow the cell dc bias light and monochromatic ac light to shine on the cell. To further ensure that ambient light does not enter the rectangular opening, the C-M-QE system has a shroud that lowers when the system is collecting data. Figure 25 shows an example of a cell under test with the vinyl mask covering the cell. This image was taken with the shroud in the 'up' position and it cannot be seen in the photo. The 0.4 x 0.6 cm monochromatic light with frequency of 530 nm (green light) is seen in the center of the rectangular opening.
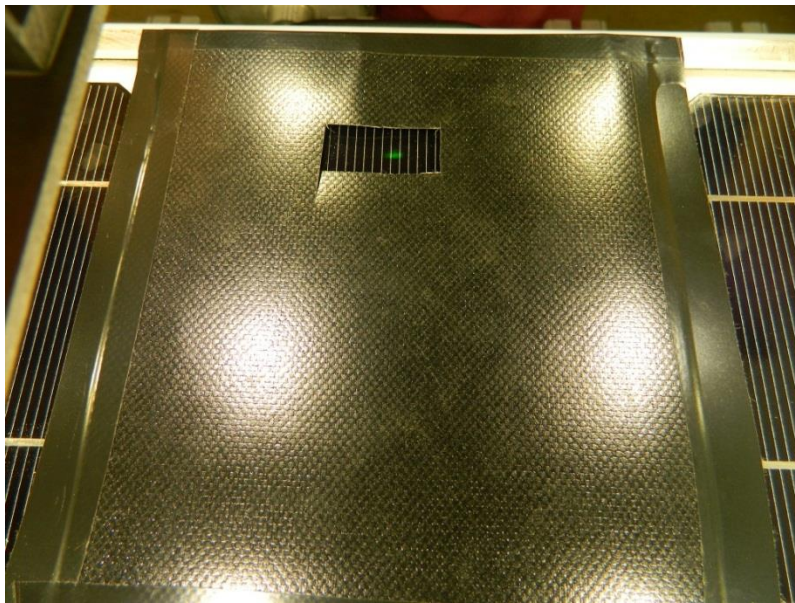

Figure 25.   Cell 9 covered with vinyl material where the green dot in the center of the rectangular opening is the 530 nm monochromatic light. The white lights gleaming off the vinyl surface are due to the module bias lights that were set to 25% intensity

Once the cell under test has been covered to make it the current limiting cell, the C-M-QE system leads are connected to the desired string of cells. For this example, n = 2 and the leads are connected to the negative ribbons of the cell under test and the positive ribbons of the second cell in series.

Module bias light is applied via manual controls in the C-M-QE system software. Bias light is applied to make the component cells in the string forward bias. When the component cells are forward bias, the cell under test becomes negatively biased with the voltage proportional to the sum of the Voc of the cells connected in series. Therefore, a positive voltage bias must be applied to bring the cell under test close to zero volts. The amount of voltage bias to be supplied is given by Equation (8). In this example, the Voc of each cell is 0.6 and there are two cells in the string (n=2). Using Equation (8), the voltage bias applied therefore becomes:

$$V_b = \frac{n-1}{n}V_{OC} = \frac{2-1}{2}(1.2V) = \mathbf{0.6V}$$

It is important to note that Voc in this equation is the open circuit voltage of the series connected string of cells (in this case Voc for two cells). Testing conditions are not performed at the standard testing conditions specified by the module manufacturer data. The temperature of the module during the measurement will affect the Voc in Equation (8) and thus affect the amount of bias voltage applied to the circuit. Therefore, the Voc must be measured at the time of test then used in the Equation (8). After the module bias light and bias voltage is applied, the QE measurement can be collected.

Measuring Cell-Module Quantum Efficiency (C-M-QE)

The same methodology for measuring multiple cells in series is applied when measuring the QE of a cell within a module. The cell under test is masked in the same way as the previous section. Module light bias is applied to illuminate the component cells in the module. Voltage bias is then applied to bring the cell under test to zero volts. The main difference in cell-module level measurements is that now the C-M-QE system leads are attached to the external module leads. Figure 26 gives the connection diagram for the 60 cell monocrystalline module used in this study.
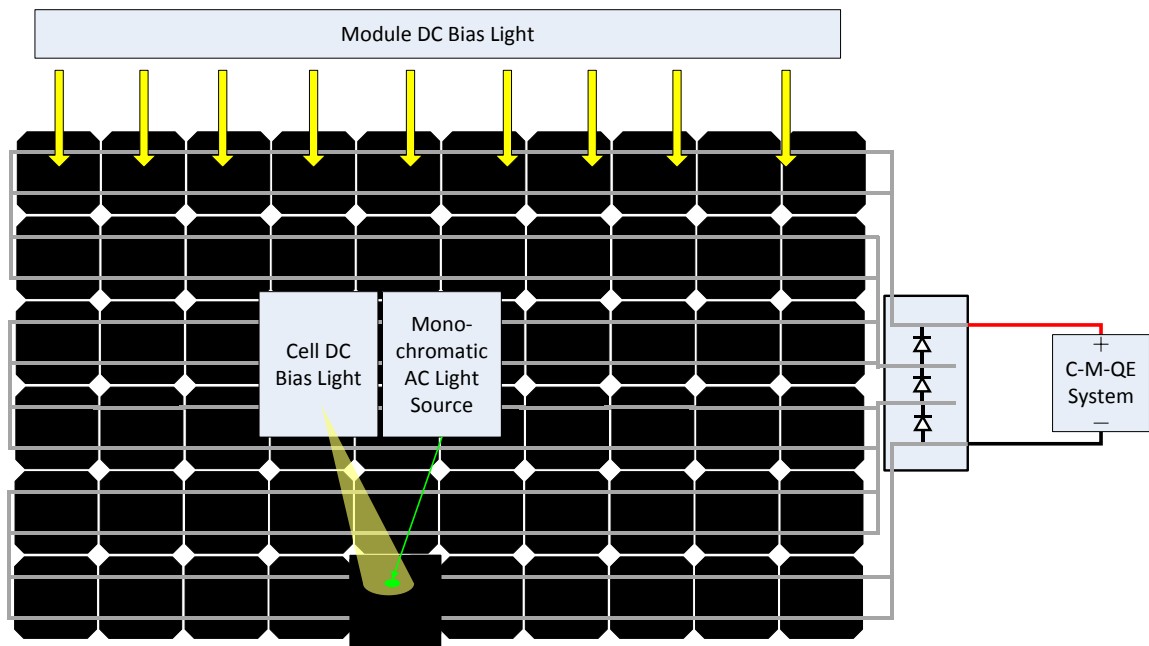

Figure 26.   Diagram for the connections and setup of C-M-QE measurements where the junction box is enlarged to show the bypass diodes

One concern when connecting to the external leads of the module is that if the bypass diodes are activated, the signal will be lost. The bypass diode is connected in parallel with a string of series connected cells but with opposite polarity. If the string is operating

55

in forward biased, the bypass diode is in reverse bias and will effectively be an open circuit. There are three bypass diodes in the module used for this test. Therefore, one bypass diode is connected in parallel with 20 series connected cells. If one or more cells is reversed biased due to shading or mismatched current, the bypass diode will activate allowing the current from the good strings to flow in the external circuit. This will prevent reverse biased cells from hot-spot heating which may lead to severe problems within the cell and module.

To ensure that the bypass diodes did not affect C-M-QE measurements, the leads of the QE system were connected to the external module leads and the internal module ribbons (Figure 27). For both cases, a voltage bias was applied according to Equation (2). Connecting to the internal module ribbons effectively circumvents the bypass diodes to ensure that they do not affect the measurement. The C-M-QE measurements for both cases were compared and it was shown that bypass diodes did not affect the QE measurement.
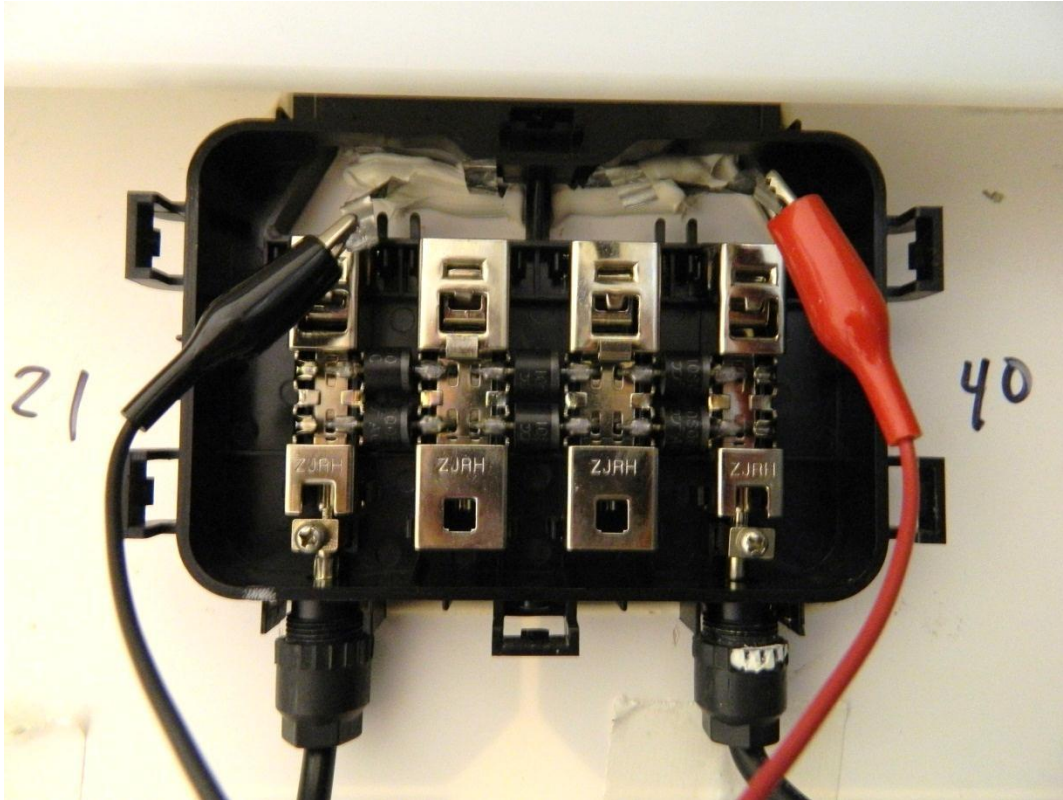
Figure 27.   C-M-QE leads connected to ribbons directly from cells and successfully circumventing the bypass diodes.

The three main adjustable parameters when measuring C-M-QE are: module light bias, cell light bias, and voltage bias. The goal is to adjust these input parameters so that the C-M-QE curve is equal to the direct cell QE curve. This report will present results for C-M-QE curves measured for various input parameter conditions. The C-M-QE curves with various module light bias, cell light bias, and voltage bias inputs will be compared to direct cell QE curves to determine the influence of each parameter.

2-4 RESULTS AND DISCUSSION

Direct Cell Results

To fully understand the results of C-M-QE measurements, data from three different characterization tests was used: I-V, EL, and Dark IV. The results for light I-V curves of cells 1 to 9 are given in Figure 28. To obtain these I-V curves, the terminal leads of the I-V curve tracer where connected directly to the ribbons soldered to the interconnects of the cells. A class A solar simulator was used to illuminate the cell under test at 1,000 W/m^2. The simulator was calibrated for uniformity to within +/-2% before the I-V curves were measured to ensure a uniform distribution of intensity was incident on the cell under test. The I-V curves are plotted on one graph and shown in Figure 28. Table 3 provides the specification for each cell and Figure 29 provides the EL image for cells 1 to 9.
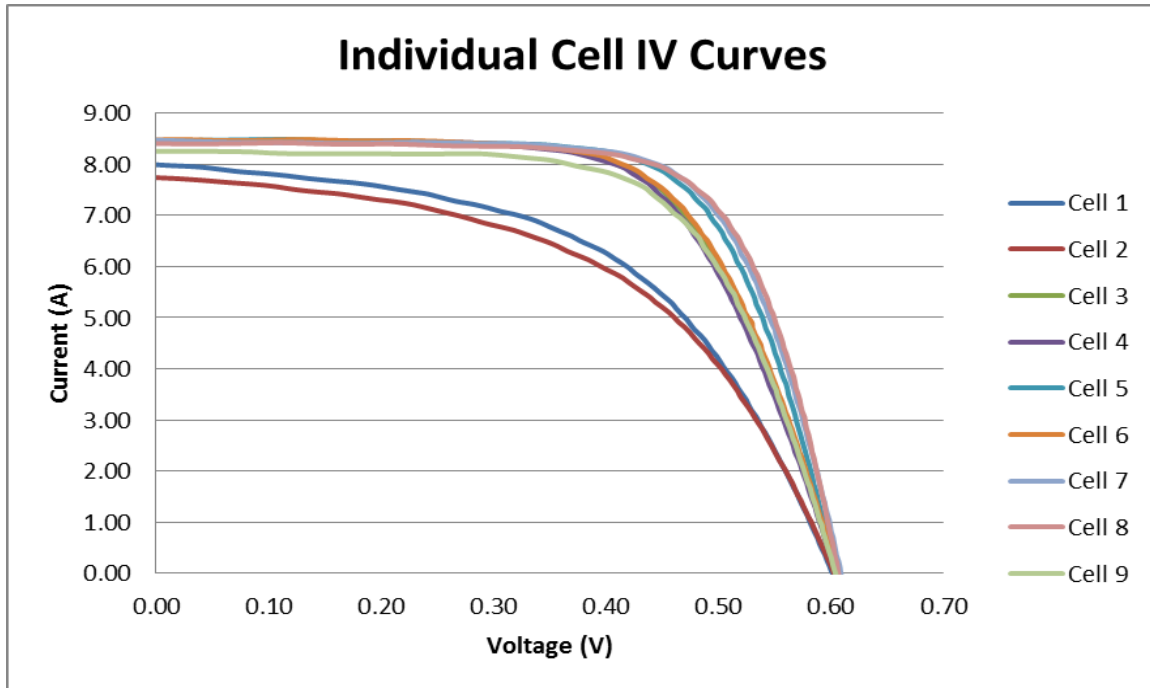

Figure 28.   Individual I-V curves for cells 1 to 9 1000W/m^2 and approximately 25°C

	Cell 1	Cell 2	Cell 3	Cell 4	Cell 5	Cell 6	Cell 7	Cell 8	Cell 9
V_{oc} (V)	0.6041	0.6028	0.6045	0.6053	0.6046	0.6057	0.6087	0.6066	0.6041
I_{sc} (A)	8.00	7.74	8.45	8.46	8.47	8.48	8.47	8.40	8.26
FF (%)	52.27	51.39	66.03	65.23	69.32	66.00	70.09	71.03	65.75
P_{max} (W)	2.53	2.40	3.37	3.34	3.55	3.39	3.61	3.62	3.28

Table 3.   Measured characteristics for cells 1 to 9 1000W/m^2 and approximately 25°C
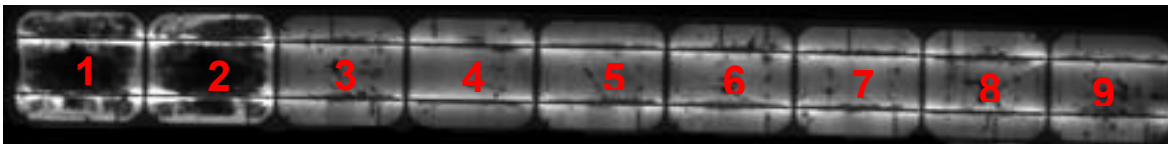

Figure 29.   Electroluminescence images for cells 1 to 9

Direct cell measurements for cells 1 to 9 were obtained by the methodology previously outlined in this thesis. The results for direct cell measurements are given in Figure 30.
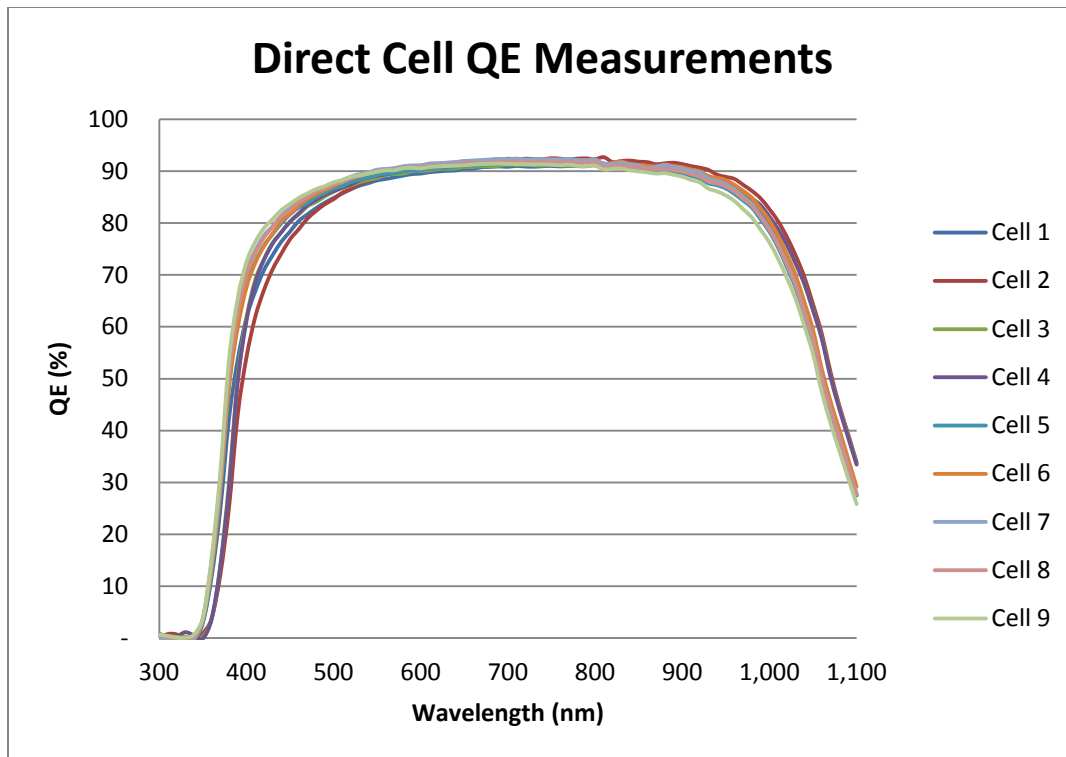
Figure 30.   Direct QE measurements for cells 1 to 9.

The major conclusions drawn from analyzing I-V, EL and QE for cells 1 to 9 are discussed in this section. Observation of the light I-V curves for 1,000 W/m^2 clearly shows that cells 1 and 2 are experiencing shunting effects. This is indicated by the deceased slope near Isc. This information also appears in the EL image. Cells 1 and 2 are much darker than cells 3 to 9 indicating a lower performance due to shunt resistance. Data from the QE curves shows that cells 1 and 2 have a lower QE for lower wavelengths (about 400nm to 500nm). However, the differences between shunted and non-shunted cells in the QE curves are a bit more subtle than the differences seen in I-V and EL images.

Multiple Cell Results (with module light bias, no voltage bias)

This section will detail the results of QE measurements for multiple cells connected in series within the module. This test was performed with module light bias but no voltage bias. The purpose of measuring QE for multiple cells in series with no voltage bias is to determine the effect on the QE curves as more cells are added in series. The graph presented in Figure 31 displays nine QE measurements resulting in nine QE curves. The position of the monochromatic light on the cell under test remained constant throughout all nine measurements. Module bias lighting also remained constant. The different curves were measured by moving positive leads of the QE system to the positive ribbons of series connected cells to increase the number of cells in the string (starting with n=1 and ending with n = 9). The legend in the graph indicates the position of the QE leads. For example, if the QE of cell 9 were measured through 5 cells with the negative of the QE leads connected to cell 9 and the positive connected to cell 5, the legend would read: cell 9 to 5 (n = 5).
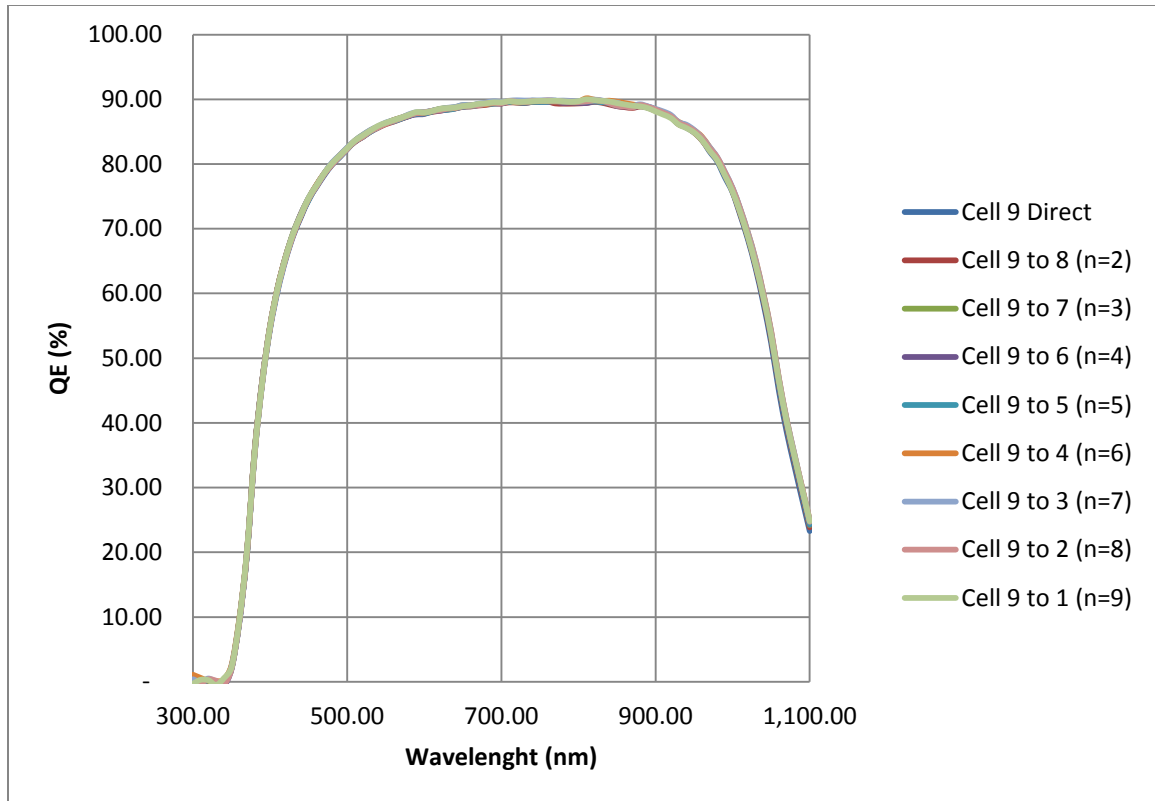
Figure 31.   QE of cell 9 through multiple cells

The results for this section show that all QE curves are identical when measured through 9 cells without applying voltage bias. This indicates that the cell under measurement (cell 9 in this case) can withstand a large negative voltage bias without decreasing current output.

To further explore QE curves without voltage bias applied, it was necessary to connect more cells in series to identify when the cell under test would reach the breakdown voltage. At the time of measurement, cell 9 could only be measured to cell 1 (n=9) because of the difficulty accessing module interconnects. For this test, cell 22 (good cell) was chosen as the cell under test because more cells could be connected in series. Direct cell measurements were obtained according to the methodology outlined in

this thesis. The QE system positive test leads were then moved to the adjacent cells connected in series. For this test, the voltage of the cell under test (cell 22) was also monitored with a voltmeter. The resulting QE curves are given in Figure 32.
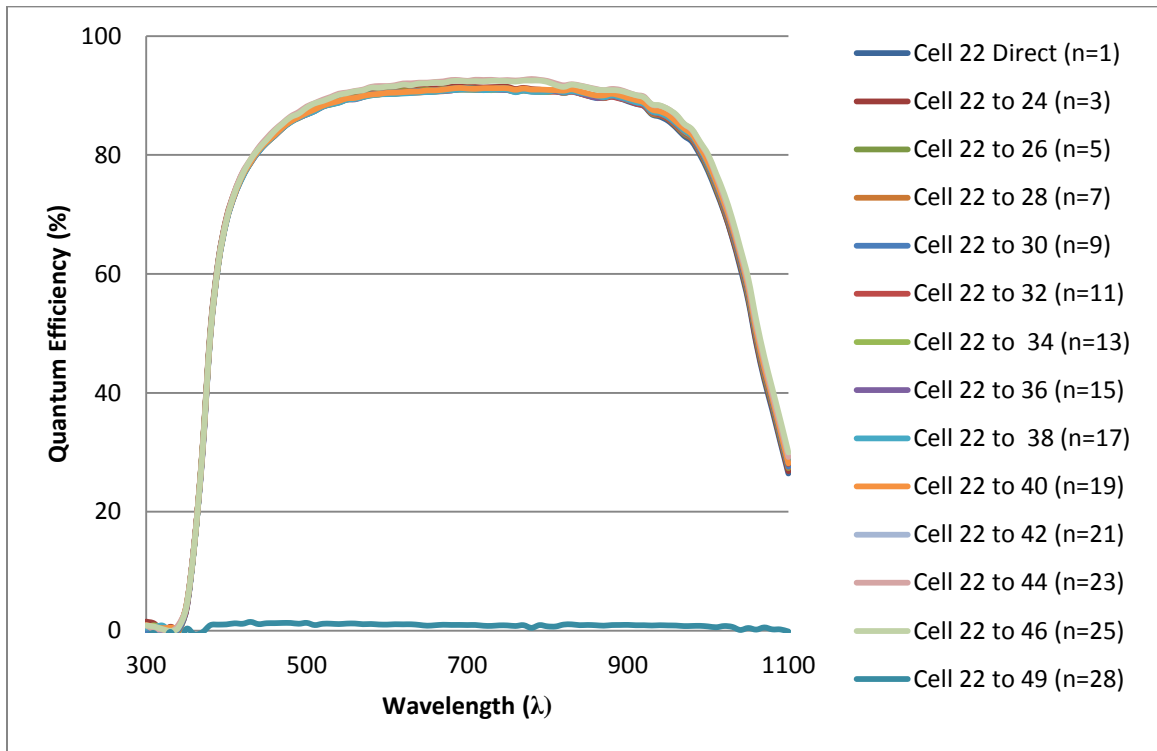

Figure 32.   QE of cell 22 (good cell) through multiple cells

The results of this test show that the QE curves for cell 22 (good cell) remained approximately constant until 28 cells were connected in series. Closer inspection of the graph shows that the QE curve actually varies slightly as more cells were connected in series. However, the fluctuation in QE was extremely small and within the +/-1% uncertainty value given by the manufacturer specifications. When the 28th cell was connected, the QE curve dropped to zero for all wavelengths. The voltage of the cell was measured at this voltage as -12.44V.

To further explain the reason that the QE of cell 22 (good cell) could still be measured at -12.44V a dark I-V curve was measured. The results of the dark I-V are given in Figure 33. The dark I-V data shows that a negative voltage bias can be applied to cell 22 up to about -10 volts before the breakdown voltage is reached.
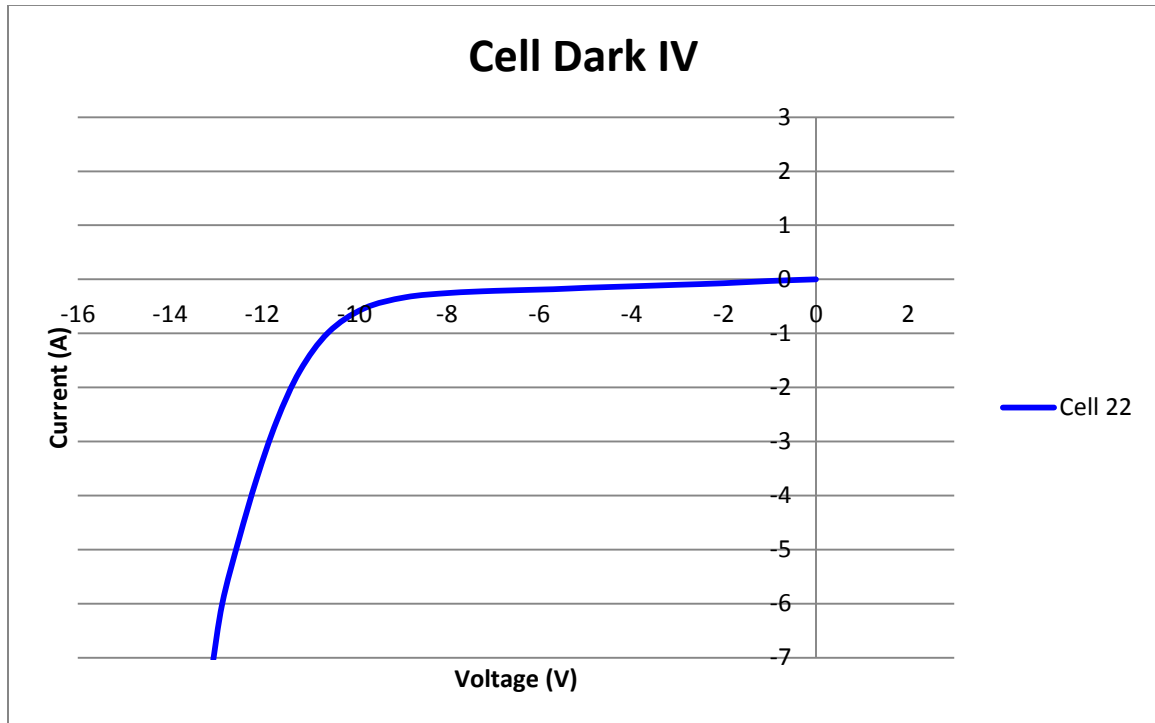

Figure 33.   Dark I-V for cell 22 (good cell)

The major conclusions that can be drawn from these multiple cell measurements is that the same QE can be obtained even if the cell under test is reverse biased. Ideally, the cell under test should always be measured at zero volts. However, future tests will not have the advantage of cutting into the backsheet to monitor the exact voltage of the cell under test. This study shows that even if the cell under test is negatively biased, QE measurements can still be obtained.

Multiple Cell Results (with module light bias and voltage bias)

Results from the multiple cell measurements show that QE measurement can be obtained even if the cell is negatively biased. However, QE measurements should always be measured as close to zero volts as possible. Also, C-M-QE tests will usually be performed for commercial modules where the number of cells connected in series will contribute to an extremely high negative voltage on the cell under test. Therefore, a voltage bias feature must be used for C-M-QE measurements.

Voltage bias feature of the C-M-QE system at ASU-PRL was used in this experiment. The purpose of the voltage bias is to correct for the negative voltage across the cell under test caused by multiple cells connected in series. Applying a voltage bias as indicated in Equation (2) will effectively cancel the negative voltage across the cell under test. Figure 32 shows the QE curve dropped to zero for all wavelengths when 28 cells were connected in series (corresponding to -12.44V across the cell under test). This section shows that the QE curve can be fully recovered by applying bias voltage. Figure 34 shows the resulting QE curves after bias voltage is applied.
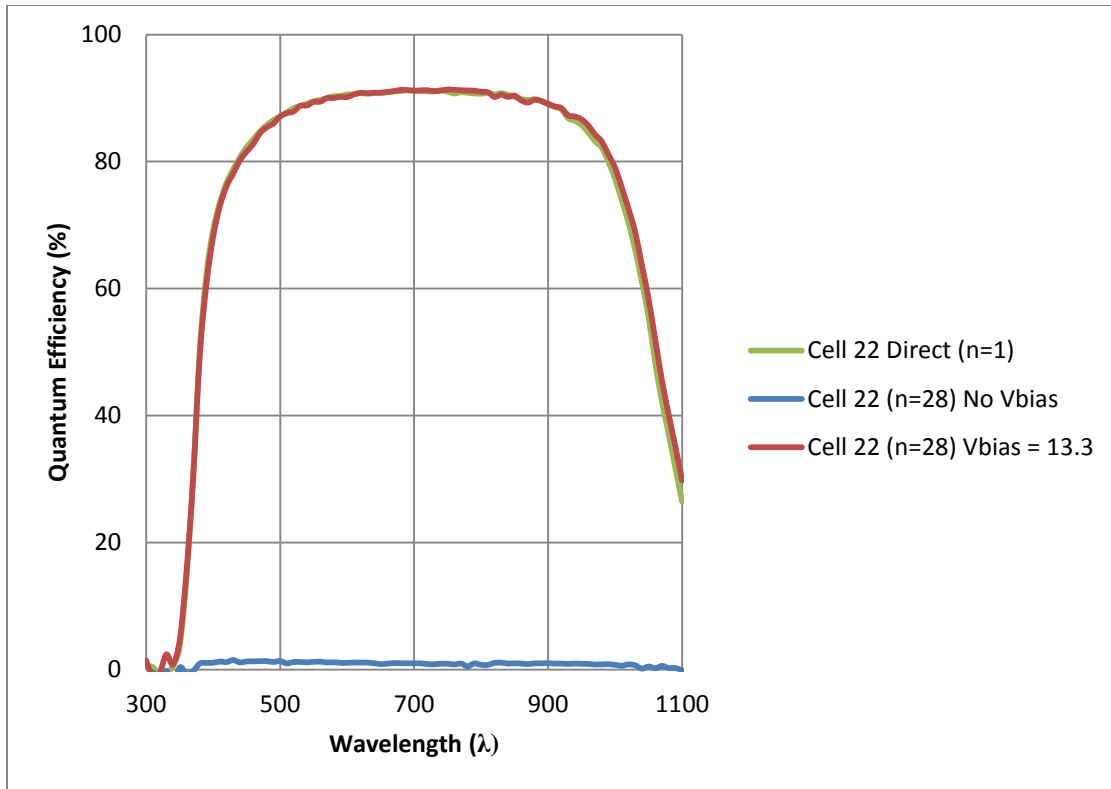
Figure 34.   QE curves for cell 22 (good cell) with voltage bias compared to direct and no voltage bias QE curves

Figure 34 shows that applying voltage bias shifts the QE curve of the cell under test back to that of the original direct QE curve for cell 22. The voltage bias of 13.3 volts was determined by measuring the Voc of the test string and applying Equation (2). Measurements were continued by adding more cells in series and applying voltage bias according to Equation (2). Measurements were taken until the number of cells in the string reached 39 (n=39). Figure 35 shows that QE curves can be accurately measured for 39 cells in series.
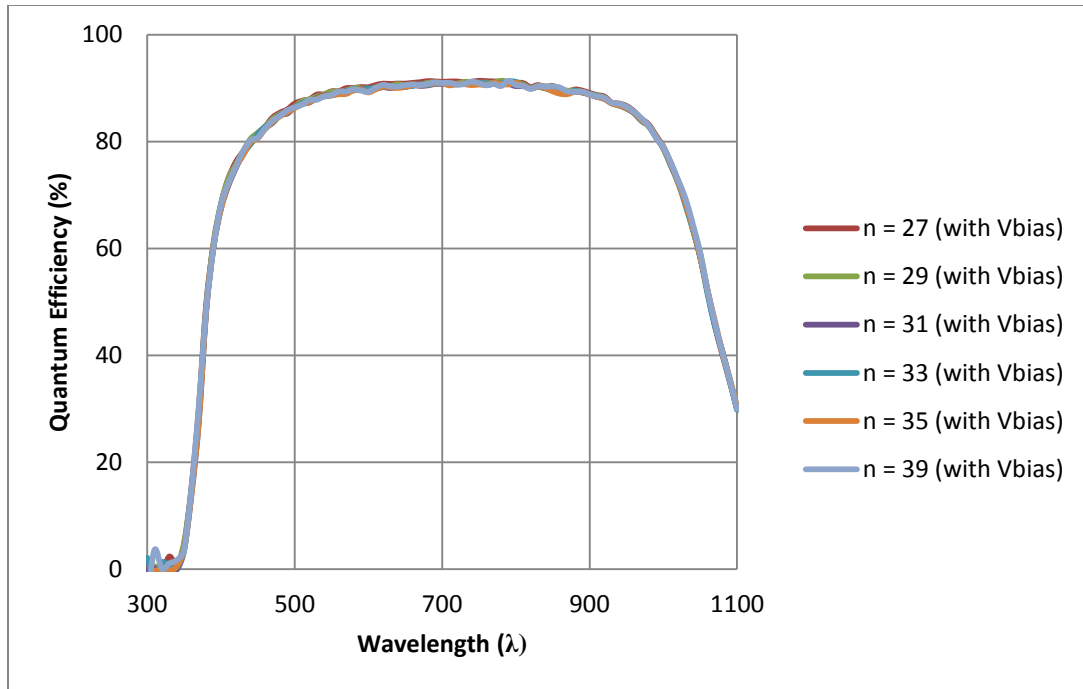
Figure 35.   QE measurements for Cell 22 (good cell) with multiple cells connected in series from n=27 to n=39

Cell-Module QE Measurements (with various module light biases)

The C-M-QE system comes equipped with LED module light bias. The purpose of this light bias is to forward bias all the cells in the module (except the cell under test which is shaded to make it the current limiting cell). The light bias is controlled using the C-M-QE system software. The amount of module light bias can be adjusted from 0% to 100%. The corresponding intensity for a range of light bias settings is given in Table 4.

LED (%)	Module Light Bias Irradiance (W/m^2)
25	68
50	119
75	156
100	208

Table 4.   List of LED light bias percentages and the corresponding module light bias irradiance

The intensity of the LED module light bias was calculated using two calibrated crystalline silicon reference cells. The reference cells were mounded on flat metal surface and placed on top of the module under test inside the C-M-QE system. The spacial uniformity of the LED lights varies by an average of +/-8 W/m^2. The values given in Table 4 are an average intensity with the spacial uniformity taken into account.

C-M-QE measurements were taken for various module light bias intensities. The results are shown in Figures 36 and 37.
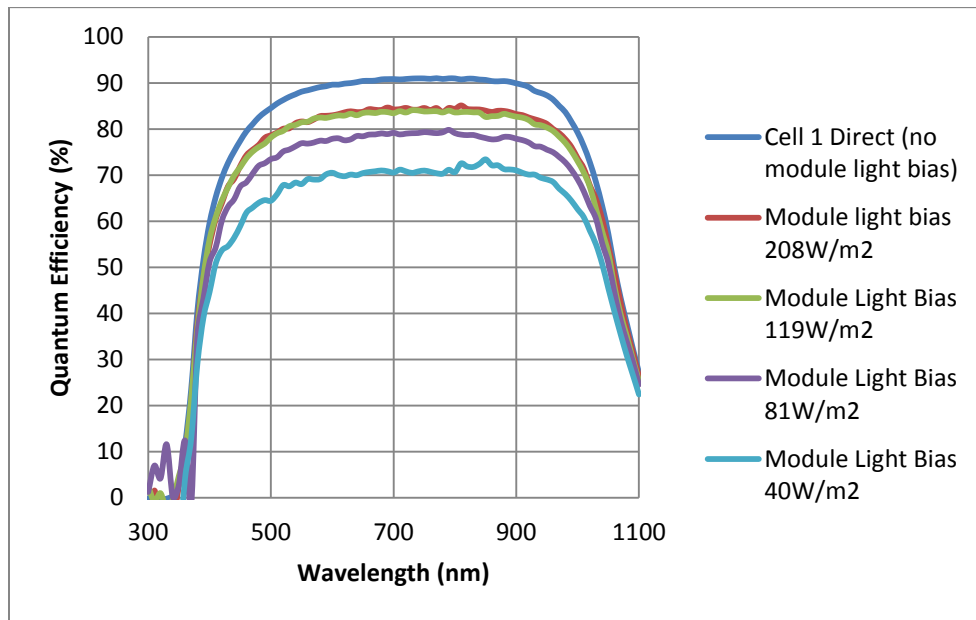

Figure 36.   Cell 1 (Shunted cell) with increasing levels of module light bias intensity
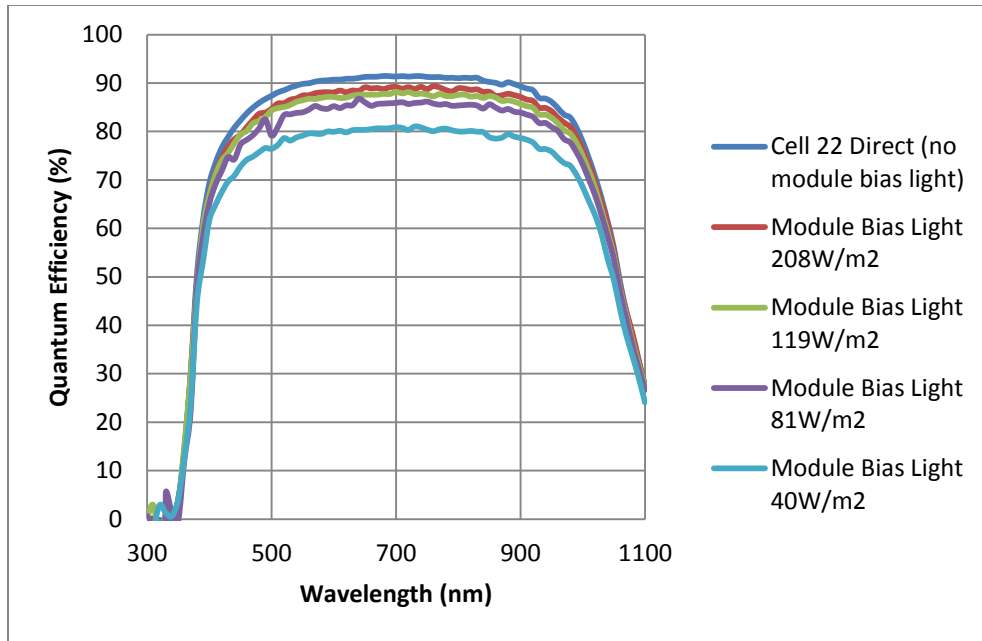
Figure 37.   Cell 22 (good cell) with increasing levels of module light bias intensity

Both graphs of cell 1 (Shunted cell) and cell 22 (good cell) indicate that increasing the module bias light intensity also increases the QE curve. The reason for this increase is attributed to the module bias light increasing the slope of the series connected cells I-V curves near Voc. This will minimize the voltage shift in the cell under test and allow the C-M-QE curve to be measured closer to Isc. To ensure that increasing module bias light did increase the slope of the curve near Voc for the cells, I-V curves were measured. Figure 38 shows the I-V curves measured for cell 3 at module bias light intensities of 69, 126, 174, and 214 W/m^2. Figure 39 provides the slops of the I-V curves near Voc for high and low intensities of irradiance.
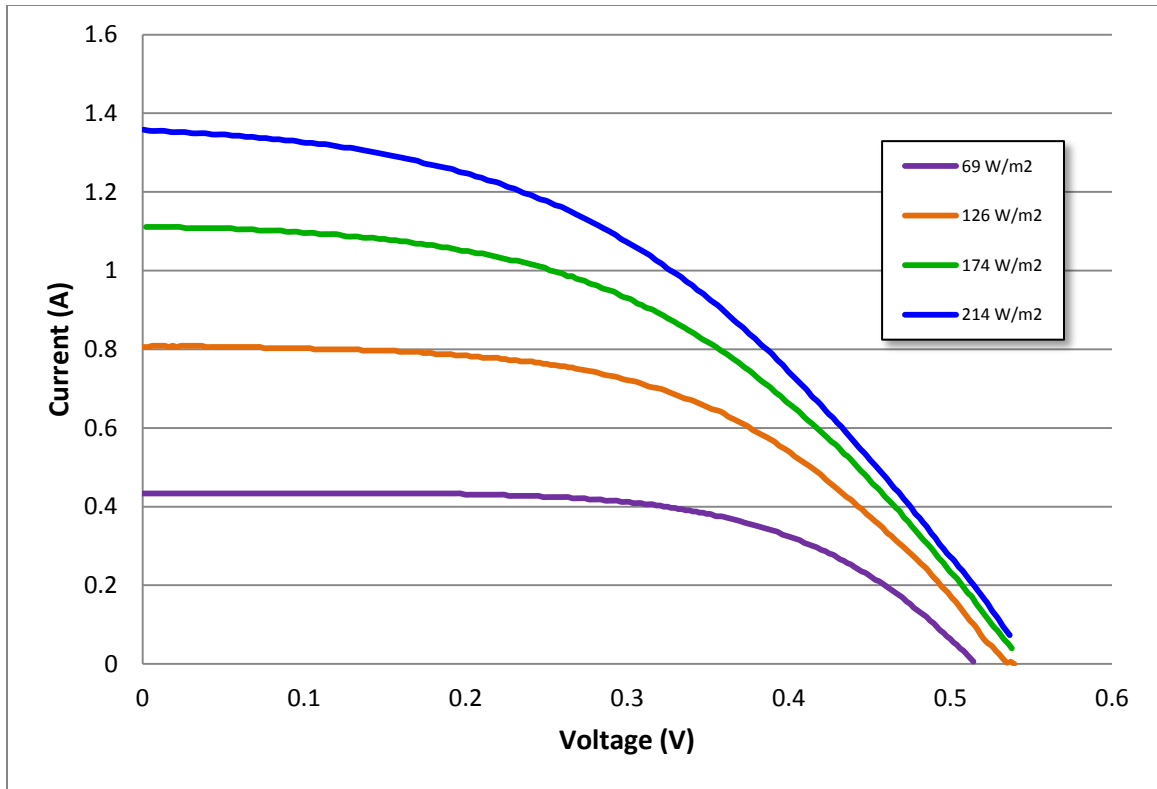
Figure 38.   I-V curves for Cell 2 under LED module bias lights at various intensities
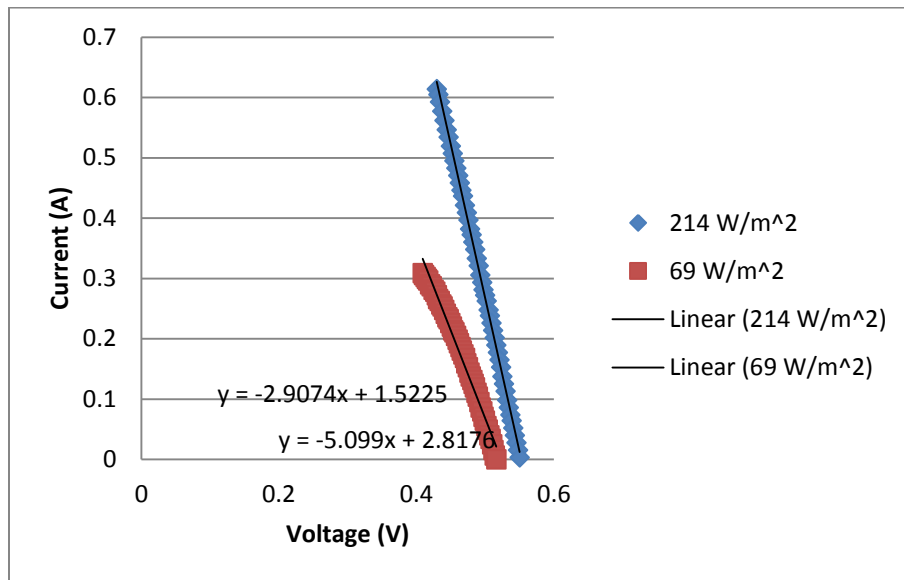

Figure 39.   Slope of the I-V curve for cell 2 near Voc for high irradiance (214 W/m^2) and low irradiance (69 W/m^2)

Cell-Module QE Measurements

The previous sections showed QE measurements for a cell with an increasing number of cells connected in series. A PV module is nothing more than a certain number of solar cells connected in series. The module measured in this test had 60 monocrystalline cells connected in series. To measure C-M-QE, the QE leads were connected to the external module leads. Module light bias and voltage were applied according to the methodology described in the previous chapter. The C-M-QE curve measured for cell 22 (good cell) is plotted and compared to the direct cell 22 measurement in Figure 40.
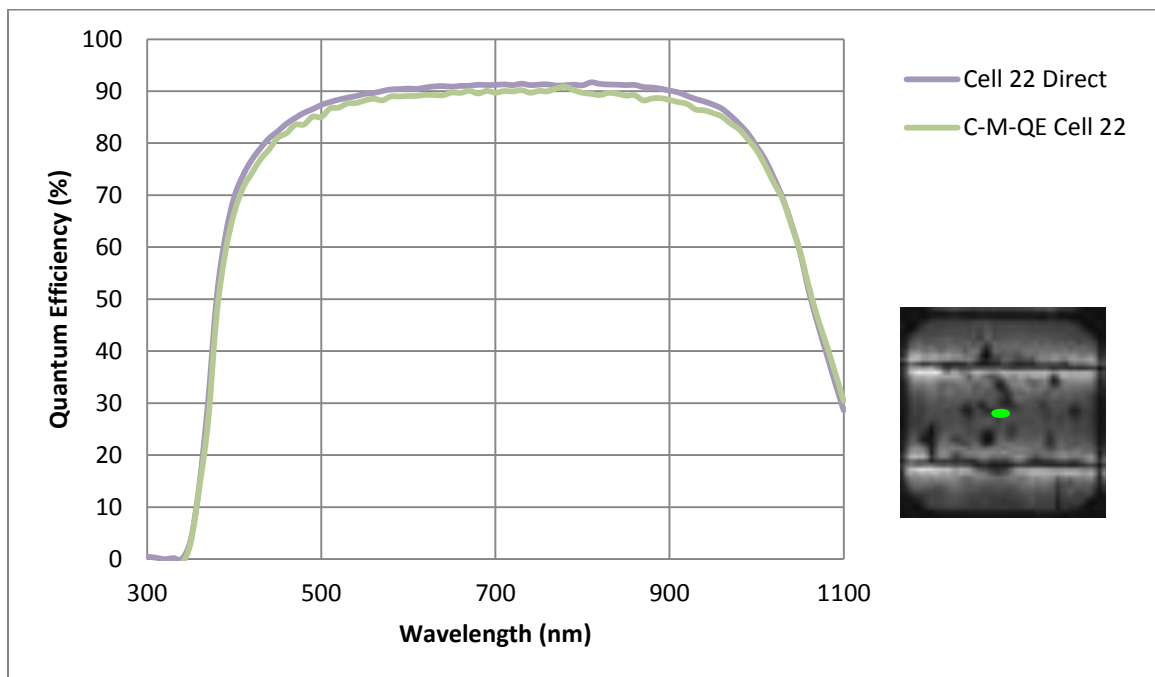

Figure 40.   C-M-QE measurements for cell 22 (good cell) compared to direct cell measurements.

Figure 40 shows that when the QE of cell 22 (good cell) is measured through the module via connecting to the external module leads; it is slightly lower than the direct cell measurements. To obtain a quantitative comparison for both curves, the deviation of

the C-M-QE curve from the direct QE curve was calculated between 400nm and 1000nm. The difference between the QE measurements in Figure 40 is 1.8%. The EL image and location of the monochromatic beam (shown in green) for the cell 22 is given below the legend in Figure 40.

The same procedure was repeated for cell 1 (Shunted cell). However, cell 1 (Shunted cell) has a lower FF than cell 22 (good cell) due to shunting. The data for cell 1 (Shunted cell) is given in Figure 41 with the EL image and location of the monochromatic beam shown below the legend. The difference between the direct QE measurement and the C-M-QE measurement is 6.2%.
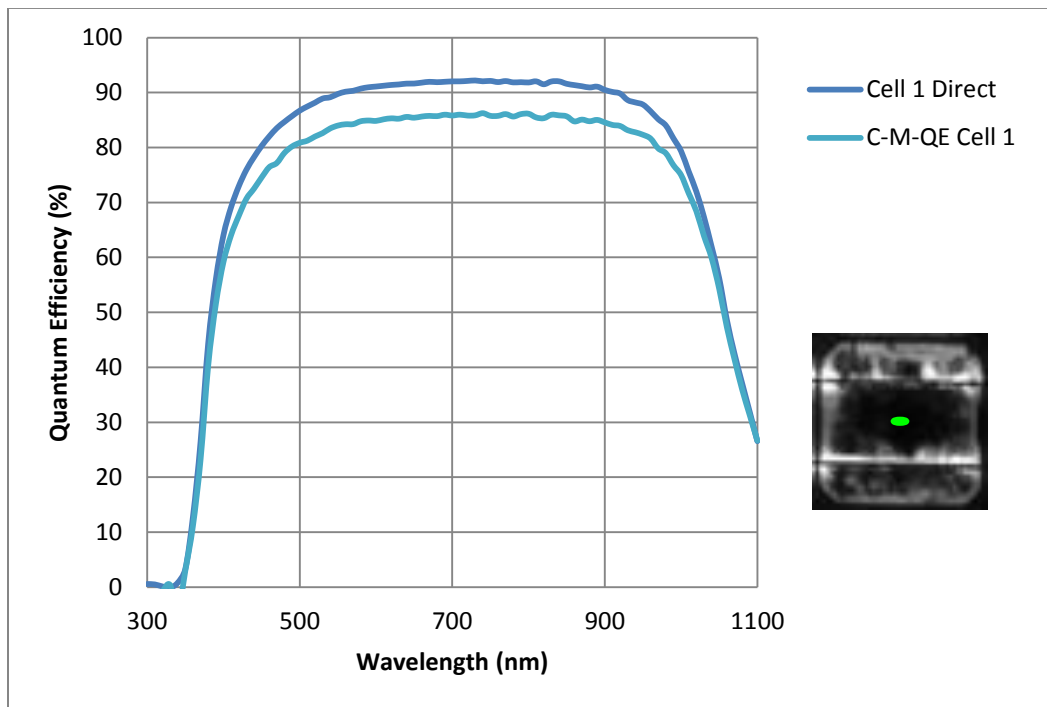

Figure 41.   C-M-QE measurements for cell 1 (Shunted cell) compared to direct cell measurements.

The main difference between cell 1 and cell 22 is that cell 1 has a lower FF due to shunting. Therefore, the difference between the C-M-QE curve and the direct curve is larger for cell 1 because of the shunting effect. The difference between the curves was calculated between 400nm and 1000nm to be 6.2%.

2-5 CONCLUSION

The data collected from this study shows that it is possible to obtain a reasonably accurate QE measurement for a cell within a module by implementing a non-intrusive testing methodology. Application of module light bias, cell light bias, and voltage bias are necessary to obtain C-M-QE curves.

- **Module Light Bias**: Module light bias should be set to maximum intensity during the QE measurement. For the C-M-QE system, maximum efficiency corresponded to approximately 200 W/m^2. Future tests should explore possibilities for increasing the module light bias intensity.

- **Cell Light Bias**: Data from this study shows that cell light bias intensity does not affect QE measurements. C-M-QE curves were measured with cell light bias intensities ranging from 0 W/m^2 to 485 W/m^2. All the QE curves measured were within +/-1%.

- **Voltage Bias**: This study showed that voltage bias is necessary when measuring C-M-QE curves. The correct voltage to be applied is given by Equation (1). When using this equation it is essential to use Voc at the operating conditions of the time of measurement (for example in this case for 200 W/m^2 and 25°C). If the QE curve is not maximized, decrease the voltage bias intensity until maximum QE is reached. For the shunted cells the C-M-QE will need to be improved possibly by a pulse-voltage biasing technique which has been recently explored by other researchers.

C-M-QE measurements were also performed for high and low FF cells within a module and compared to direct cell measurements. For high FF cells, the C-M-QE

measurement was within 98.2% of the direct cell measurement. For low FF cells, the C-

M-QE was within 93.8% of the original measurement.

REFERENCES

[1] D. L. King, "Measuring Angle of Incidence (AOI) Influence on PV Module Performance," Private communication (this document is reproduced in Appendix A of this Report), June 2012.

[2] N. Martin and J. M. Ruiz, "Annual Angular Reflection Losses in PV Modules," in *Progress in Photovoltaics*, pp. 75-84.

[3] International Electrotechnical Commission (IEC) 61853-2 (Draft), "Photovoltaic (PV) Module Performance Testing and Energy Rating - Part 2: Spectral Response, Incident Angle, and Module Operating Temperature Measurements," May 2012.

[4] C. Honsberg and S. Bowden, "PV Education," PVCDROM. [Online]. [Accessed 22 August 2013].

[5] American Society for Testing and Materials (ASTM), "Standard Test Method for Spectral Responsivity Measurements of Photovoltaic Devices E1021-12," ASTM International, West Conshohocken, 2013.

[6] X. Deng and E. A. Schiff, "Amorphous Silicon-based Solar Cells," in *Handbook of Photovoltaci Science and Engineering*, Hoboken, John Wiley & Sons, 2003, pp. 542-556.

[7] American Society for Testing and Materials (ASTM), "Standard Test Methods for Measurement of Electrical Performance and Spectral Response of Nonconcentrator Multijunction Photovoltaic Cells and Modules E2236-10," ASTM International, West Conshohocken, 2010.

[8] R. Steve, E. Keith, F. Halden, M. Tom, A. Allan, D. Don and O. Larry, "PV Cell and Module Performance Measurement Capabilities at NREL," in *NCPV Photovoltaics Program Review*, Golden, 1999.

[9] J.-J. Li, S. H. Lim and Y.-H. Zhang, "A Novel Method to Eliminate the Measurement Artifacts of External Quantum Efficiency of Multi-junction Solar Cells Caused by the Shunt Effect," in *Physics, Simulation, and Photonic Engineering of Photovoltaic Devices*, Tempe, 2012.

[10] D. L. King, J. A. Kratochvil and W. E. Boyson, "Measuring Solar Spectral and Angle-of-Incidence Effects on Photovoltaic Modules and Solar Irradiance Sensors.," Paper presented at IEEE Photovoltaic Specialists Conference, Anaheim, California, 1997.

[11] E. A. Sjerps-Koomen, E. A. Alsema and W. C. Turkenburg, "A Simple Model for

PV Module Reflection Losses Under Field Conditions," in *Solar Energy*, 1997, pp. 421-432.

[12] W. D. Soto, S. A. Klein and W. A. Beckman, "Improvement and Validation of a Model for Photovoltaic Array Performance," in *Solar Energy*, 2006, pp. 78-88.

[13] T. Moriarty and K. Emery, "Procedures at NREL for Evaluating Multijuntion Concentrator Cells," National Renewable Energy Laboratory, Golden.

[14] K. Emery, D. Dunlavy, H. Field and T. Moriarty, "Photovoltaic Spectral Responsivity Measurements," *Proc. 2nd World Conference and Exhibition on Photovoltaic Solar Energy Conversion,* vol. 18656, pp. 2298-2301, July 1998.

[15] B. Knisely, S. V. Janakeeraman, J. Kuitche and G. Tamizhmani, "Validation of Draft International Electrotechnical Commission 61853-2: Angle of Incidence Effect on Photovoltaic Modules," Solar America Board for Codes and Standards, March 2013. [Online]. Available: http://www.solarabcs.org/about/publications/reports/aoi/pdfs/ABCS-29_AOI-SR-3-4.pdf.

APPENDIX A

SANDIA PROCEDURE TO DETERMINE RELATIVE OPTICAL RESPONSE,

$f_2(AOI)$

Measuring Angle-of-Incidence (AOI) Influence on PV Module Performance

Private Communication with David L. King (June 2012)

There are two AOI influences that need to be considered, one is "mechanical" and the other is "optical." The mechanical influence really doesn't have anything to do with the module itself, but rather its orientation relative to the incident sunlight, often called the "cosine effect." The beam solar irradiance incident on the module is reduced by cos(AOI). The optical effect is due to the surface characteristics of the module, which can be highly planar (float glass), dimpled (rolled glass), coated with anti-reflection (AR) coatings, heavily textured for light gathering at large AOI, or specifically patterned for optical concentration purposes. The primary influence on the optical effect is increasing reflectance loss as AOI increases. Both of these AOI influences apply primarily to the beam or direct component of sunlight, rather than the diffuse component of sunlight. The Sandia module performance model attempts to account for both these influences using an expanded expression for the solar irradiance, called the effective solar irradiance (E_e), which in turn determines the module's short-circuit current (I_{sc}). Equation (A1) gives the Sandia expression for E_e, and Equation (A2) gives the resulting equation for I_{sc}. The intent of this document is to provide a discussion of the procedures that can be used to empirically measure the optical effect, f_2(AOI).

$$E_e = [E_{dni}*\cos(AOI)*f_2(AOI)+f_d*(E_{poa} - E_{dni}*\cos(AOI))]/E_o \qquad (A1)$$

$$I_{sc} = I_{sco} * [1+\alpha_{Isc}*(T_c -25)]*f_1(AM_a)*E_e \qquad (A2)$$

79

Where:

E_e = Solar irradiance actually captured and used by module (dim or suns)

E_{dni} = Direct normal solar irradiance (W/m^2)

E_{poa} = Global solar irradiance in the plane-of-array (module) (W/m^2)

E_o = Reference global solar irradiance, typically 1000 W/m^2

f_d = Fraction of diffuse irradiance used by module, typically assumed = 1 (dim)

AOI = Angle between solar beam and module normal vector (deg)

T_c = Measured module (cell) temperature (°C)

α_{Isc} = Short-circuit current temperature coefficient (1/°C)

$f_1(AM_a)$ = Empirical relationship for solar spectral influence on I_{sc} versus air mass

I_{sco} = Module short-circuit current at STC conditions (A)

I_{sc} = Measured short-circuit current (A)

Direct Measurement of f₂(AOI)

The direct procedure for measuring $f_2(AOI)$ involves measuring module I_{sc} as the module is moved in angular increments using a solar tracker through a wide range of AOI conditions, 0 deg to 90 deg. The challenge is to conduct the test in a way that either minimizes or compensates for all the factors in Equations (A1) and (A2) that influence the measured I_{sc} values. The following bullets identify desirable conditions and approaches, depending on the capabilities of the test equipment available.

Conduct test during clear sky conditions when the direct normal irradiance is the dominant component, e.g. when the ratio of direct normal divided by global normal

80

irradiance is greater than about 0.85. This reduces the influence of diffuse irradiance on the determination of $f_2(AOI)$.

Conducting the test near solar noon also has a couple advantages, variation in the solar spectrum during the test is minimized, and the full range for AOI can typically be achieved by changing only the elevation angle of a two-axis solar tracker.

Measure I_{sc}, E_{dni}, E_{poa}, and T_c associated with each AOI increment. E_{dni} should be measured with a thermopile pyrheliometer, and E_{poa} should ideally be measured using a thermopile pyranometer that has been calibrated as a function of AOI.

Module temperature will vary during the test, so measured temperature should be used to translate measured I_{sc} values to a common temperature, e.g. 25°C.

If possible, record data over the full range of AOI as rapidly as possible, so that solar spectral variation can be ignored, less than 30-min test period is desirable. If the test period must be longer, then a spectral correction to measured I_{sc} can be done using a previously determined $f_1(AM_a)$ relationship.

The Sandia model Equations (A1) and (A2) can be solved to provide an equation for the angle-of-incidence relationship, $f_2(AOI)$, as a function of the measured variables, Equation (A3).

$f_2(AOI)=\{[I_{sc}*E_o/(I_{sco}*f_1(AM_a)*(1+\alpha_{Isc}(T_c-25)))]-f_d*(E_{poa}-E_{dni}*\cos(AOI))\}/(E_{dni}*\cos(AOI))$ (A3)

In order to simplify, recognize that by definition $f_2(AOI)=1$ when AOI=0 degrees. Therefore, Equation (A3) can be solved for the I_{sco} value at the start and end of the

outdoor test period when AOI=0 degrees. The value solved for is not exactly I_{sco} at STC because the air mass value may not be exactly $AM_a=1.5$ at the time of day when the AOI=0 deg conditions were achieved. This calculated value is only intended to provide a reference value for short-circuit current in order to normalize $f_2(AOI)=1$ when AOI=0 deg, so to avoid confusion call the calculated value I_{scr}.

$$I_{scr} = I_{sc}*E_o/\{f_1(AM_a)*(1+\alpha_{Isc}(T_c-25))*(E_{dni}+f_d*(E_{poa}-E_{dni}))\} \qquad (A4)$$

After determining the value for I_{scr} using the average value for several measurements when AOI=0 deg, the measured values for $f_2(AOI)$ can be determined using Equation (3), by substituting the I_{scr} value for I_{sco}.

Further simplification in the determination of $f_2(AOI)$ can be made for conventional flat-plate modules, depending on the test procedure and assumptions made. If data for the full range of AOI is recorded in a relatively short period of time, then the influence of varying solar spectrum is likely to be negligible. In addition, for conventional flat-plate modules the assumption is usually made that they capture both diffuse and direct irradiance; therefore $f_d=1$. Under these simplified conditions, Equations (A3) and (A4) can be rewritten as Equations (A5) and (A6).

$$I_{scr} = I_{sc}*(E_o/E_{poa})*(1+\alpha_{Isc}(T_c-25)) \qquad (A5)$$

$$f_2(AOI) = [E_o* (I_{sc}/(1+\alpha_{Isc}(T_c-25)))/I_{scr} -(E_{poa}-E_{dni}*\cos(AOI))]/(E_{dni}*\cos(AOI)) \qquad (A6)$$

For conventional flat-plate glass modules, this procedure should result in empirical $f_2(AOI)$ relationships similar to those shown in Figure A1. As previously mentioned, AR-coated glass or heavily textured glass will provide different results. For the simple case with a planar glass surface, Snell's and Bougher's optic laws along with glass optical properties (index of refraction, extinction coefficient, thickness) can also be used to calculate a theoretical relationship for $f_2(AOI)$, as done by DeSoto in Reference [1].
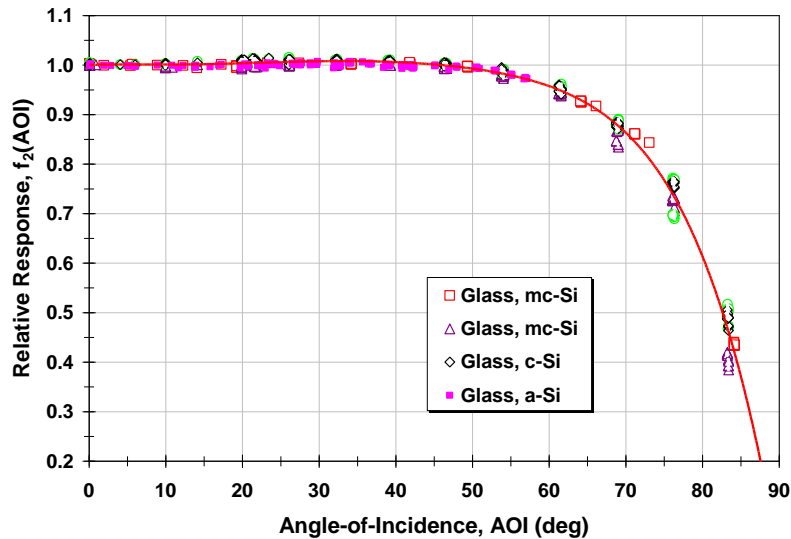
Figure A1: Empirical $f_2(AOI)$ measurements by Sandia National Laboratories for conventional flat-plate modules with a planar glass front surfaces.

Although polynomial fits to measured data can be problematic, ten years ago when the procedure was developed and the Sandia module database initiated, a fifth order fit was used to represent the measured data. There are probably better ways to represent the data, but at this point the Sandia module database has gained enough inertia that it would be difficult to change the model coefficients used to match the measured data. The

"generic" polynomial used for the majority of typical glass-surface modules is given below.

$f_2(AOI)=1-2.4377E-3(AOI)+3.1032E-4(AOI)^2-1.2458E-5(AOI)^3+2.1122E-7(AOI)^4-1.3593E-9(AOI)^5$

Relative (Comparison) Measurements for $f_2(AOI)$

Although not presented in this document, an alternative test procedure providing simultaneous measurements of the I_{sc} of a test module and a reference module may possibly provide a more accurate and repeatable process. The reference module is assumed to have "known $f_2(AOI)$" characteristics. The reference device could be a module or an individual reference cell, ideally with matching cell technology to provide equivalent solar spectral sensitivity. For a reference device with ideally planar glass surface, the "known $f_2(AOI)$" could be derived from optical laws, perhaps providing a more fundamental basis for the outdoor test procedure.

References
[1] W. DeSoto, S.A. Klein, W.A. Beckman, "Improvement and Validation of a Model for Photovoltaic Array Performance," Solar Energy, August 2005.

APPENDIX B

CROSSCHECKING OF AOI DEVICE USING A MANUAL METHOD

In this study, the AOI was directly determined using an AOI device purchased from MicrStrain. However, in the absence of this device, the AOI value can also be determined using a manual calculation (Equation B1) provided by Sandia National Laboratories[2].

$$AOI = \cos^{-1}(\cos(T_m)\cos(Z_s) + \sin(T_m)\sin(Z_s)\cos(AZ_s - AZ_m)) \quad (B1)$$

Where:

AOI = solar angle of incidence (degrees)

T_m = tilt angle of module (degrees, 0° is horizontal)

Z_s = zenith angle of the sun (degrees)

AZ_m = azimuth angle of module (0°=North, 90°=East)

AZ_s = azimuth angle of sun (degrees)

As shown in Figure B1 (azimuth rotation) and Figure B2 (elevation rotation) below, the accuracy of the AOI device used in this project was crosschecked with the manual method using Equation (B1) given above. These plots confirm that the AOI data obtained using the MicroStrain device was reliable and accurate.
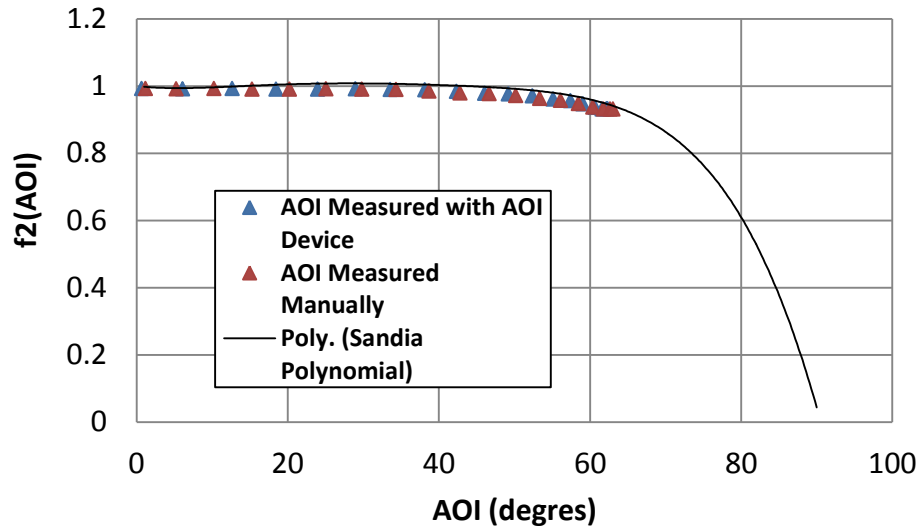
Figure B1: Comparison of relative optical responses obtained using the AOI hardware and AOI calculation for a CdTe module with glass superstrate for azimuth rotation (direct to global ratio was 0.89)
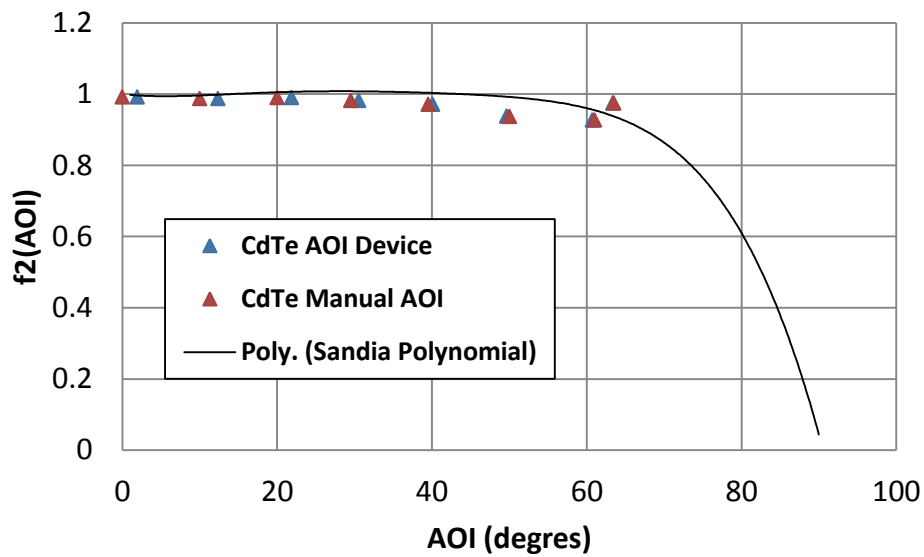

Figure B2: Comparison of relative optical responses obtained using the AOI hardware and AOI calculation for a CdTe module with glass superstrate for elevation rotation (direct to global ratio was 0.89)

For azimuth angle, the tracker was allowed to rotate to its full Westward rotation angle and tracked azimuthally to the East. The azimuth angle of the module was manually measured by dividing the diameter of the tracker pole into 360° and fixing a dial to the rotating head of the tracker to indicate its change in angle. Since the azimuthal rotation of the tracker was limited, azimuth verification could only be obtained for AOI up to 63°. For elevation angle, the two-axis tracker was tilted to the maximum horizontal position of 11° (where 0° is horizontal) and tilted downward to a maximum angle of 74.5°. The $f_2(AOI)$ data for elevation angle deviates from the generalized polynomial for higher tilt angles due to the inconsistent reflectance throughout the measurement. When the modules are at 11° tilt (close to horizontal), they 'see' only the sky. As they are tilted downward, the ground reflection could interfere with the data accuracy. This phenomenon does not occur for azimuth angles because the modules are essentially seeing the same ratio of sky and ground (they were at 30° tilt angle for the duration of the azimuth rotation).

The purpose of this experiment was to verify that the manual method and AOI device measurements were consistent. Both methods proved to be accurate. The standard deviation between manually calculated AOI and the AOI device measurement for azimuth angle was 1.66°. The standard deviation between manually calculated AOI and AOI device measurement for elevation tilt was 1.08°.

APPENDIX C

LESSONS LEARNED 1: ROUND 1 MEASUREMENTS USING A MULTI-CURVE

TRACER

The data presented in the main body (round 3; final round) of the report evolved from previous two rounds of data collections and reductions. Improvements to the experimental setup and data processing were made for each round. For round 1 of data collection, a DayStar (DS3200) multi-curve tracer was used to measure and record Isc, module temperature, and irradiance sensor readings. The main problems concerning round 1 measurements were:

The fastest time the multi-curve tracer could record and store data was one minute intervals. This was due to a software limitation of the multi-curve tracer, not a hardware issue. The multi-curve tracer saves data files onto the harddrive by automatically assigning them a file name based on the time the data was collected. The data file is named only for the hour and minute it is stored (not for the second). The physical capabilities of the tracer allow it to take data for the five modules in ten seconds. However, since the files are automatically assigned a name based on the time they were taken, the minimum time interval the data could be recorded and stored was one minute. For this experiment, the tracker was rotated by 5° AOI every one minute until it reached a maximum of 77° AOI. The experiment was performed in 16 minutes and a total of 16 data points were collected. The 16 data points in 16 minutes is sufficient to comply with the IEC 61853-2 standard which states for devices with rotational symmetry of the reflectivity with respect to the module normal, do a minimum of 9 different angles to span the angles from 0 to 80° for one direction. To confidently validate this statement, more data points were needed. Since data should be recorded as quickly as possible to reduce the spectral change during the experiment, round 2 was proposed to be carried out using equipment that could measure and record data in less than one minute intervals.

90

The irradiance sensors used for measuring global irradiance in the plane of array (pyranometers) and direct normal irradiance (pyrheliometer) had not been calibrated, and therefore, the accuracy of the measurements could not be confirmed and the uncertainty could not be calculated.

The relative Isc obtained versus AOI plot is shown in Figure C1. Using Equation (A6) of Sandia, the relative optical response data, f_2(AOI) data, was plotted (symbol) versus AOI as shown in Figure C2. The plotted data (symbols) was then compared to the "generic" polynomial curve (solid line) empirically derived by Sandia National Laboratories. As can be seen in Figure C2, there is a significant difference between the f_2(AOI) data calculated using the experimental data and the generic polynomial curve (between 60° and 75°). This difference warranted further investigation.

A further investigation revealed a human error that was made in constructing the Equation (A6) in the Excel spreadsheet. This error was fixed in the final rounds of data processing.

Nevertheless, the multi-curve tracer method, as opposed to the transducer/data logger method, was not continued for the second and final rounds of measurements due to the limitation on the number of data points that could be collected during the short duration of tracker rotation.
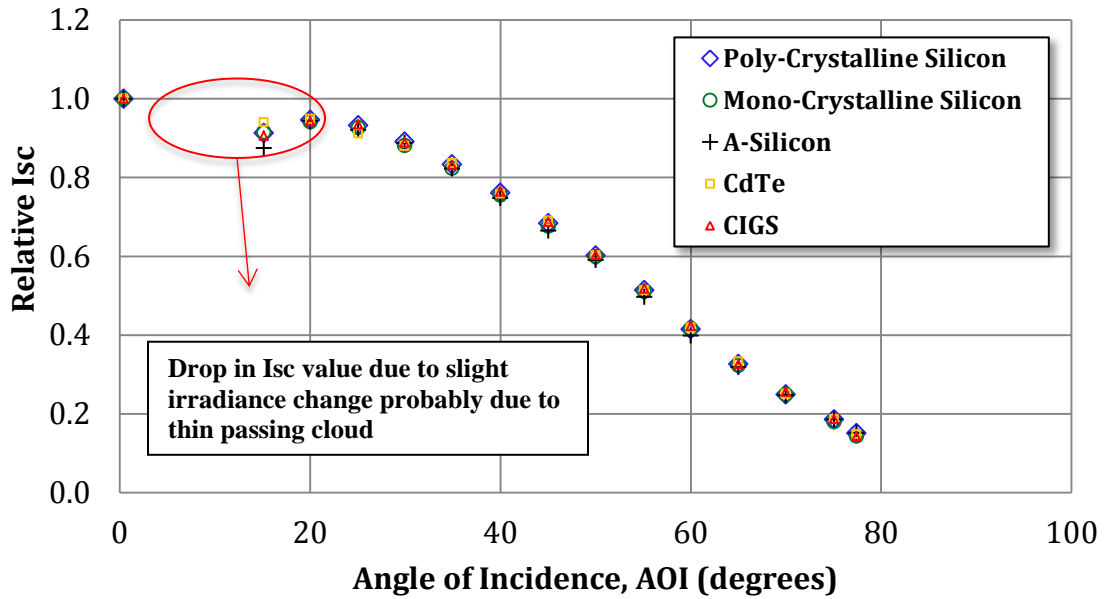
Figure C1: Round 1 – Relative short circuit current verses AOI for five modules (Multi-curve tracer method)
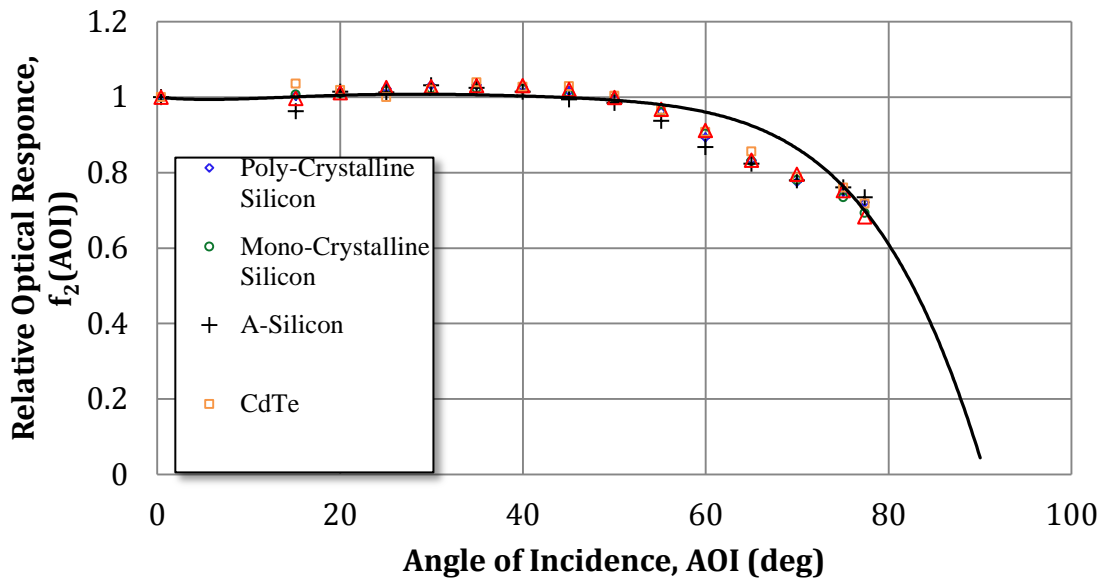

Figure C2: Round 1 - Data for five modules where $f_2(AOI)$ was _erroneously_ calculated using Equation (A6) (Muti-curve tracer method)

APPENDIX D

LESSONS LEARNED 2: ROUND 2 MEASUREMENTS USING TRANSDUCERS

AND DATA LOGGER

Round 2 data used CR-magnetic DC current transducers and a Campbell Scientific CR1000 datalogger and multiplexer to measure and record Isc, module temperature, and reference cell readings. The problems apparent in round 1 were addressed in round 2 and are as follows:

The fastest time interval the multi-curve tracer could measure and store data was one minute. For round 2, the fastest time interval that the datalogger and multiplexer could store data was 30 seconds. For round 2, 16 data points were collected where the total time for the experiment was 9.5 minutes.

The human error that was present in round 1 when constructing Equation (A6) in the Excel spreadsheet was identified and corrected for round 2. Therefore, all plots presented in round 2 used the correct $f_2(AOI)$ equation.

The reference devices had yet to be calibrated for this experiment. Therefore, uncertainty analysis of $f_2(AOI)$ could not be calculated.

For round 2 measurements, the relative Isc obtained versus AOI is shown in Figure D1. The plot of $f_2(AOI)$ versus AOI which was correctly generated using the Sandia Equation (A6) is given in Figure D2.
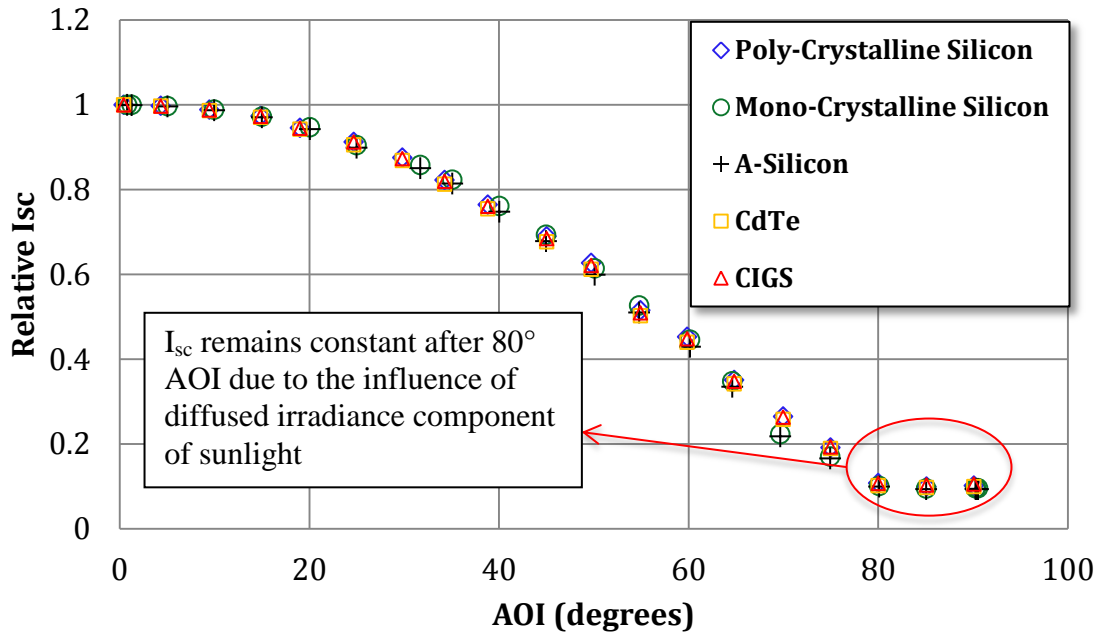
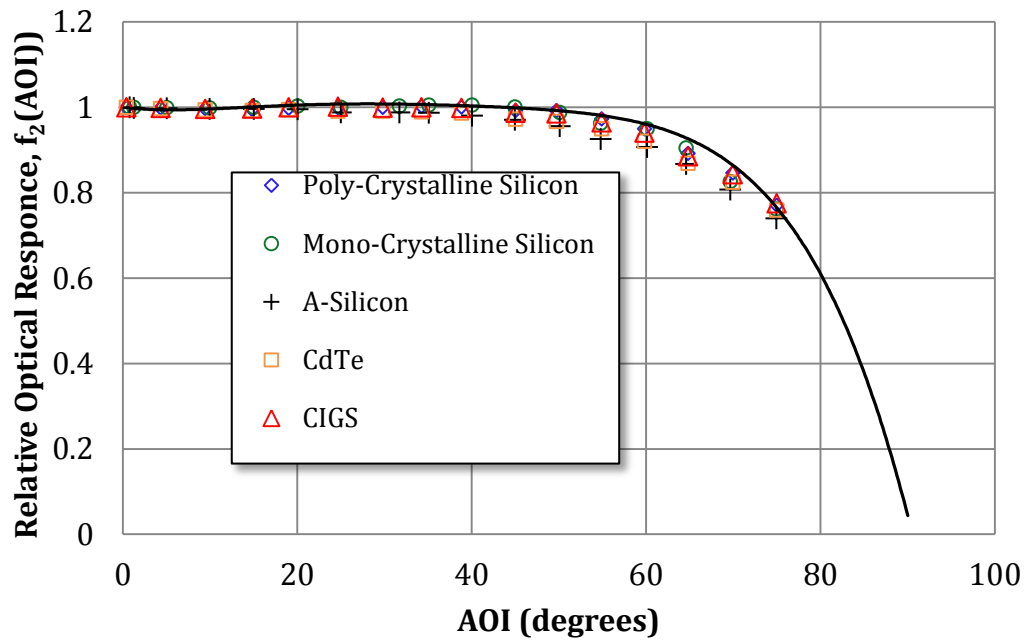Figure D1: Round 2 – Relative short circuit current verses AOI for five modules (Data logger method)

Figure D2: Round 2 - Data for five modules where f_2(AOI) was correctly calculated using Equation (A6) (Data logger method)

APPENDIX E

INTER-COMPARISON AND CROSSCHECKING OF PYRANOMETERS

For this experiment, a calibrated Eppley PSP pyranometer was used to measure global irradiance in the plane of array and it was cross referenced with a Kipp & Zonen CMP21. The f_2(AOI) calculation proved to be extremely sensitive to the accuracy of the global irradiance measurements. The pyranometers were mounted coplanar to the PV modules and in positions on the tracker so that no shading of the modules or the other reference devices occurred. The Epoa measurements for both devices were recorded simultaneously by the CR1000 datalogger and are shown in Table E1. The AOI experiment was performed on several different days with various ratios of direct normal irradiance to global irradiance (Edni/Epoa). For each case, the standard deviation of the pyranometers' measured global irradiance in the plane of array (Epoa) increased as AOI increased. Figure E2 gives Epoa measured for both pyranometers and their standard deviation as measured for an 87% Edni/Epoa ratio.
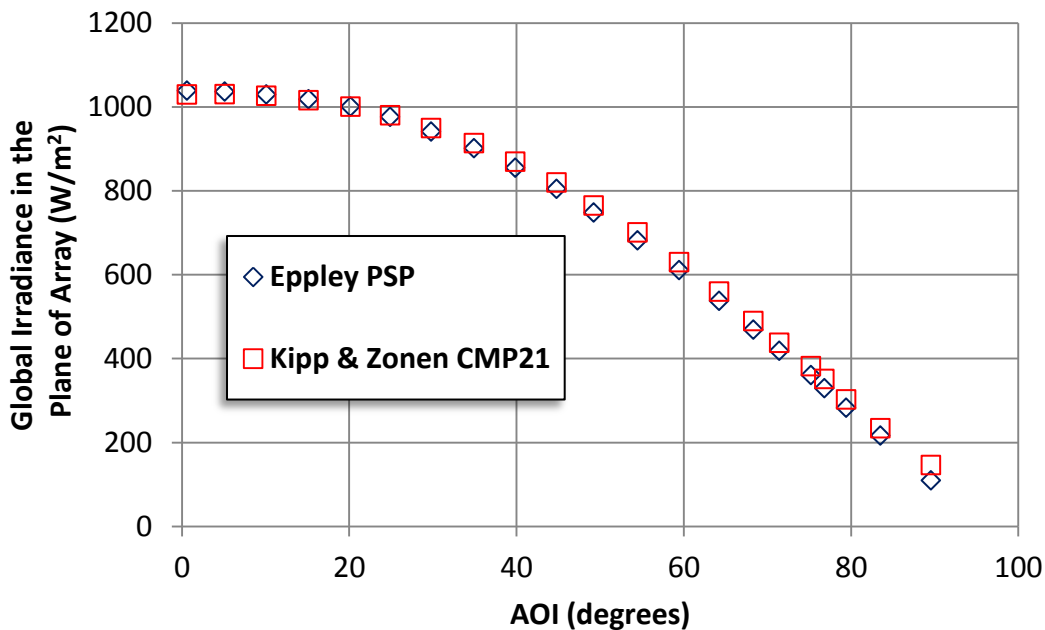

Figure E1: Global irradiance as measured by the Kipp & Zonen CMP21 and Epply PSP pyranometer for 87% Edni/Epoa

88% Edni to Epoa Ratio			
AOI (degrees)	Kipp & Zonen Epoa (W/m^2)	Eppley Epoa (W/m^2)	Difference (%)
0.6	1029.3	1038.6	0.9%
5.1	1030.3	1036.4	0.6%
10.1	1026.0	1029.5	0.3%
15.1	1015.2	1018.2	0.3%
20.2	1000.0	1000.0	0.0%
24.9	979.4	976.1	0.3%
29.8	949.1	940.9	0.9%
34.9	913.3	901.5	1.3%
39.9	868.9	854.4	1.7%
44.8	819.7	804.4	1.9%
49.2	764.8	747.8	2.3%
54.5	700.4	681.5	2.8%
59.5	629.9	610.2	3.2%
64.2	559.0	537.4	4.0%
68.3	489.3	468.4	4.5%
71.4	437.2	418.3	4.5%
75.2	381.8	359.9	6.1%
76.8	351.1	329.2	6.7%
79.4	302.6	282.5	7.1%
83.5	233.9	215.8	8.4%
89.6	146.0	109.2	33.7%

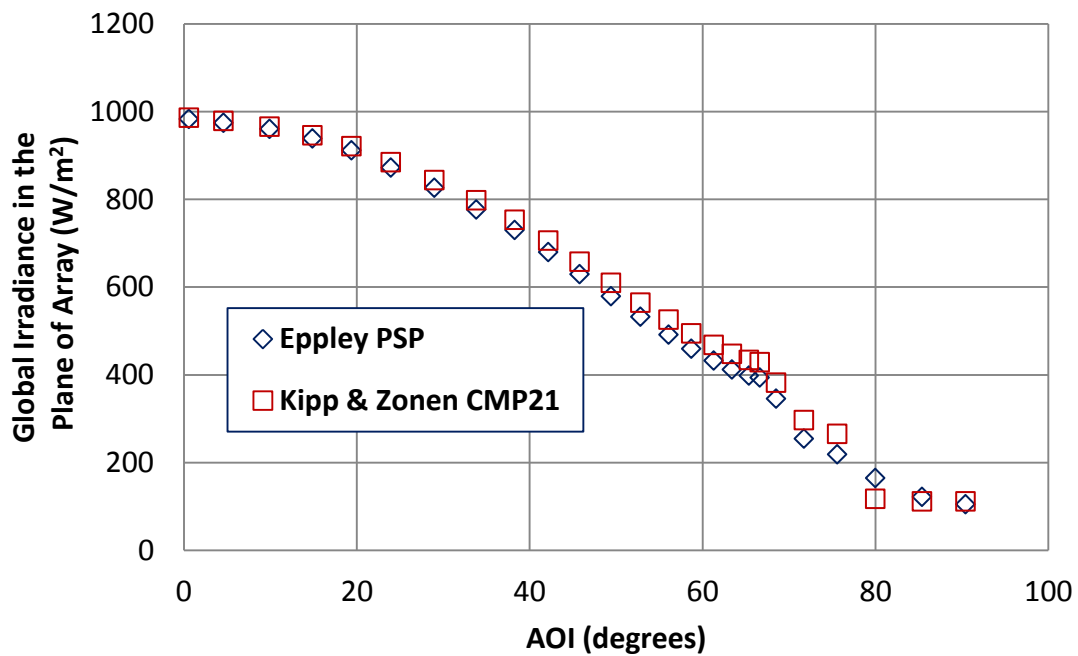Table E1: Comparison of Kipp & Zonen CMP21 verses Eppley PSP measured global irradiance in the plane of array for 87% direct to global irradiance ratio

The data presented above represents the data used in the main body of this report. However, experiments were also performed for other days with various direct to global irradiance ratios. Figure E3 gives a comparison of irradiance data for a direct to global irradiance ratio of 81%. This data also shows a higher standard deviation for higher AOI. For AOI from 0° to 66° the average standard deviation is 4% whereas for AOI from 67° to 90° the average standard deviation is 15%. Figure E4 gives a comparison of irradiance data for an overcast day where the ratio of direct to global irradiance was 2%. For this data, the standard deviation between the two pyranometers remained approximately constant, but higher, for all AOI.

Figure E3: Comparison of Kipp & Zonen CMP21 verses Eppley PSP measured global irradiance in the plane of array for 81% direct to global irradiance ratio
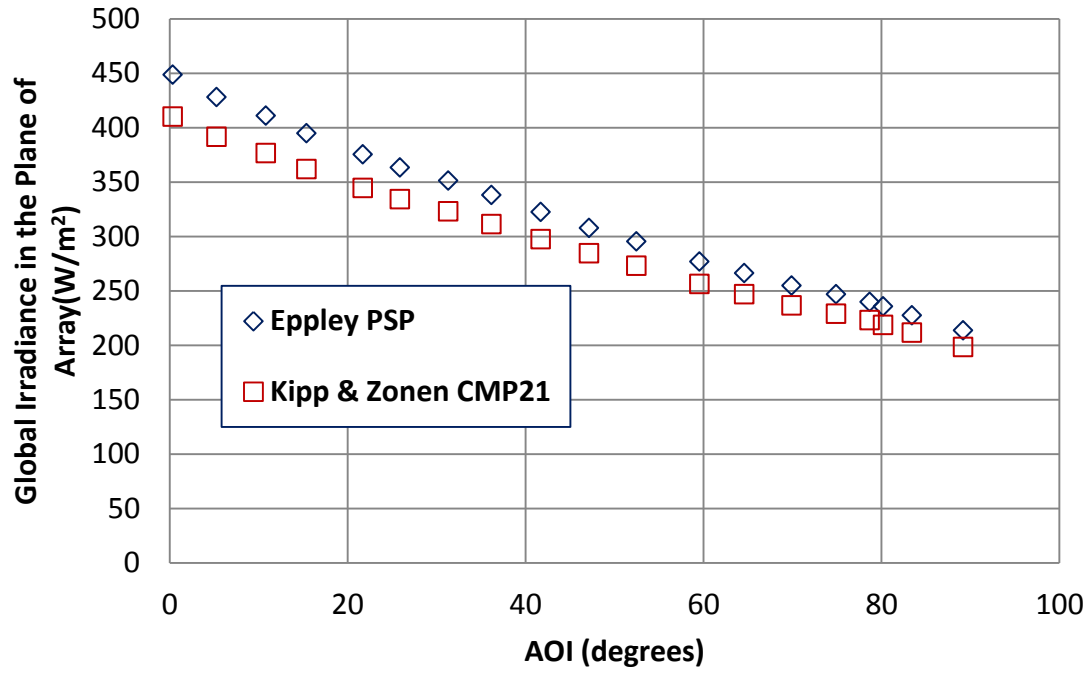
Figure E4: Comparison of Kipp & Zonen CMP21 verses Eppley PSP measured global irradiance in the plane of array for 2% direct to global irradiance ratio

APPENDIX F

MEASUREMENT OF f_2(AOI) VERSES AOI IN THE OPPOSITE DIRECTION

To obtain Figure 8 in the main body of this report, experimental data was collected at 14:37:30 MST and the tracker was rotated from the West (starting at 0.59° AOI) to the East (ending at 83.50° AOI). This experiment took 10 minutes to complete. To verify the rotational symmetry of the reflectivity with respect to module normal as called for in IEC 61853-2, the data was also collected for the five modules in the opposite direction (East to West). This experiment started at 14:47:30 MST. The tracker was set to automatic mode and allowed to track the opposite direction (from East to West). The data was processed using Sandia Equation (A6) and the corresponding graph of f_2(AOI) is given in Figure F1.
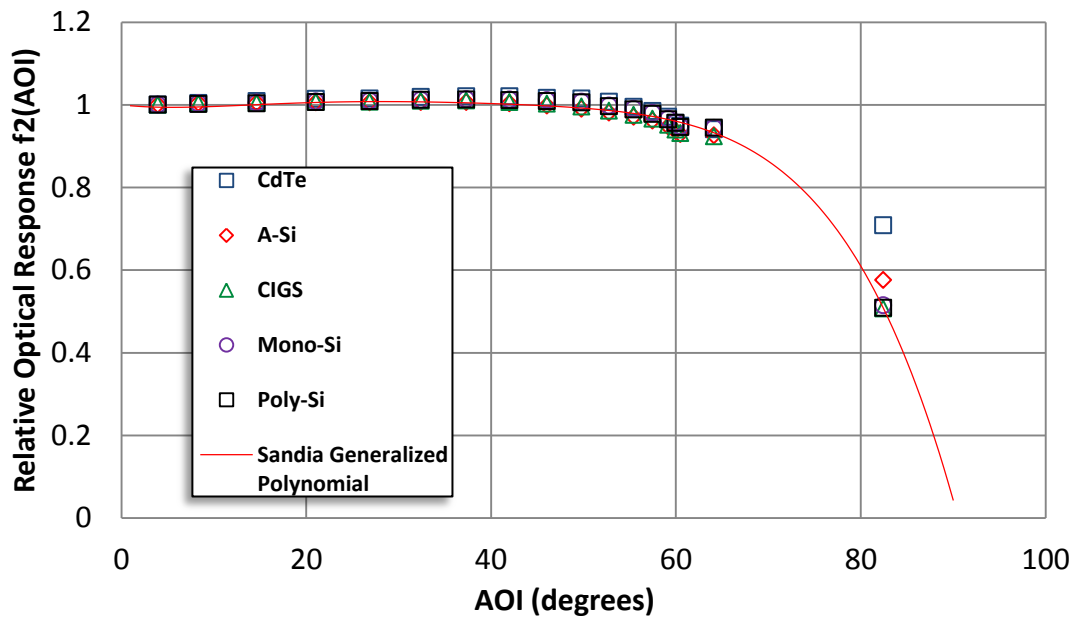
Figure F1: Round 3 - Data for five modules where f_2(AOI) was calculated when the tracker was rotated in the opposite direction (East to West)

Using the automatic function to track in the opposite direction had a few disadvantages. In the manual mode, the tracker was rotated in both azimuth and elevation proportionally. However, when the tracker was set to automatic mode to track back to

zero AOI, it first adjusted elevation angle, then tracked back azimuthally. This is not expected to affect the relative optical response of the module; however, it does limit the amount of data points collected. Tilting the tracker's elevation changes the AOI much faster than rotating azimuthally. Since the tracker tilted the modules in elevation for the first 30 seconds, data could only be recorded for AOI of 83° (the starting point taken at 14:37:30) and 63° (the next point taken at 14:38:00). After the tracker adjusted its elevation angle it began tracking azimuthally and more data points could be obtained. Figures F2 to F6 provide the plots for $f_2(AOI)$ calculated for each module technology tracking in both directions (East to West and West to East). The data for each technology is consistent for AOI when rotated in both directions from 0 to 63°.
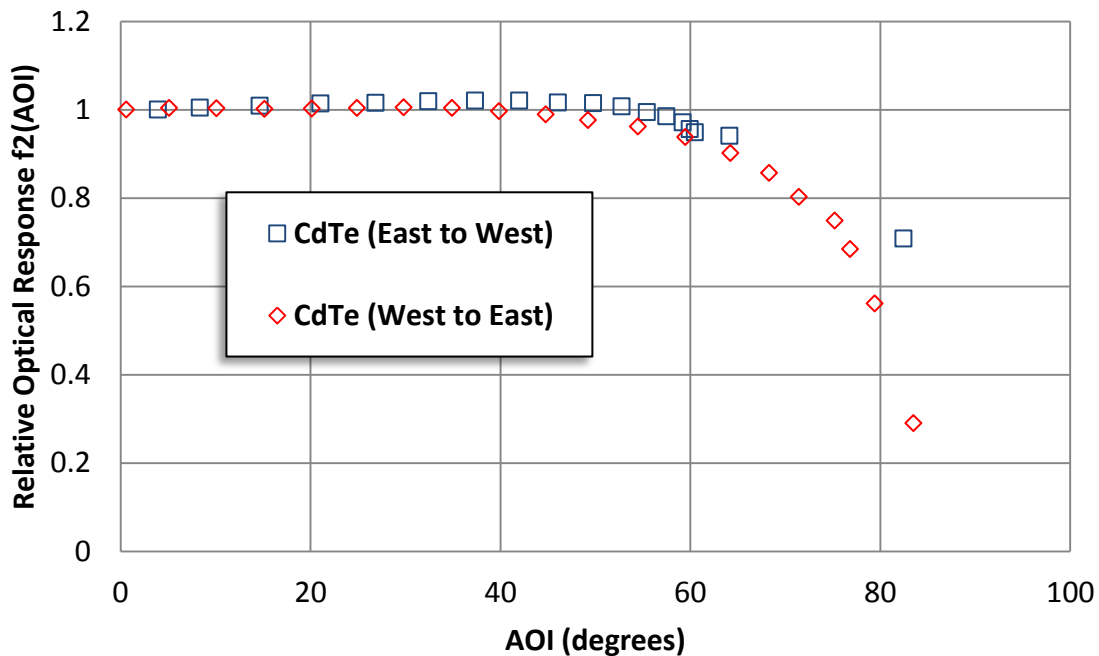

Figure F2: Round 3 - Data for $f_2(AOI)$ calculated for CdTe from West to East compared to data when the tracker was rotated in the opposite direction (East to West)

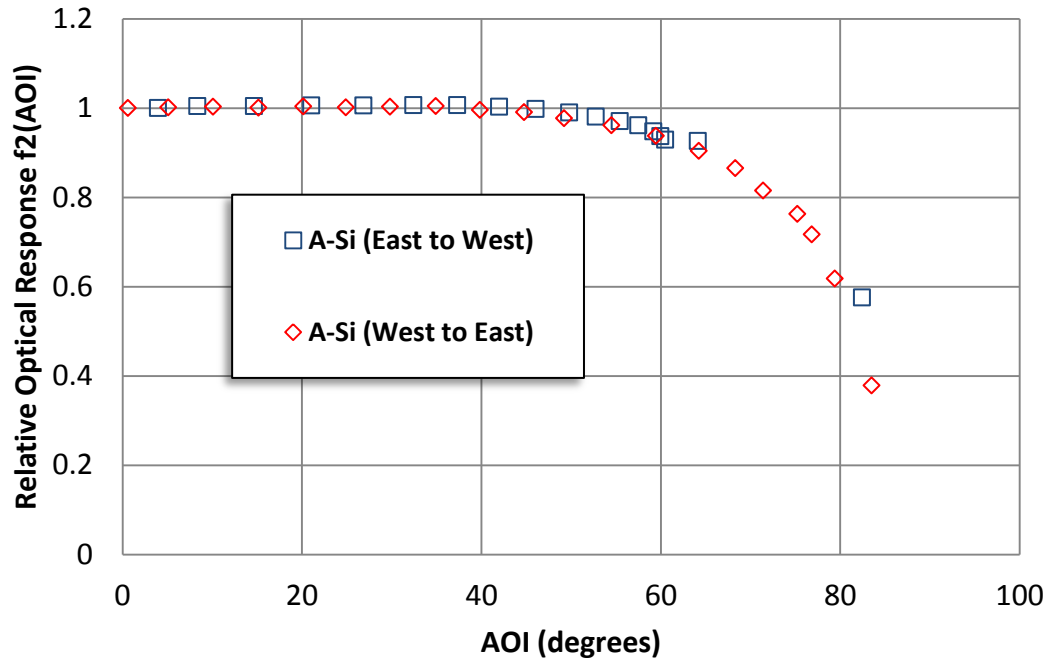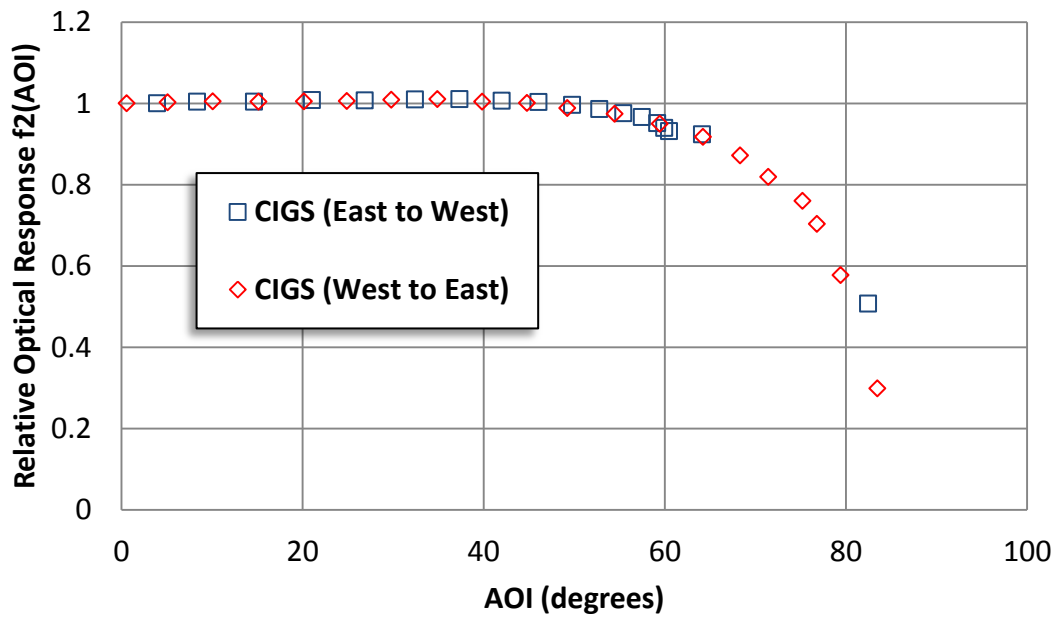Figure F3: Round 3 - Data for f_2(AOI) calculated for a-Si from West to East compared to data when the tracker was rotated in the opposite direction (East to West)

Figure F4: Round 3 - Data for f_2(AOI) calculated for CIGS from West to East compared to data when the tracker was rotated in the opposite direction (East to West)
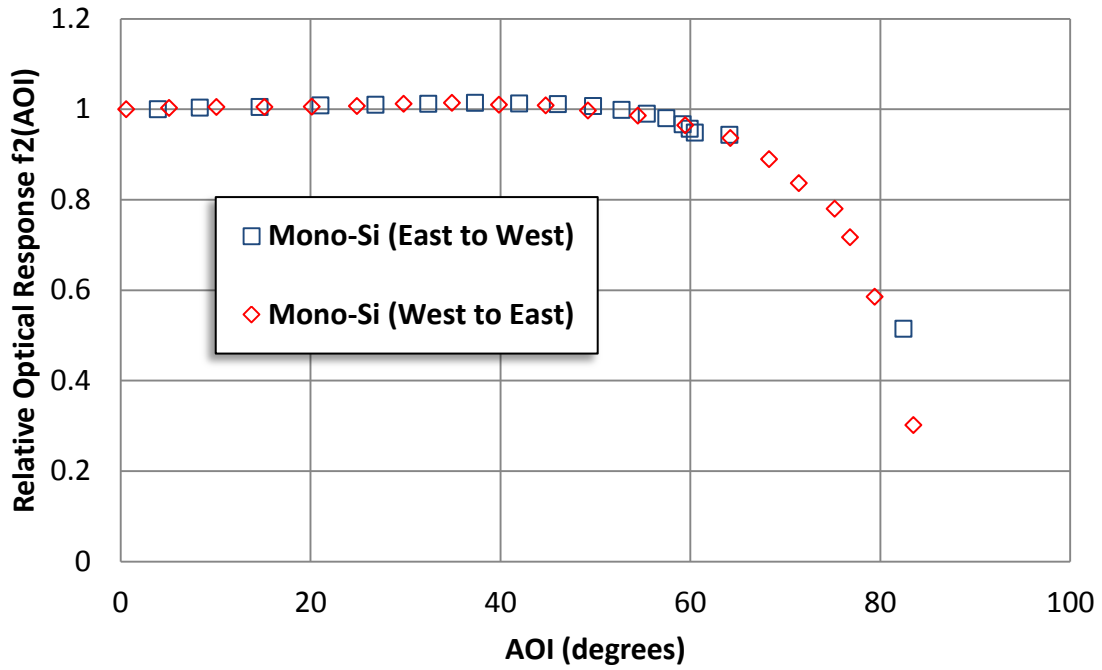
Figure F5: Round 3 - Data for $f_2(AOI)$ calculated for Mono-Si from West to East compared to data when the tracker was rotated in the opposite direction (East to West)

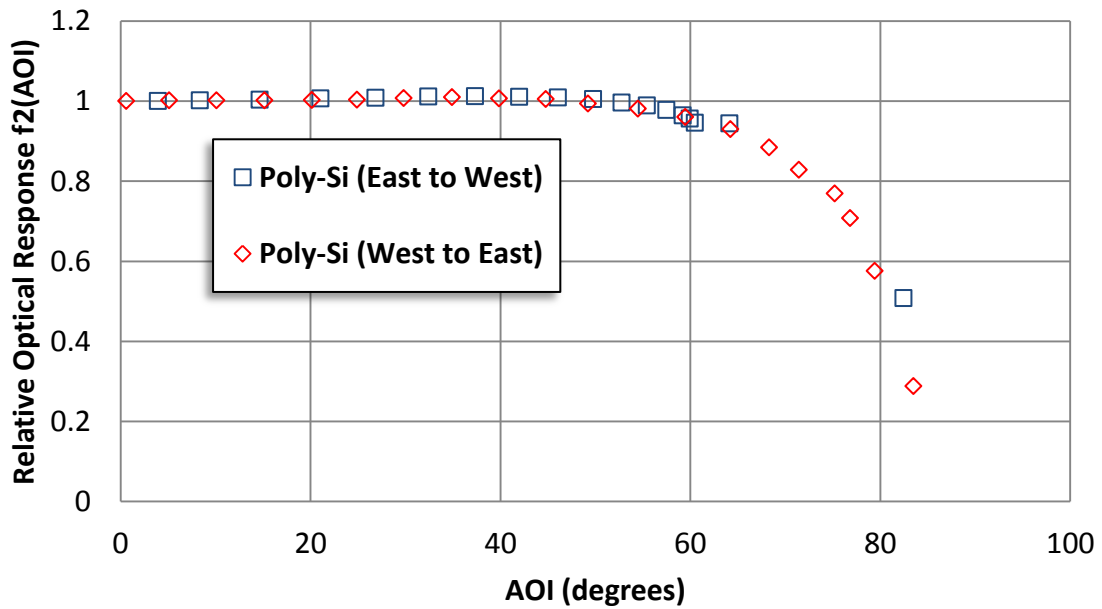
Figure F6: Round 3 - Data for $f_2(AOI)$ calculated for Poly-Si from West to East compared to data when the tracker was rotated in the opposite direction (East to West)

APPENDIX G

DETERMINING HOW MUCH VOLTAGE BIAS TO APPLY

When measuring QE for more than two cells connected in series, it is essential to use voltage bias to keep the cell under test near zero volts. The amount of voltage bias that should be applied is provided in ASTM E1021-12 as:

$$V_b = \frac{n-1}{n} V_{OC} \qquad (8)$$

This equation was used when measuring M-C-QE for this experiment. It is extremely important to note that Voc in this equation must be measured at the time of test. However, even correct application of this calculation might not yield the maximum QE curve. Therefore, this equation was used as a starting point for voltage bias application. Once the voltage bias was applied, the QE at one wavelength was monitored. The voltage bias was then slightly increased or decreased until the QE was maximized. Also, if Voc at the time of test is not known, the manufacturer's specified Voc can be used and the voltage bias can be adjusted according to the previous statement. An example of M-C-QE measurement with various voltage biases applied is given in this section.

For this C-M-QE measurement, the manufacturer's specified Voc was used as a starting point. The Voc for this module was 35.4V and the number of cells was 60. Equation (8) was used to determine the voltage bias.

$$V_b = \frac{n-1}{n} V_{OC} = \frac{60-1}{60} 35.4V = \mathbf{34.8V}$$

Once the voltage bias of 34.8V was applied, the voltage was decreased and QE curves were measured until a maximum QE curve was obtained. The resulting QE curves are given in Figure G1, where V_b indicated the applied voltage bias.
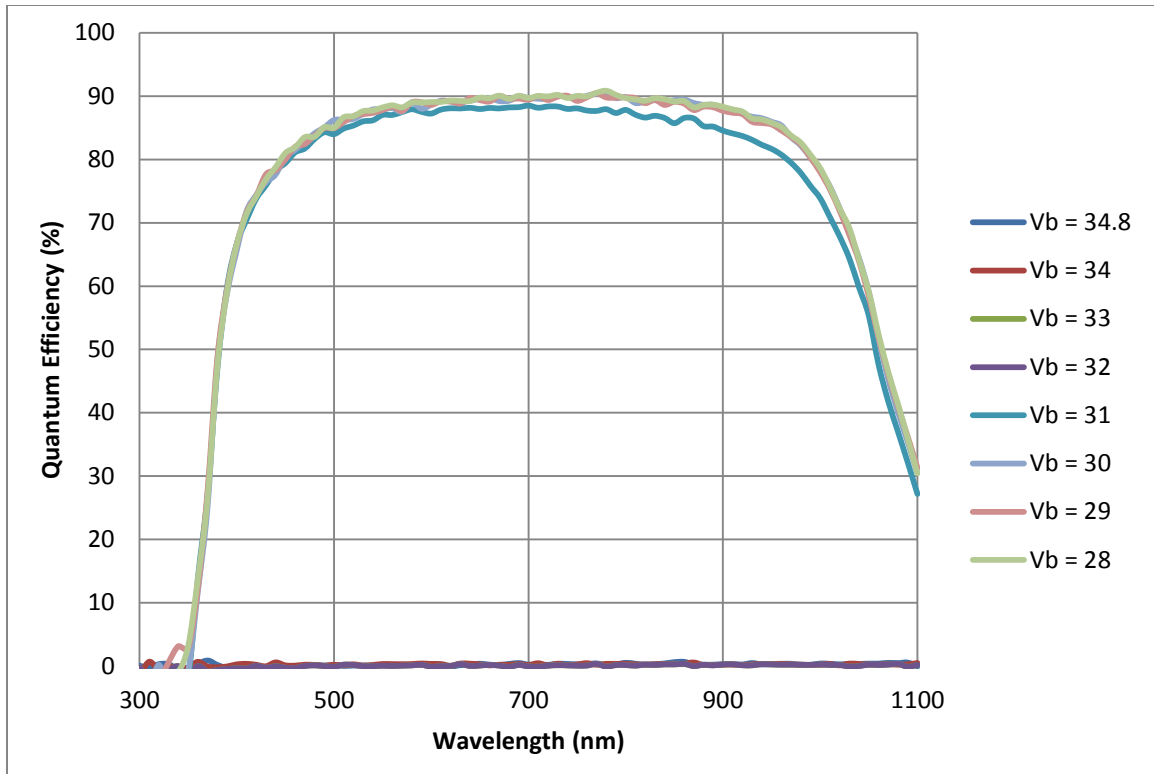
Figure G1.   C-M-QE curves with various voltage bias (V_b) applied

The results displayed by this graph show the ideal amount of voltage bias to apply for this case was between 30V and 28V. When a voltage bias of 31V was applied, the curve decreased a bit because the cell was slightly forward biased (the voltage at the end of the measurement was measured at 0.1V). When a voltage bias of 32V or higher was applied, the resulting QE curves were zero. The reason is that too much voltage bias was causing the cell under test to operate near Voc conditions (voltage measured near 0.44V). A summary of the voltage biases applied and the corresponding voltage of the cell under test (V_{CUT}) is given in Table G1.

V_{BIAS} Applied	V_{CUT}
34.80	0.45
34.00	0.44
33.00	0.44
32.00	0.44
31.00	-0.16
30.00	-0.85
29.00	-1.10
28.00	-1.90

Table G1.   Module voltage bias applied to each cell and corresponding cell voltages

APPENDIX H

THE EFFECT OF TEMPERATURE ON QE CURVES

During the test, the module is illuminated with module bias light of 200W/m^2. This will increase the temperature of the module and the cell under test. An increase in module temperature will lead to a decrease in voltage for all cells in the module. The voltage of the cell under test is negative and equals the sum of all the other cells in the module. Therefore, if the voltage of the cells within the module decreases, the voltage of the cell under test will increase (or become less negative).

The C-M-QE equipment at ASU-PRL incorporates heat sinks and fans to keep the testing temperature from getting too hot. However, the fans must be off during measurements to degrease the electrical noise inherent in ac fans. It takes five minutes to measure a full QE curve and the temperature of the module during the measurement is expected to increase during the QE measurement process. A slight increase in temperature during the test will not significantly affect the QE curve. However, the shift in voltage due to the increase in temperature will affect the QE curve.

This temperature effect can be countered by ensuring the cell under test is measured at a starting voltage bias lower than zero volts. This will allow for the voltage of the cell under test to increase slightly during the measurement, but still remain below zero volts for the duration of the test. This can be achieved by applying voltage bias as indicated in the previous section, then decreasing the voltage bias by another 1V to account for the expected voltage shift due to the temperature effect. If the voltage bias is not set low enough, the QE curves will decrease at higher wavelengths (due to the module heating up as the test is running). An example of a QE curve decreased due to the temperature effect is given in Figure H1.
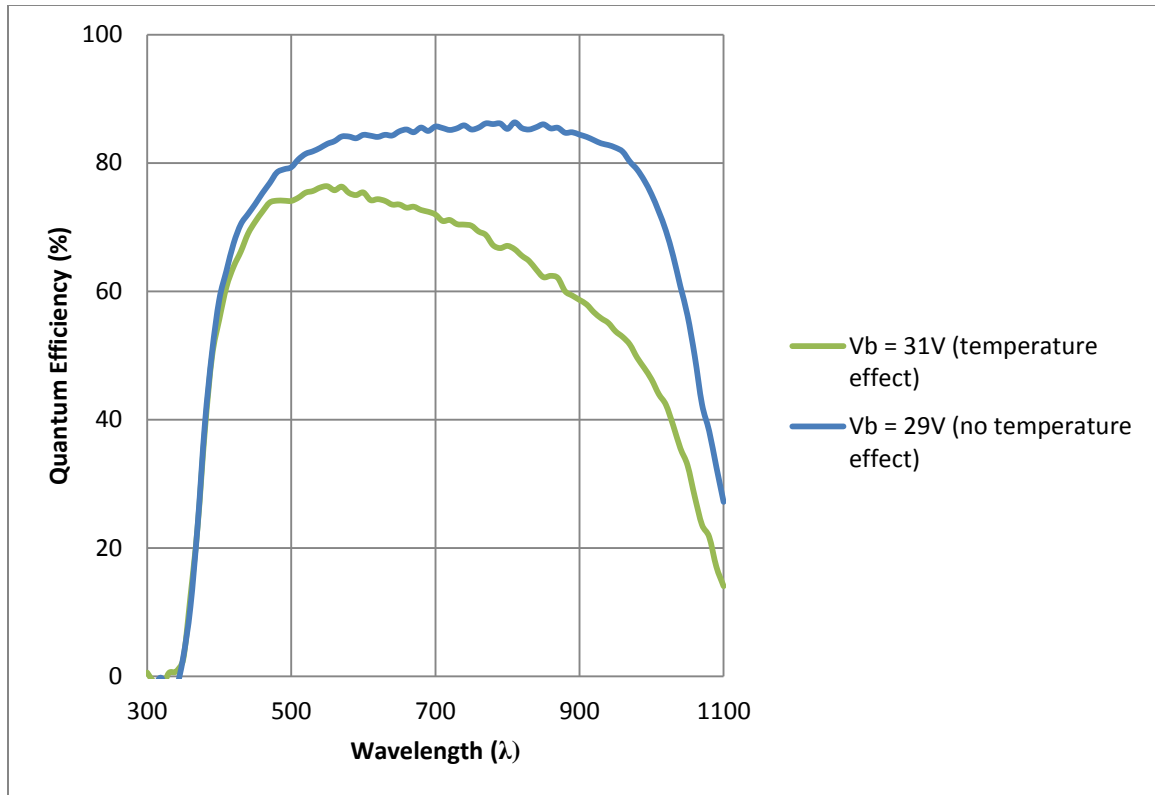
Figure H1.　　C-M-QE curves for cell 1 (Shunted cell) where the green curve shows the decrease in QE at higher wavelengths due to the temperature effect and the blue curve shows the recovered curve.

For both curves shown in Figure H1, the change in temperature during the course of the measurement was the same (about a 2°C increase during the test). This 2°C increase in temperature corresponds to a 0.28V increase in the voltage of the cell under test. If this voltage causes the voltage of the cell under test to increase into the positive region, then the current will be lost because the cell in no longer operating at Isc. Therefore, to ensure that the voltage of the cell under test does not increase past zero, the voltage bias must be adjusted lower. The blue curve shows the recovered QE after the voltage bias is decreased from 31V to 29V.

APPENDIX I

CELL BIAS LIGHT

The purpose of the cell bias light is to induce a dc current in the cell under test. The cell light bias is superimposed with the ac monochromatic beam to increase the photoconductivity of the cell under test. Since the intensity of the monochromatic beam is extremely low, it is sometimes necessary to induce a base amount of dc current so that the signal processor or lockin amplifier can accurately measure the current induced by the ac monochromatic light from the dc cell bias light. Increasing or decreasing the intensity of the cell bias light should not affect the QE curve because quantum efficiency is calculated based on the current inducted from the monochromatic light.

For this experiment, various intensities of bias light were shined on the module and the corresponding C-M-QE curves were measured. The cell light bias of the C-M-QE system at ASU-PRL uses a 12V 75W halogen lamp. The lamp intensity is adjusted via a physical dial on the power supply stack for the system. The dial can be adjusted from 0V to 12V. The intensities of cell bias light at various voltages were measured using a monocrystalline silicon reference cell. The resulting values are given in Table I1. The C-M-QE curves were compared to ensure that the measurements were consistent for different intensities of cell bias light. Figure I1 shows the C-M-QE curves for cell 22 (good cell) at various levels of cell bias light.

Voltage (V)	Cell Bias Light Intensity (W/m^2)
2	1.5
5	44.8
10	328.6
12.5	545.2

Table I1.   Voltage indicated by the C-M-QE system and the corresponding cell bias light intensity
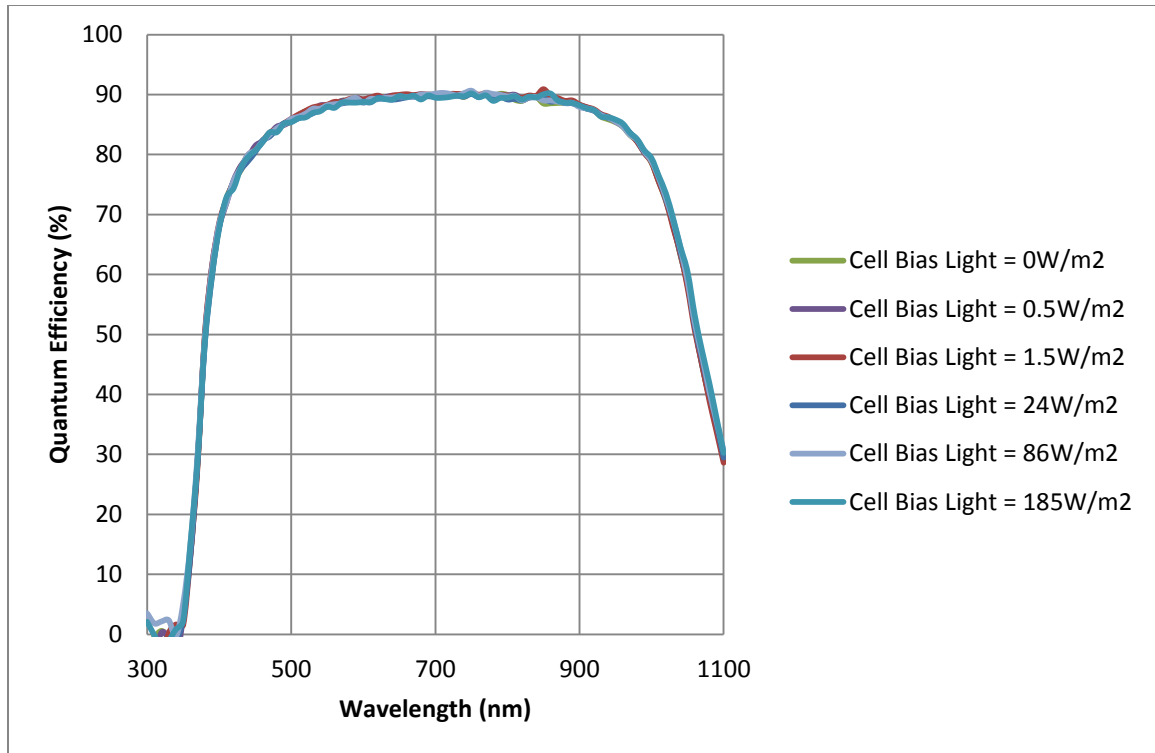
Figure I1.   QE curves for cell 22 (good cell) measured at various cell bias light intensities

The C-M-QE curves measured at various light bias intensities matched each other within the 1% uncertainty specified by the manufacturer. Also, even if the cell bias light was turned off, an accurate C-M-QE curve could be generated. This result indicates that cell bias light intensity does not influence the C-M-QE measurement when measurements for a high FF cell were performed.

Figure I2 shows the C-M-QE curves for cell 1 (shunted cell) at various levels of cell bias light.
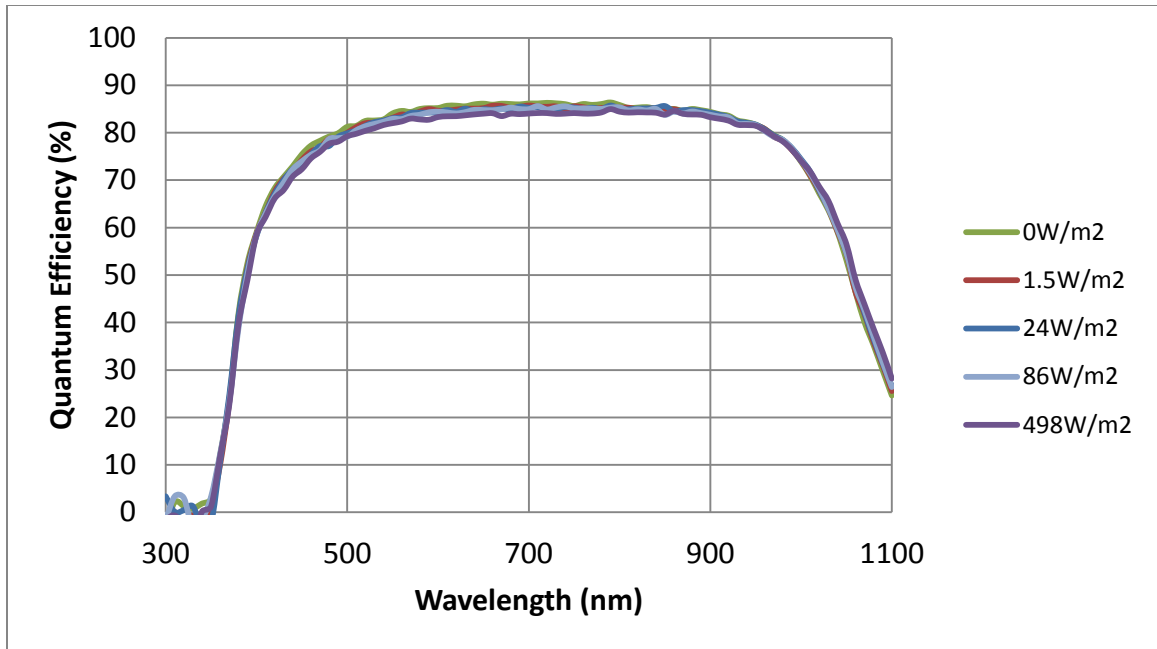
Figure I2.   QE curves for cell 1 (shunted cell) measured at various cell bias light intensities

Figure I2 shows that the intensity of the cell bias light does not have a major impact on the C-M-QE of a shunted cell for lower intensities (below 24W/m^2). However, for higher intensities of cell bias light (86W/m^2 and above) the QE curve decreases slightly with increasing cell bias light intensity. Therefore, for accurate C-M-QE measurements the cell bias light should be set to a lower intensity (below 86W/m^2). For this thesis, all C-M-QE measurements were performed with the cell bias voltage set to 1.5 W/m^2.

APPENDIX J

ADDITIONAL DATA FOR CELL 1 (SHUNTED CELL) AND CELL 22 (GOOD

CELL)

The main focus of part 2 of this thesis was to measure the accuracy of C-M-QE measurements compared to direct cell measurements for good cells (high FF) and shunted cells (low FF). To accomplish this task, cell 22 (good cell) and cell 1 (shunted cell) were targeted for comparison measurements. The characterization tests performed for these two cells are presented in this section.

First, the light I-V for cell 1 (shunted cell) and cell 22 (good cell) were measured. The I-V curves were measured by using a class A solar simulator to illuminate the target cells with 1,000 W/m^2 light. The I-V curve for cell 22 (good cell) is given in Figure J1 and the I-V curve for cell 1 (shunted cell) is given in figure J2.
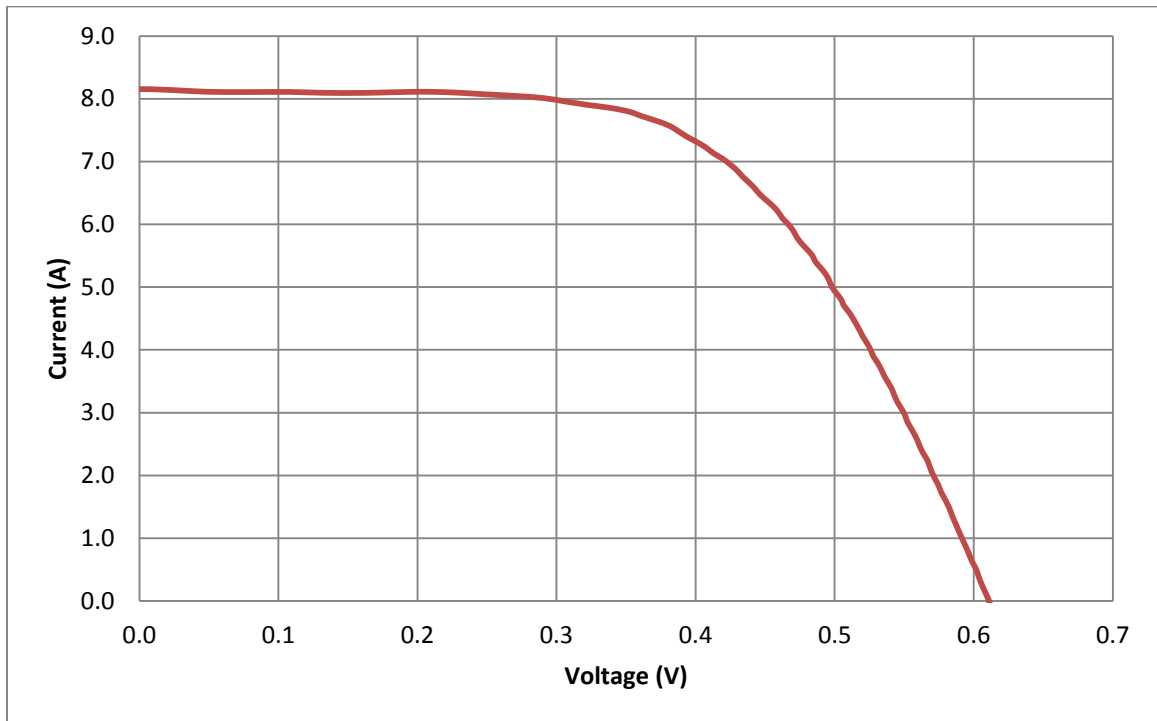

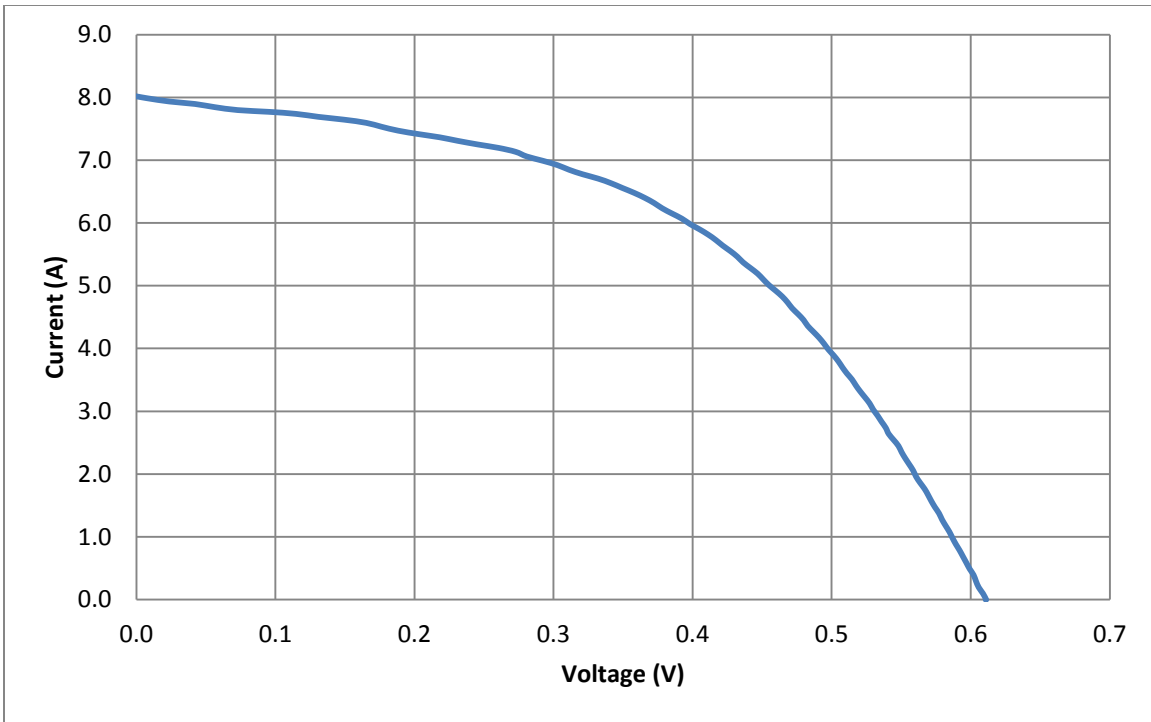Figure J1.　　I-V curve for cell 22 (good cell) at 1,000 W/m^2

Figure J2.   I-V curve for cell 1 (shunted cell) at 1,000 W/m^2

Dark I-V curves were also measured for cell 22 (good cell) and cell 1 (shunted cell). The results of the dark I-V curves are given in figures J3 and J4. The relevant data provided by the dark I-V curves and light I-V curves are provided in Table J1.
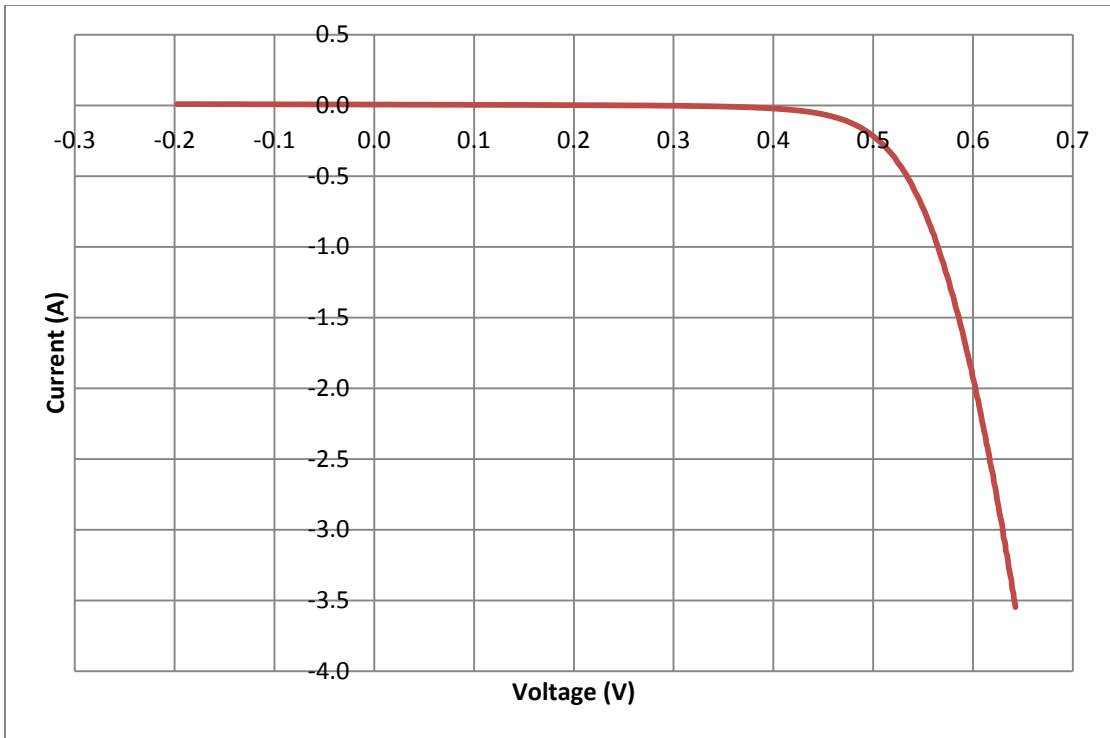
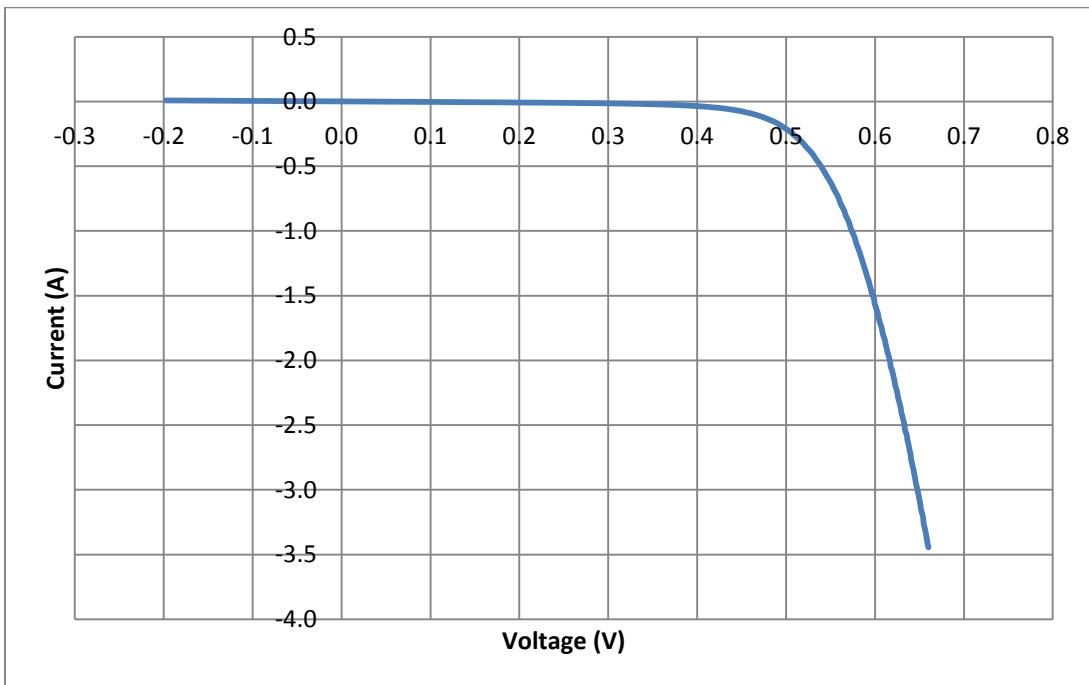Figure J3.   Dark I-V curve for cell 22 (good cell)

Figure J4.   Dark I-V curve for cell 1 (shunted cell)

	Cell 1 (Shunted Cell)	Cell 22 (Good Cell)
Voc (V)	0.61	0.61
Isc (A)	8.01	8.15
Fill Factor (%)	48.8	59.30
Pmax (W)	2.39	2.96
Vmax (V)	0.41	0.42
Imax (mA)	5.82	7.04
LIV Rshunt (Ω)	0.48	2.70
Dark Rshunt	25.70	55.60
Dark Rseries	0.036	0.021

Table J1.   Specifications for Cell 1 (shunted cell) and Cell 22 (good cell) derived from light I-V and dark I-V measurements